MECHANIK

RESEARCH REPORT

Asymptotic Analysis of the Load Transfer on Double-Lap Bolted Joints

Jan Kratochvíl

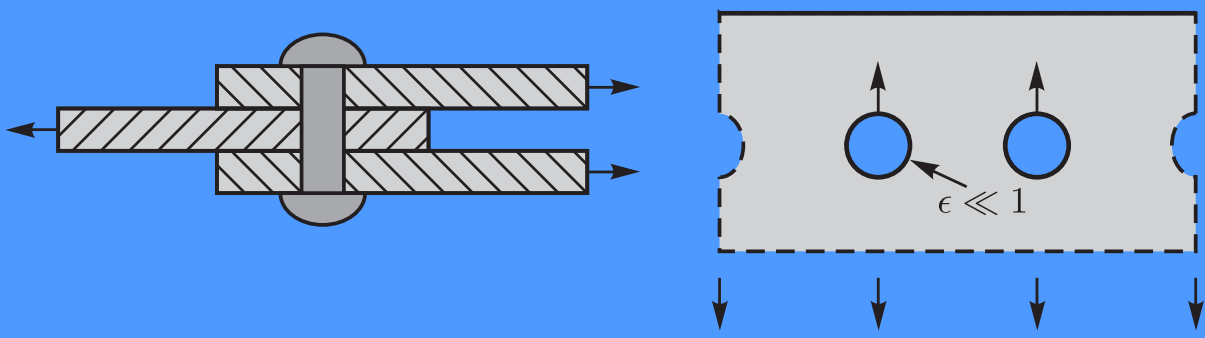

$$\varphi = \sum_{n=0}^{\infty} \epsilon^n \left[\varphi_0^n(z) + \sum_{q=1}^{N_H} \left(\varphi_q^n(\zeta_q) + A_q^n \ln \zeta_q \right) \right]$$

$$\psi = \sum_{n=0}^{\infty} \epsilon^n \left[\psi_0^n(z) + \sum_{q=1}^{N_H} \left(\psi_q^n(\zeta_q) - \frac{\overline{c}_q}{\epsilon \rho_q} \frac{\mathrm{d}\varphi_q^n}{\mathrm{d}\zeta_q} + B_q^n \ln \zeta_q - \frac{A_q^n \overline{c}_q}{\epsilon \rho_q \zeta_q} \right) \right]$$

TECHNISCHE UNIVERSITÄT DARMSTADT

Volume 24

Asymptotic Analysis of the Load Transfer on Double-Lap Bolted Joints

Vom Fachbereich Maschinenbau
an der Technischen Universität Darmstadt
zur
Erlangung des Grades eines Doktor-Ingenieurs (Dr.-Ing.)
genehmigte

D i s s e r t a t i o n

vorgelegt von

Mgr. Jan Kratochvíl

aus Prag (Tschechische Republik)

Berichterstatter:	Prof. Dr.-Ing. W. Becker
Mitberichterstatter:	Prof. Dr.-Ing. H. Altenbach
Tag der Einreichung:	12.03.2012
Tag der mündlichen Prüfung:	04.05.2012

Darmstadt 2012
D17

Herausgeber:

Studienbereich Mechanik
Technische Universität Darmstadt
Hochschulstr. 1
D-64289 Darmstadt
Germany

ISBN 978-3-935868-24-2

Acknowledgement

This thesis is a result of my research activities at the chair of Structural Mechanics at Technische Universität Darmstadt. Its completing would never have been possible without support, advice and encouragement from many persons.

First and foremost, I would like to thank my supervisor Prof. Dr.-Ing. Wilfried Becker for giving me the opportunity to work at the chair of Structural Mechanics, patiently guiding me throughout the graduation process and for many fruitful discussions during the research work. I also wish to thank Prof. Dr.-Ing. Holm Altenbach for his interest on my work and for reviewing it.

Furthermore, I want to express my gratitude to my colleagues from Technische Universität Darmstadt for helping me with various problems and creating a warm atmosphere both during and after the core hours.

Last but not least, I would like to thank my family for the motivation and support they provided to me over the long distance.

Darmstadt, May 2012 Jan Kratochvíl

Contents

Kurzfassung

In der vorliegenden Arbeit wird die Methode der komplexen Potentiale zusammen mit der Methode der zusammengesetzten asymptotischen Entwicklung auf ausgewählte Probleme der ebenen Elastizitätstheorie angewendet, die mit der Problematik der Bolzenverbindung zusammenhängen. Der Beitrag dieser Arbeit liegt in der Konstruktion geschlossen-analytischer Näherungslösungen der betrachteten Probleme.

Nach einer kurzen Einführung der theoretischen Begriffe in Kapitel 2 wird im Kapitel 3 ein mathematisches Modell der zweischnittigen Bolzenverbindung vorgestellt. Das Modell ist sehr einfach, um die analytische Behandlung zu ermöglichen. Es setzt den (generalisierten) ebenen Spannungszustand und eine einfache sinusförmige Verteilung des Kontaktdruckes zwischen dem Bolzen und der Scheibe voraus und führt somit auf das erste Randwertproblem der ebenen Elastizitätstheorie.

Im Kapitel 4 wird eine formale asymptotische Lösung des ersten Randwertproblems für eine unendlich ausgedehnte Ebene und Halbebene konstruiert, die entweder durch eine endliche Anzahl oder eine unendliche symmetrische Anordnung von kleinen Löchern geschwächt ist. Als kleiner Parameter wird dabei der relative Lochradius verwendet. Es werden drei verschiedene zugrundeliegende partielle Differentialgleichungen betrachtet, nämlich die Laplacegleichung, die Bipotentialgleichung und eine allgemeinere elliptische Gleichung vierter Ordnung mit konstanten Koeffizienten. Für jede Gleichung wird eine asymptotische Entwicklung der komplexen Potentiale hergeleitet, die gleichmäßig in dem ganzen Gebiet d.h. sowohl in der Umgebung von jedem Loch als auch in dem Fernfeld gültig ist. Die Lösung wird in Form von Algorithmen für ein Computeralgebrasystem zusammengefasst und in MATHEMATICA implementiert. Um die asymptotische Lösung zu verifizieren, wird ein parametrisiertes Finiten-Elemente Modell des betrachteten Problems mit Hilfe des kommerziellen Softwarepaketes ABAQUS und seiner PYTHON Programmierschnittstelle entwickelt.

Im Kapitel 5 wird diese allgemeine Lösung auf drei Arten von Problemen angewendet. Als Erstes wird die Problematik der Spannungskonzentration an unbelasteten Löchern betrachtet mit dem Ziel, die Möglichkeiten der benutzten Methode anhand von vergleichsweise einfachen Problemen zu untersuchen. Danach wird die Nachgiebigkeit einer unendlichen Reihe von kleinen belasteten Löchern in einer isotropen Ebene und Halbebene betrachtet. Es wird eine geschlossen-analytische Näherungsformel für die Nachgiebigkeit hergeleitet, die im Gegensatz zu den in der Industrie häufig verwendeten semiempirischen Formeln den Beitrag der Scheibenverformung zur Nachgiebigkeit der Verbindung richtig abbildet. Schließlich wird die Lastverteilung sowohl an einer finiten Anzahl als auch an unendlichen Reihen von Bolzen untersucht. Auch in diesem Fall werden die Lösungen in Form von

geschlossen-analytischen Näherungsformeln konstruiert.

Ein durch die Art der Lösung bedingtes Problem ist die Konvergenz der asymptotischen Entwicklungen. Deswegen wurden numerische Konvergenzstudien durchgeführt. Sie zeigen, dass die Methode in dem technisch relevanten Bereich der kleinen Löcher befriedigende Ergebnisse liefert.

Im Fall von anisotropem Materialverhalten ist die Abhängigkeit der Lösung von den Materialparametern sehr komplex. Eine wesentliche Vereinfachung der Ergebnisse wird durch die Annahme starker Orthotropie und die Entwicklung nach dem mit dieser Annahme verbundenen kleinen Parameter erreicht. Es stellt sich heraus, dass diese Art der Entwicklung zu gutem Konvergenzverhalten führt und sich damit kompakte geschlossen-analytische Formeln für Konfigurationen mit endlicher Anzahl von Löchern gewinnen lassen. Leider wurden keine solchen Lösungen für unendliche Reihen in anisotropen Scheiben gefunden, weil der Algorithmus in diesem Fall auf unendliche Summen führt, die sich nicht analytisch auswerten lassen.

Nomenclature

Notation

grad	Gradient operator
div	Divergence operator
rot	Curl operator
Δ	Laplace operator
$\frac{\partial}{\partial n}$	Normal derivative with respect to the normal vector $\vec{n}$
Tr	Trace of a tensor
Re	Real part
Im	Imaginary part
Int	Interior of a curve
Ext	Exterior of a curve
sec	Secant function
csc	Cosecant function
sech	Hyperbolic secant function
csch	Hyperbolic cosecant function
$\overline{(..)}$	Complex conjugate
$(..)^{\mathrm{T}}$	Tensor transpose
$(..)'$	The first derivative with respect to a real or a complex argument
$\|..\|$	Absolute value, norm
$[..]_{..}^{..}$	Difference of function values at the endpoints of an interval
$\lceil .. \rceil$	Ceiling function
[../..]	Paddé approximant
$\binom{..}{..}$	Binomial coefficient

Latin symbols

a	Constant
a^n_{pk}, a^n_{pjk}	Laurent series coefficient
A, A_p, A^n_p	Factor at a logarithmic term
b	Constant
b^n_{pk}, b^n_{pjk}	Laurent series coefficient
$\vec{b}$	Vector of volume forces
B, B_p, B^n_p	Factor at a logarithmic term

c_p	Complex coordinate of the hole centre
c_{pj}	Affine transformation of the complex coordinate of the hole centre
C	Compliance of a row of pin-loaded holes
$C^{(\mathrm{P})}$	Compliance of a bolt
$C^{(\mathrm{J})}$	Compliance of a joint
C_j	Complex constant
$\mathbb{C}$	Fourth-order stiffness tensor, complex numbers
d	Bolt diameter
d_{pk}^n	Laurent series coefficient
e	Euler's number
e_{pk}^n	Laurent series coefficient
$\vec{e}$	Direction of the position vector
E, E_1, E_2	Young's modulus
f, f_p, f_p^n	Boundary condition for the first fundamental problem
f_x, f_y, f_{xp}, f_{yp}, f_{xp}^n, f_{yp}^n	Cartesian component of the boundary condition for the first fundamental problem
f^*, f_p^*, f_p^{*n}	Boundary condition for the first fundamental problem after subtraction of logarithmic terms
f_x^*, f_y^*, f_{xp}^*, $f_{yp}^*, f_{xp}^{*n}, f_{yp}^{*n}$	Cartesian component of the boundary condition for the first fundamental problem after subtraction of logarithmic terms
$f_{\mathrm{SP0}}, f_{\mathrm{SPL}}, f_{\mathrm{SPp}}$	Boundary condition for a subproblem
$f_{x\,\mathrm{SP0}}, f_{y\,\mathrm{SP0}}$, $f_{x\,\mathrm{SPL}}, f_{y\,\mathrm{SPL}}$, $f_{x\,\mathrm{SPp}}, f_{y\,\mathrm{SPp}}$	Cartesian component of the boundary condition for a subproblem
$F^{(\mathrm{J})}$	Force transmitted over a joint
F, F_p, F_p^n, $F^{(k)}$	Force normalised by plate thickness
F_x, F_y	Cartesian component of the force normalised by plate thickness
g_k	Load coefficients
$g_n(\epsilon)$	General asymptotic sequence
G, G_{12}	Shear modulus, Lamé coefficient
h, h_k	Nondimensionalised edge distance
i	Imaginary unit, Index denoting a vector or a tensor component
j	Index denoting an anisotropic complex potential or a vector or a tensor component
k	Index denoting a plate, Auxiliary index
k_A, k_B, k_C, k_D, k_0	Stress concentration factor
K_{pk}^n, K_{pjk}^n	Auxiliary coefficient
l	Auxiliary index
L_{pk}^n	Auxiliary coefficient
m	Auxiliary variable, index
m_p	Minor semiaxis of an ellipse with unit major semiaxis
n	Index denoting the power of ϵ
$\vec{n}$	Normal vector
N	Approximation order
N_A	Number of auxiliary functions
N_C	Number of categories
N_g	Number of nonzero load coefficients

N_H	Number of holes
$\mathbb{N}$	Natural numbers
$\mathbb{N}_0$	Natural numbers with zero
o, O	Landau symbols
p	Index denoting a hole number
p_j	Complex parameter
P^n	Far-field operator
q	Index denoting a hole number
q_j	Complex parameter
Q^n, Q_p^n	Near-field operator
r	Radius, polar coordinate
Δr	Clearance
$\vec{r}$	Position vector
$\mathbb{R}$	Real numbers
S_{ij}	Compliance coefficient for plane stress in the Voigt notation
S'_{ij}	Compliance coefficient for plane strain in the Voigt notation
S^m_{pqk}, S^m_{pqjk}	Complex coefficient defined as an infinite sum
$\boldsymbol{S}^n_{pk}$	Auxiliary stress tensor
$\mathbb{S}$	Fourth-order compliance tensor
t, $t^{(k)}$	Plate thickness
t_x, t_y	Cartesian component of the stress vector
t_r, t_θ	Polar component of the stress vector
$\vec{t}$	Stress vector
T^m_{qk}, T^2_q, T^1_{qjk}, T^2_{qj}	Holomorphic function defined as an infinite sum
u	Displacement in the x-direction
u_i	Component of the displacement vector
$\overline{u}$	Displacement in the x-direction averaged over the plate thickness
u_r, u_θ	Polar component of the displacement vector
$u_r^{\mathrm{P}}, u_\theta^{\mathrm{P}}$	Polar component of the displacement vector on the bolt
$\vec{u}$	Displacement vector
U	Airy stress function
v	Displacement in the y-direction
$\overline{v}$	Displacement in the y-direction averaged over the plate thickness
$V, V_p, V_p^{(k)}$	Bolt displacement
w	Displacement in the z-direction
$w(z_j)$	Conformal mapping of the exterior of an ellipse onto the exterior of a unit circle
w_k	Width in physical dimensions
x	Cartesian coordinate
y	Cartesian coordinate
z	Cartesian coordinate, Complex coordinate
z_j	Affine transformation of the complex coordinate
$\mathbb{Z}$	Integer numbers

Greek symbols

α, α_j	Auxiliary complex coefficient
β, β_j	Auxiliary complex coefficient
γ	Unit circle, Euler–Mascheroni constant, Auxiliary complex coefficient
γ_j	Auxiliary complex coefficient
Γ, Γ_k	Boundary, Gamma function
$\delta_{kn}, \delta_{\text{condition}}$	Kronecker symbol
ϵ	Small parameter accounting to relative hole radius
$\boldsymbol{\varepsilon}$	Linearised strain tensor
ε_{ij}	Component of the linearised strain tensor
$\varepsilon_x, \varepsilon_y, \varepsilon_z,$ $\frac{\gamma_{xy}}{2}, \frac{\gamma_{xz}}{2}, \frac{\gamma_{yz}}{2}$	Cartesian component of the linearised strain tensor
$\overline{\varepsilon}_x, \overline{\varepsilon}_y, \frac{\overline{\gamma}_{xy}}{2}$	Cartesian component of the linearised plane strain tensor averaged over the plate thickness
$\varepsilon_x^*, \varepsilon_y^*, \frac{\overline{\gamma}_{xy}^*}{2}$	Cartesian component of the linearised plane strain tensor in the comparative plate
ζ, ζ_p	Scaled complex coordinate
ζ_j, ζ_{pj}	Affine transformation of the scaled complex coordinate
η	Small parameter accounting to strong orthotropy
θ	Angle, polar coordinate
κ	Material parameter
λ	Lamé coefficient
λ, λ_p, $\lambda_p^{(k)}$	Load distribution coefficient
μ	Complex parameters
ν, ν_{12}, ν_{21}	Poisson's ratio
π	Ludolph's number
ρ	Norm of scaled position vector
$\rho_p\epsilon$	Nondimensionalised hole radius
$\vec{\rho}$	Scaled position vector
σ	Point on the unit circle
σ_{ij}	Component of the Cauchy stress tensor
$\sigma_x, \sigma_y, \sigma_z,$ $\tau_{xy}, \tau_{xz}, \tau_{yz}$	Cartesian component of the Cauchy stress tensor
$\overline{\sigma}_x, \overline{\sigma}_y, \overline{\tau}_{xy}$	Cartesian component of the plane Cauchy stress tensor averaged over the plate thickness
$\sigma_r, \sigma_\theta, \tau_{r\theta}$	Polar component of the Cauchy stress tensor
$\sigma_x^\infty, \sigma_y^\infty,$ $\tau_{xy}^\infty, \tau_{xz}^\infty, \tau_{yz}^\infty,$ $\sigma_x^n, \sigma_y^n,$ $\tau_{xy}^n, \tau_{xz}^n, \tau_{yz}^n$	State of stress at infinity
$\boldsymbol{\sigma}$	Cauchy stress tensor
$\boldsymbol{\sigma}_0^n$	Outer auxiliary stress tensor
$\boldsymbol{\sigma}_1^n$	Inner auxiliary stress tensor
φ, φ_j	Complex potential

φ_p^n, φ_{pj}^n	Inner auxiliary complex potential
φ_0^n, φ_{0j}^n	Outer auxiliary complex potential
$\hat{\varphi}_p^n$, $\hat{\varphi}_{pj}^n$	Given complex potential that defines the load on the pth hole
$\hat{\varphi}_0^n$, $\hat{\varphi}_{0j}^n$	Given complex potential that defines the load in the far-field
$\varphi_{\mathrm{SP0}}, \varphi_{\mathrm{SPL}}, \varphi_{\mathrm{SPp}},$ $\varphi_{j,\mathrm{SP0}}, \varphi_{j,\mathrm{SPL}}, \varphi_{j,\mathrm{SPp}}$	Solution to a subproblem
χ, χ_j	Complex potential
ψ	Complex potential
ψ_p^n	Inner auxiliary complex potential
ψ_0^n	Outer auxiliary complex potential
$\hat{\psi}_p^n$	Given complex potential that defines the load on the pth hole
$\hat{\psi}_0^n$	Given complex potential that defines the load in the far-field
$\psi_{\mathrm{SP0}}, \psi_{\mathrm{SPL}}, \psi_{\mathrm{SPp}}$	Solution to a subproblem
Ψ_n	Polygamma function of the order n
Ω, Ω_ϵ	Two- or three-dimensional domain

Chapter 1

Introduction

1.1 Motivation

Bolted joints belong to classical connection techniques and are widely used in many areas of mechanical and civil engineering. Their main advantages are technological simplicity and the possibility of disassembling without causing any damage to the structure. While there exists sufficient empirical experience with bolted joints of metallic plates, the same cannot be said about laminates and other types of modern composite materials. This lack of practical experience creates a demand for a better understanding of the mechanical behaviour of this type of joints.

Mathematical modelling of bolted joints leads to boundary value problems of the theory of elasticity. These problems can be solved either with numerical or with analytical methods. Because of their universality and simplicity of application, numerical methods and especially the finite element method experienced an unprecedented increase in popularity over the last decades. The disadvantage of numerical solution is that a single simulation does only provide results for one combination of input values and it can be a non-trivial task to determine the interaction of different parameters. Simple closed-form solutions that cover the dependence of the results on the relevant parameters are therefore still popular among engineers. Deriving such solutions with analytical methods is only possible for comparatively simple problems though and even then, such derivation is rather nontrivial.

The set of problems that can be treated by analytical methods can be significantly extended by using approximate analytical methods. An important subclass of these are the asymptotic methods. They are applicable if the considered problem involves some intrinsic parameter which is small in magnitude. This parameter can then be considered as a perturbation of some simpler problem and the solution of the perturbed problem is expressed as a series in terms of the small parameter.

In the problem of bolted joints, a possible small parameter is the relative hole radius, which is denoted by ϵ throughout this thesis. In the case of two holes in an unbounded plate, the hole radius related to their respective distance is subject to the geometric restriction $0 < \epsilon < 1/2$ and in the case of a single hole near an edge, its radius related to the edge distance fulfils the condition $0 < \epsilon < 1$. However, from the design point of view,

a recommended minimal distance between two bolts is 5 times the bolt diameter and a minimal edge distance three times the bolt diameter (cf. Schürmann [85], Rolbicki [81]). In the first above mentioned situation, this results in the restriction of the technically relevant domain $\epsilon < 0.1$ and in the second situation $\epsilon < 0.17$. The fact that the technically relevant domain is much smaller than the geometrically possible one suggests that the solution constructed on the basis of the assumption of small holes should give satisfactory results for practically relevant problems.

Since the holes degenerate to singular points as $\epsilon \to 0$, the considered perturbation problem is of the so-called singular type. This makes its treatment using asymptotic methods more challenging in comparison to regular problems that do not degenerate at the limit $\epsilon \to 0$.

1.2 Current state of research

In this section, an overview of relevant literature for this thesis is given without any claim on completeness. The literature is divided into several topics.

The problem of holes in plane elasticity

The problem of a plane or half-plane weakened by holes has a long history that goes back to the 19^{th} century. Early works in this area employ the Airy stress function formulation, while later, the more convenient complex potential method is used more frequently.

Exact solutions of the fundamental problems for the isotropic half-plane and for the infinite isotropic plane weakened by a single circular hole based on the complex potential method have been given in the classical work of Muskhelishvili [71]. An exact series solution of the problem of two holes in an infinite isotropic plane has been given by Ling [57] using the Airy stress function in bipolar coordinates and by Haddon [29] using the complex potential method and conformal mapping. The problem of a single hole in a half-plane has been solved by Mindlin [70] using the Airy stress function in bipolar coordinates.

A possible approach to the problem of multiple holes is based on the Laurent series expansion. First, the complex potentials are written as a sum of power series, each originating at one of the holes. The series are then truncated after a finite number of terms and from the underlying boundary conditions a coupled system of linear equations for the unknown coefficients is constructed. Finally, the system must be solved numerically. Several methods for the construction of the system of equations have been proposed, such as boundary collocation, Fourier transform (e.g. Kushch et al. [53]) or the body force method (e.g. Duan et al. [15]). An older approach based on an ansatz for the Airy stress function is due to Howland and Knight [33]. Numerical results for many practically relevant situations may be found in reference books of Neuber [73], Pilkey and Pilkey [75] or Radaj and Schilberth [78].

A perturbation approach to the problem of multiple small holes, originally developed by Isida [39] for the analysis of crack problems, has been used for example by Chao et al. [11] and Gong and Meguid [25] for the study of interacting small circular inclusions. In

this approach, first, a system of linear equations is constructed using the same method as described above. Then, all the unknowns are assumed as power series in terms of a relative hole size and their coefficients are determined successively by use of the boundary conditions.

Comparatively less work has been devoted to anisotropic material behaviour. Exact analytical solutions for the half-plane and for the infinite plane weakened by a single ellipse based on the complex potential method can be found in the classical references Lekhnitskii [56] or Savin [83]. As for multiple holes in both infinite and finite domains, the problem is typically treated using numerical or semi-analytical methods such as hybrid FEM (Rhee and Rowlands [80]) or the complex potential method combined with boundary collocation (Xu et al. [96], Sergeev et al. [86]), to name a few. Although these methods deliver accurate numerical results for a wide range of configurations, they do not provide much insight into the analytical structure of the results.

In his Ph.D. thesis [21], Engels has developed a method for the analysis of elliptical domains containing circular or elliptical holes. His method has been implemented for problems involving bending-extension coupling and is based on an ansatz for the complex potentials that consist of two parts: the first of them corresponds to the solution of the classical problem of an infinite plane weakened by an elliptic opening loaded along its edge, the second one to the problem of an elliptical plate loaded along its edge. The unknown coefficients comprised in the ansatz are determined from the underlying boundary conditions. Engels applied his method to the analysis of an elliptically reinforced circular hole in an anisotropic plate or laminate [23] and to the analysis of external patch repairs of laminate plates [22]. This method has been applied to the problem of bolted joints by the author (see Kratochvil and Becker [51]) and served as one of the motivations of the present work.

Modelling of bolted joints

Two review papers dedicated to the mechanics of bolted joints are due to Thoppul et al. [91] and Camanho and Matthews [10]. The early development of the subject is described in the work of de Jong [14].

The problem of contact between an isotropic elastic plane with a hole and a rigid or elastic pin with a radius only slightly different from the hole radius has been treated by Persson [74]. The problem is reduced to a singular integro-differential equation whose solution gives the contact pressure as a function of the angle. If the material parameters of the pin and the plate are equal, the integro-differential equation can be solved in a closed form. Otherwise, a numerical solution using the method of Vekua is employed.

A model of bolted joints of anisotropic plates based on the complex potential method and involving an approximate solution of the contact problem is due to de Jong [14]. He considered a single pin-loaded hole and an infinite row of pin-loaded holes in an infinite anisotropic plate and proposed a suitable series representation of the complex potentials: a power series in the case of a single hole and a linear combination of the zeta-function and its derivatives in the case of an infinite row of holes. The boundary conditions were satisfied in an approximate sense using a collocation method. Further similar works based on the

collocation technique are due to Mangalgiri et al. [60, 61], Rangavittal et al. [79], Madenci et al. [58], Wei-Xun and Chun-Tu [93], Xiong [95] or recently Aluko and Whitworth [3], to name a few.

Another approach to the modelling of bolted joints on the basis of the complex potential method is due to Kradinov et al. [47]. (see also Kradinov et al. [49, 48], Sergeev et al. [86]). In their study, they have combined the complex potential method with a variational approach. They proposed a power series expansion for the complex potentials and then derived the governing equations by requiring the first variation of the total potential energy to vanish. Using this numerical scheme, they determined contact stress, contact region and the bolt load distribution in single- and double-lap joints of composite laminates with arbitrary shape and arbitrary location of the bolts.

A further approach to the problem of pin-loaded holes in orthotropic plates is due to Berbinau and Soutis [9]. It is based on an ansatz for the complex potentials which automatically satisfies the stress-free boundary conditions on the unloaded part of the hole. The unknown coefficients in the ansatz are determined numerically from the underlying boundary conditions. A single pin-loaded hole in an infinite plate including bending-coupling effects has been studied by Grüber [27, 28] using the extension of the complex potential method proposed by Becker [7].

A large amount of publications is devoted to the numerical simulation of bolted joints using the finite element method. Since the numerical modelling is not the main concern of this thesis, only some most relevant contributions in this direction of research are listed. An extensive numerical and experimental study including the effects of three-dimensional geometry, clearance and degradation has been carried out by McCarthy and McCarthy [65, 66, 67]. Another extensive study is due to Ekh and Schön [17, 18, 19] and Ekh et al. [20]. Further works worth mentioning are for example by Frizzell et al. [24], Hühne et al. [34], Gray and McCarthy [26], Tomas and Ireman [92] or Zerres [97].

There have been a number of attempts to derive a semi-empirical formula for the joint compliance by fitting results of experimental tests. An early work in this area is due to Tate and Rosenfeld [90]. Besides a formula for joint compliance, they have proposed a spring-based model for the determination of load distribution on bolts in a double-lap joint of isotropic plates. This work has been extended by Nelson et al. [72] to single-lap joints of composite materials. The probably most widespread formula for joint compliance has been proposed by Huth [35, 36]. It describes the dependence of the joint compliance on Young's moduli of the plate and the bolt materials, bolt diameter and thickness of the plates. Single- and double-lap configurations of both isotropic and composite materials are considered. For a list of (partly unpublished) semi-empirical formulae used in the industrial environment, the reader is referred to Huth [35], Postupka et al. [76] or Anton [5]. In all mentioned formulae, the bolt diameter is related to plate thickness and therefore they cannot take correctly into account the contribution of the plane deformation of the plates to the overall compliance. Recently, a simplified method for the investigation of the effects of bolt–hole clearance on the load distribution in composite multibolt joints was presented by McCarthy et al. [68].

Method of compound asymptotic expansions

The first one to systematically use asymptotic methods in connection with ordinary differential equations was Poincaré (1854-1912) within his investigations in celestial mechanics. The boundary layer theory founded by Prandtl [77] in 1904 is the first example of a singular perturbation problem with small parameter at the highest derivative solved using the matching principle. The application of the matching principle to boundary value problems involving a singular perturbation of the boundary originated in the 1970s (see e.g Il'in [37]). This work is summarised in the monographs by Il'in [38] or Leguillon and Sanchez-Palencia [55]. A more detailed description of the development of this subject can be found in Il'in [38], Dyke [16] or Andrianov and Manevitch [4].

Starting with the paper by Maz'ya et al. [63] in 1979, Maz'ya, Nazarov and Plamenevskii developed the method of compound asymptotic expansions for the treatment of elliptic partial differential equations in singularly perturbed domains. The results of their work on this area, originally published in papers with low circulation, are summarised in the monograph Mazja et al. [62] (English translation Maz'ya et al. [64]). This method found application to the computation of stress intensity factors on crack tips, solution of boundary value problems in thin domains or homogenisation of equations with rapidly oscillating coefficients (see Maz'ya et al. [64]). Another application is the evaluation of the so-called topological derivative (Sokolowski and Zochowski [88]) which provides the variation of a response functional when a small hole is introduced into the domain (Silva et al. [87]). The last application worth mentioning is the analysis of fields in multi-structures, i.e. domains dependent on a small parameter ϵ in such a way that as $\epsilon \to 0$, they tend to a region consisting of subsets of different space dimensions (Kozlov et al. [44, 45, 46]).

1.3 Objectives and outline of the thesis

As documented by the survey in the previous section, the available literature already covers the influence of all possible parameters on the practically relevant questions related to bolted joints. These parameters include the material properties of the plates such as anisotropy and lamination, the geometry of the plate, interaction among several bolts, three-dimensional effects, clearance and friction between plate and bolt or material degradation. However, the largest amount of the models lead to a numerical scheme, even if they are based on the complex potential method. On the other hand, analytical investigations limit themselves either to one-dimensional modelling or to fitting the experimental data by a formula of 'guessed' type that lacks any deeper mathematical or physical justification.

A systematic analytical investigation of the in-plane deformations in a double-lap bolted joint to author's knowledge is missing. Therefore, the main objective of this thesis is to construct closed-form approximate solutions to problems of the plane theory of elasticity related to bolted joints based on the assumption of small relative hole size.

This thesis is structured in six chapters. Chapter 2 briefly reviews basic theoretical concepts that are relevant for the thesis. It covers the fundamentals of linear elasticity theory, the complex potential method for the solution of plane problems of elasticity and the fundamentals of the asymptotic analysis with major focus on the method of compound

asymptotic expansions.

In Chapter 3, a simple mathematical model of a bolted joint is presented. Only double-lap configurations where the tilting of the bolts can be neglected are considered. The model assumes the state of (generalised) plane stress in each of the plates and a simple sinusoidal normal stress distribution in the bolt-to-hole contact and mathematically leads to the first fundamental problem of the plane theory of elasticity.

A formal asymptotic solution of the first fundamental problem for an infinite plane or half-plane weakened by a finite number or an infinite symmetric array of small holes is given in Chapter 4. Several types of deformations with three different underlying partial differential equations are considered, namely antiplane strain described by the Laplace equation, plane stress and plane strain in isotropic plates described by the bipotential equation and plane stress and generalised plane stress in anisotropic plates described by a more general linear elliptic fourth-order partial differential equation with constant coefficients. A general geometric configuration with arbitrary location of holes is considered. The solution is based on the combination of the complex potential method and the method of compound asymptotic expansions. It delivers an iterative procedure for the construction of an asymptotic expansion of the complex potentials to an arbitrary order of approximation. The solution is uniformly valid in the whole domain, i.e. both in the vicinity of each of the holes as well as in the far-field.

The proposed solution and especially the derivation of higher order approximations is very intensive in routine algebraic calculation. Therefore, it is summarised in form of algorithms for a computer algebra system and implemented in the commercial package MATHEMATICA [94]. All solutions to particular problems presented later in this thesis are generated using this implementation.

Since this thesis is focused on solving a real-world problem, only the formal asymptotic solution is constructed. This means that no mathematical proof of the validity of the solution and error estimates is given. Instead, the correctness and usefulness of the proposed formal solution is proved by numerical convergence studies and comparison to solutions obtained by numerical means. For this purpose, a parametrised finite element model of the considered problem has been created using the commercial FE software ABAQUS and its PYTHON scripting interface.

In Chapter 5, several examples solved using this algorithm are presented. The first part of this chapter discusses the stress concentration on unloaded holes. The purpose of this section is to evaluate the capabilities of the algorithm from Chapter 4 by means of relatively simple problems. In the second part, several configurations involving infinite rows of pin-loaded holes are considered. The main focus is laid on the evaluation of the compliance of such configurations. The final topic is the load distribution on both finite configurations and infinite rows of pin-loaded holes. In all cases, closed-form analytical approximations to the solution of the problem are given.

Finally, the results of the thesis are concluded and several possibilities of further research in this area are suggested in Chapter 6.

Chapter 2

Theoretical background

In this chapter, the theoretical concepts upon which this work is based are recapitulated for further reference. No attempt is made to derive the results and no claim is raised to comprehensiveness. In the first section, the basics of linear elasticity theory are summarised. After that, the complex potential method for solving two-dimensional linear-elastic problems is presented. Finally, the basic notions of the asymptotic analysis and the method of compound asymptotic expansions are outlined.

A standard notation for the field variables and operations is used. Scalar quantities are denoted by italic letters, vectors by a symbol with an arrow, second-order tensors by boldface symbols and fourth-order tensors by blackboard symbols. Although the fundamental field equations are first given in the coordinate-free form, for the solution of specific problems, they must be given with respect to an appropriate coordinate system (cylindrical or polar). Summation convention is not adopted, sums over indices are always given explicitly.

2.1 Linear elasticity theory

All results of this work relate to the linear elasticity theory. This theory assumes small deformations and linear elastic material behaviour. In this section, the fundamental concepts of the linear elasticity theory are summarised. These include the notions of the displacement vector, strain and stress tensors, equilibrium conditions and Hooke's law. Special attention is paid to two-dimensional deformations such as antiplane stress, plane stress and plane strain which play the central role in this work. For more details the reader is referred to standard textbooks as e.g. Becker and Gross [8], Sadd [82] or Howell et al. [32].

2.1.1 Kinematics

The position of a material point in a continuous body is described by its position vector $\vec{r}$. In a Cartesian coordinate system, its components are the coordinates x, y and z of the

considered point. The length of the position vector is denoted by r.

The transformation of a continuous body from the undeformed state to the deformed state is described by the displacement vector $\vec{u}$ whose components in a Cartesian coordinate system are traditionally denoted by

$$u_i = \begin{bmatrix} u \\ v \\ w \end{bmatrix}. \tag{2.1}$$

The state of deformation of the body within the framework of the small deformation theory is described by the linearised strain tensor

$$\boldsymbol{\varepsilon} = \frac{1}{2}\left(\operatorname{grad}\vec{u} + (\operatorname{grad}\vec{u})^{\mathrm{T}}\right) \tag{2.2}$$

the components of which are traditionally denoted by

$$\varepsilon_{ij} = \begin{bmatrix} \varepsilon_x & \frac{\gamma_{xy}}{2} & \frac{\gamma_{xz}}{2} \\ \frac{\gamma_{xy}}{2} & \varepsilon_y & \frac{\gamma_{yz}}{2} \\ \frac{\gamma_{xz}}{2} & \frac{\gamma_{yz}}{2} & \varepsilon_z \end{bmatrix}. \tag{2.3}$$

From the equation (2.2), the Saint-Venant's compatibility condition

$$\operatorname{rot}(\operatorname{rot}\boldsymbol{\varepsilon})^{\mathrm{T}} = 0 \tag{2.4}$$

follows by differentiation. It represents six different equations.

2.1.2 Stress tensor and equilibrium

The state of stress at a given point of an elastic body is described by the Cauchy stress tensor $\boldsymbol{\sigma}$. This tensor is symmetric and its components in a Cartesian coordinate system are traditionally denoted by

$$\sigma_{ij} = \begin{bmatrix} \sigma_x & \tau_{xy} & \tau_{xz} \\ \tau_{xy} & \sigma_y & \tau_{yz} \\ \tau_{xz} & \tau_{yz} & \sigma_z \end{bmatrix}. \tag{2.5}$$

The stress vector $\vec{t}$ acting on an infinitesimal area element with the normal $\vec{n}$ is given by the Cauchy formula

$$\vec{t} = \boldsymbol{\sigma} \cdot \vec{n}. \tag{2.6}$$

The differential form of the equilibrium condition for a continuous body reads

$$\operatorname{div}\boldsymbol{\sigma} + \vec{b} = 0, \tag{2.7}$$

where $\vec{b}$ is the vector of volume forces.

2.1.3 Linear elastic behaviour

A linear elastic material is characterised by a linear relation between stress and strain tensors called Hooke's law

$$\boldsymbol{\sigma} = \mathbb{C} : \boldsymbol{\varepsilon}, \tag{2.8}$$

where $\mathbb{C}$ is the fourth-order stiffness tensor or, inversely,

$$\boldsymbol{\varepsilon} = \mathbb{S} : \boldsymbol{\sigma}, \tag{2.9}$$

where $\mathbb{S}$ is the compliance tensor.

For a fully anisotropic body, 21 out of the 81 components of the stiffness tensor are independent. The number of independent stiffness coefficients further reduces for materials with certain symmetries:

- Monoclinic material possesses one plane of material symmetry and is characterised by thirteen independent elastic moduli.
- Orthotropic material possesses three mutually perpendicular planes of symmetry and is characterised by nine independent elastic moduli.
- Transversely isotropic material possesses an axis of symmetry and is characterised by five independent elastic moduli.
- Isotropic material is completely symmetric and is characterised by two independent elastic moduli.

For an isotropic material, Hooke's law becomes

$$\boldsymbol{\sigma} = \lambda(\operatorname{Tr}\boldsymbol{\varepsilon})\mathbf{I} + 2G\boldsymbol{\varepsilon}, \tag{2.10}$$

where λ and G are the Lamé constants which are related to the Young's modulus E and the Poisson's ratio ν by

$$\lambda = \frac{\nu E}{(1+\nu)(1-2\nu)}, \quad G = \frac{E}{2(1+\nu)}. \tag{2.11}$$

2.1.4 Formulation of boundary value problems

The kinematic equations (2.2), the equilibrium equations (2.7) and Hooke's law (2.8) represent in a full three-dimensional setting a system of 15 partial differential equations for 15 unknown components of the displacement vector and the stress and strain tensors. In order to guarantee the uniqueness of the solution in a given domain, this system has to be supplied with appropriate boundary conditions.

The following combinations of boundary conditions are most common:

- *First fundamental problem.* The stress vector $\vec{t}$ is prescribed on the whole boundary.

- *Second fundamental problem.* The displacement vector $\vec{u}$ is prescribed on the whole boundary.
- *Problem of a mixed type.* The stress vector $\vec{t}$ is prescribed on a part of the boundary whereas the displacement vector $\vec{u}$ is prescribed on its complement. Also, tangential stresses and normal displacements or vice versa can be prescribed on certain parts of the boundary.

A special kind of mixed boundary value problems is the contact problem. Here, a certain contact condition involving the displacement is prescribed within the contact area whereas the zero traction condition $\vec{t} = 0$ is prescribed outside it. The extent of the contact area is a priori not known. Beside the three listed classical problems, other combinations of boundary conditions are conceivable as well.

Since all above listed field equations are linear, they fulfil the superposition principle: if both $\vec{u}^{(1)}$, $\boldsymbol{\varepsilon}^{(1)}$, $\boldsymbol{\sigma}^{(1)}$ and $\vec{u}^{(2)}$, $\boldsymbol{\varepsilon}^{(2)}$, $\boldsymbol{\sigma}^{(2)}$ satisfy the field equations, then so does their superposition $\vec{u}^{(1)} + \alpha\vec{u}^{(2)}$, $\boldsymbol{\varepsilon}^{(1)} + \alpha\boldsymbol{\varepsilon}^{(2)}$, $\boldsymbol{\sigma}^{(1)} + \alpha\boldsymbol{\sigma}^{(2)}$ for any $\alpha \in \mathbb{R}$.

2.1.5 Two-dimensional problems

In many practically relevant situations, the deformation of the body is exactly or at least approximately two-dimensional. In such cases, the number of equations, independent variables and unknowns reduces. Due to the reduced complexity, analytical solutions for such configurations can be found more easily. The results of this thesis are based on theories of antiplane strain, plane stress and plane strain.

Antiplane strain

The simplest two-dimensional deformation is antiplane strain. It is defined by the kinematic assumptions

$$u = 0, \quad v = 0, \quad w = w(x, y). \tag{2.12}$$

The only nonzero strain components are

$$\gamma_{xz} = \frac{\partial w}{\partial x}, \quad \gamma_{yz} = \frac{\partial w}{\partial y} \tag{2.13}$$

and in the case of an isotropic material, the only nonzero stresses are

$$\tau_{xz} = G\frac{\partial w}{\partial x}, \quad \tau_{yz} = G\frac{\partial w}{\partial y}. \tag{2.14}$$

The shear stress τ_{nz} related to a normal vector $\vec{n}$ in the xy-plane is given by the normal derivative

$$\tau_{nz} = G\frac{\partial w}{\partial n}. \tag{2.15}$$

From the equilibrium condition (2.7), it follows

$$\Delta w = \frac{\partial^2 w}{\partial x^2} + \frac{\partial^2 w}{\partial y^2} = 0. \tag{2.16}$$

Although antiplane strain only has a limited practical relevance, it serves as a model problem for more complex deformations.

Plane stress and generalised plane stress

Plane stress is defined by the relations

$$\sigma_x = \sigma_x(x,y), \quad \tau_{xy} = \tau_{xy}(x,y), \quad \sigma_y = \sigma_y(x,y), \quad \sigma_z = \tau_{xz} = \tau_{yz} = 0 \tag{2.17}$$

and describes approximately the state of stress in thin plates with a homogeneous profile loaded by in-plane forces. Hooke's law in the Voigt notation for the nonzero stress components in an anisotropic material reads

$$\begin{bmatrix} \varepsilon_x \\ \varepsilon_y \\ \gamma_{xy} \end{bmatrix} = \begin{bmatrix} S_{11} & S_{12} & S_{16} \\ S_{12} & S_{22} & S_{26} \\ S_{16} & S_{26} & S_{66} \end{bmatrix} \begin{bmatrix} \sigma_x \\ \sigma_y \\ \tau_{xy} \end{bmatrix}, \tag{2.18}$$

where S_{ij} are doubly-indexed components of the compliance tensor $\mathbb{S}$. For an orthotropic body, this equation takes the form

$$\begin{bmatrix} \varepsilon_x \\ \varepsilon_y \\ \gamma_{xy} \end{bmatrix} = \begin{bmatrix} \frac{1}{E_1} & -\frac{\nu_{21}}{E_2} & 0 \\ -\frac{\nu_{12}}{E_1} & \frac{1}{E_2} & 0 \\ 0 & 0 & \frac{1}{G_{12}} \end{bmatrix} \begin{bmatrix} \sigma_x \\ \sigma_y \\ \tau_{xy} \end{bmatrix} \tag{2.19}$$

and for an isotropic body, it reduces to

$$\begin{bmatrix} \varepsilon_x \\ \varepsilon_y \\ \gamma_{xy} \end{bmatrix} = \begin{bmatrix} \frac{1}{E} & -\frac{\nu}{E} & 0 \\ -\frac{\nu}{E} & \frac{1}{E} & 0 \\ 0 & 0 & \frac{2(1+\nu)}{E} \end{bmatrix} \begin{bmatrix} \sigma_x \\ \sigma_y \\ \tau_{xy} \end{bmatrix}, \tag{2.20}$$

where the engineering constants E_1, E_2, G_{12} and ν_{12} are independent and ν_{21} is given by the reciprocity relation

$$\frac{\nu_{12}}{E_1} = \frac{\nu_{21}}{E_2}. \tag{2.21}$$

The plane stress formulation can easily be generalised to plates with a symmetric nonhomogeneous profile by introducing the values of the stress, displacement and strain components averaged over the plate thickness t

$$\overline{\sigma}_x = \frac{1}{t}\int_{-t/2}^{t/2} \sigma_x \,\mathrm{d}z, \quad \overline{\sigma}_y = \frac{1}{t}\int_{-t/2}^{t/2} \sigma_y \,\mathrm{d}z, \quad \overline{\tau}_{xy} = \frac{1}{t}\int_{-t/2}^{t/2} \tau_{xy} \,\mathrm{d}z, \tag{2.22a}$$

$$\overline{u} = \frac{1}{t}\int_{-t/2}^{t/2} u \,\mathrm{d}z, \quad \overline{v} = \frac{1}{t}\int_{-t/2}^{t/2} v \,\mathrm{d}z, \tag{2.22b}$$

$$\overline{\varepsilon}_x = \frac{\partial \overline{u}}{\partial x}, \quad \overline{\varepsilon}_y = \frac{\partial \overline{v}}{\partial y}, \quad \overline{\gamma}_{xy} = \frac{\partial \overline{u}}{\partial y} + \frac{\partial \overline{v}}{\partial x}. \tag{2.22c}$$

The averaged stresses and strains fulfil a relation of the same form as (2.18) where the coefficients of the compliance matrix are determined by the structure of the plate. For a laminated plate, these coefficients can be calculated by means of the classical laminate theory. For more details on modelling of laminates, the reader is referred to Becker and Gross [8], Jones [42], Altenbach et al. [2] or Christensen [12].

Plane strain

Plane strain is characterised by the kinematic assumptions

$$u = u(x, y), \quad v = v(x, y), \quad w = 0, \tag{2.23}$$

which imply that the only nonzero strain components are

$$\varepsilon_x = \frac{\partial u}{\partial x}, \quad \varepsilon_y = \frac{\partial v}{\partial y}, \quad \gamma_{xy} = \frac{\partial u}{\partial y} + \frac{\partial v}{\partial x}. \tag{2.24}$$

Hooke's law for an anisotropic material in the Voigt notation reads

$$\begin{bmatrix} \varepsilon_x \\ \varepsilon_y \\ \gamma_{xy} \end{bmatrix} = \begin{bmatrix} S'_{11} & S'_{12} & S'_{16} \\ S'_{12} & S'_{22} & S'_{26} \\ S'_{16} & S'_{26} & S'_{66} \end{bmatrix} \begin{bmatrix} \sigma_x \\ \sigma_y \\ \tau_{xy} \end{bmatrix}, \tag{2.25}$$

where

$$S'_{ij} = S_{ij} - \frac{S_{i3} S_{j3}}{S_{33}}. \tag{2.26}$$

In the case of an isotropic material, this relation becomes

$$\begin{bmatrix} \varepsilon_x \\ \varepsilon_y \\ \gamma_{xy} \end{bmatrix} = \begin{bmatrix} \frac{1-\nu^2}{E} & -\frac{\nu(1+\nu)}{E} & 0 \\ -\frac{\nu(1+\nu)}{E} & \frac{1-\nu^2}{E} & 0 \\ 0 & 0 & \frac{2(1+\nu)}{E} \end{bmatrix} \begin{bmatrix} \sigma_x \\ \sigma_y \\ \tau_{xy} \end{bmatrix}. \tag{2.27}$$

Note that by introducing the constants $E' = \frac{E}{1-\nu^2}$ and $\nu' = \frac{\nu}{1-\nu}$, the equations take exactly the same form as those for plane stress.

Airy stress function

In both (generalised) plane stress and plane strain configurations, the equations of equilibrium can be identically fulfilled by introducing the Airy stress function U through the relations

$$\sigma_x = \frac{\partial^2 U}{\partial y^2}, \quad \sigma_y = \frac{\partial^2 U}{\partial x^2}, \quad \tau_{xy} = -\frac{\partial^2 U}{\partial x \partial y}. \tag{2.28}$$

Substituting Hooke's law (2.18) into the compatibility condition (2.4) and using the definition of the Airy stress function (2.28) yields

$$S_{22} \frac{\partial^4 U}{\partial x^4} - 2S_{26} \frac{\partial^4 U}{\partial x^3 \partial y} + (2S_{12} + S_{66}) \frac{\partial^4 U}{\partial x^2 \partial y^2} - 2S_{16} \frac{\partial^4 U}{\partial x \partial y^3} + S_{11} \frac{\partial^4 U}{\partial y^4} = 0. \tag{2.29}$$

An equation for the Airy stress function with the same structure can be derived also for plane strain deformations by using the Hooke's law (2.25). In the case of plane stress in orthotropic materials, this equation becomes

$$\frac{1}{E_2} \frac{\partial^4 U}{\partial x^4} + \left(\frac{1}{G_{12}} - \frac{2\nu_{12}}{E_1} \right) \frac{\partial^4 U}{\partial x^2 \partial y^2} + \frac{1}{E_1} \frac{\partial^4 U}{\partial y^4} = 0 \tag{2.30}$$

and in the isotropic case

$$\Delta \Delta U = \frac{\partial^4 U}{\partial x^4} + 2 \frac{\partial^4 U}{\partial x^2 \partial y^2} + \frac{\partial^4 U}{\partial y^4} = 0. \tag{2.31}$$

This equation is called biharmonic equation. It arises also in other problems of structural mechanics such as bending of isotropic plates.

2.2 Complex potential method

Complex analysis provides an efficient approach to analytical solving two-dimensional problems of elasticity. This approach is based on the reduction of the original boundary value problem in the physical plane to a problem formulated in the complex domain. This is accomplished by replacing the real coordinates x and y by a complex variable $z = x + iy$. In this section, the complex potential method is presented for antiplane strain as well as plane stress and strain with both isotropic and anisotropic material behaviour. In each of the cases, the general solution of the underlying equations is presented and the solution for the half-plane and the infinite plane weakened by a single circular hole is given.

A classical monograph on the isotropic version of the complex potential method is Muskhelishvili [71], a standard monograph on the anisotropic version is Lekhnitskii [56]. Additional information can be found in Milne-Thomson [69] or Savin [83]. The presentation assumes basic background in complex analysis for which the reader is referred to classical textbooks such as Lang [54] or Henrici [30].

2.2.1 Antiplane strain

The general solution of the Laplace equation (2.16) in a two-dimensional setting is

$$w = \operatorname{Re} \varphi(z), \tag{2.32}$$

where $\varphi(z)$ is a holomorphic function of the complex variable $z = x + iy$. The normal derivative of the solution, denoted f in the following, can be expressed on the unit circle in terms of the complex potential as

$$f(z) = \operatorname{Re} z\varphi'(z) \tag{2.33}$$

and on the x-axis as

$$f(z) = -\operatorname{Im} \varphi'(z). \tag{2.34}$$

The complex potential corresponding to the homogeneous state of stress τ_{xz}, τ_{yz} is

$$\varphi(z) = \frac{\tau_{xz} - i\tau_{yz}}{G} z. \tag{2.35}$$

The solution of the first fundamental problem for a single circular unit hole in an infinite plane under zero stresses at infinity has the structure

$$\varphi(z) = A \ln z + \varphi^*(z), \tag{2.36}$$

where $\varphi^*(z)$ is a function holomorphic and single-valued on the exterior of the hole and the constant A is given as

$$A = \frac{1}{2\pi} \int_0^{2\pi} f(\theta) \, \mathrm{d}\theta. \tag{2.37}$$

The part of the boundary load corresponding to the single-valued term $\varphi^*(z)$ in (2.36) is denoted f^*, i.e.

$$f^*(z) = \frac{\partial}{\partial n} \operatorname{Re} \varphi^* = f(z) - A. \tag{2.38}$$

Then, the single-valued part of the solution is given by

$$(\varphi^*)'(z) = -\frac{1}{\pi i z}\int_\gamma \frac{f^*(\sigma)}{\sigma - z}\,\mathrm{d}\sigma, \tag{2.39}$$

where γ denotes the unit circle. The solution of the first fundamental problem for the lower half-plane is

$$\varphi'(z) = \frac{1}{\pi}\int_{-\infty}^{\infty} \frac{f(x)}{x - z}\,\mathrm{d}x. \tag{2.40}$$

2.2.2 Plane stress and strain in isotropic plates

The general solution to the biharmonic equation (2.31) in a two-dimensional setting is

$$U = \mathrm{Re}[\overline{z}\varphi(z) + \chi(z)], \tag{2.41}$$

where $\varphi(z)$ and $\chi(z)$ are two holomorphic functions of the complex variable $z = x + iy$. The in-plane stress and displacement components in a Cartesian coordinate system are related to the complex potentials by the Kolosov equations

$$\sigma_x + \sigma_y = 2\left(\varphi'(z) + \overline{\varphi'(z)}\right), \tag{2.42a}$$

$$\sigma_y - \sigma_x + 2i\tau_{xy} = 2\left(\overline{z}\varphi''(z) + \psi'(z)\right), \tag{2.42b}$$

$$2G(u_x + iu_y) = \kappa\varphi(z) - z\overline{\varphi'(z)} - \overline{\psi(z)}, \tag{2.42c}$$

where $\psi(z) = \chi'(z)$ and the constant κ is defined by Poisson's ratio ν as

$$\kappa = \begin{cases} \dfrac{3-\nu}{1+\nu} & \text{(plane stress)}, \\ 3 - 4\nu & \text{(plane strain)}. \end{cases} \tag{2.43}$$

In a polar coordinate system, the Kolosov equations read

$$\sigma_r + \sigma_\theta = 2\left[\varphi'(z) + \overline{\varphi'(z)}\right], \tag{2.44a}$$

$$\sigma_\theta - \sigma_r + 2i\tau_{r\theta} = 2\left[z\varphi''(z) + \frac{z}{\overline{z}}\psi'(z)\right], \tag{2.44b}$$

$$2G(u_r + iu_\vartheta) = \left[\kappa\varphi(z) - z\overline{\varphi'(z)} - \overline{\psi(z)}\right]\frac{\overline{z}}{|z|}. \tag{2.44c}$$

The resultant complex force acting on an arbitrary arc up to a constant is given by

$$f = i(f_x + if_y) = \varphi(z) + z\overline{\varphi'(z)} + \overline{\psi(z)}. \tag{2.45}$$

The boundary conditions of the first fundamental problem are given in terms of this function.

The complex potentials corresponding to the homogeneous state of stress σ_x, σ_y and τ_{xy} are

$$\varphi(z) = \frac{\sigma_x + \sigma_y}{4}z, \tag{2.46a}$$

$$\psi(z) = \frac{\sigma_y - \sigma_x + 2i\tau_{xy}}{2}z. \tag{2.46b}$$

The solution of the first fundamental problem for the infinite plane weakened by a unit circular hole has the structure

$$\varphi(z) = A \ln z + \varphi^*(z), \tag{2.47a}$$
$$\psi(z) = B \ln z + \psi^*(z), \tag{2.47b}$$

where $\varphi^*(z)$ and $\psi^*(z)$ are functions holomorphic and single-valued on the exterior of the hole and A and B are constants related to the total resultant acting on the hole

$$F = F_x + iF_y = -i[f(\theta)]_0^{2\pi} \tag{2.48}$$

by

$$A = \frac{-F}{2\pi(1+\kappa)}, \tag{2.49a}$$
$$B = \frac{\kappa\overline{F}}{2\pi(1+\kappa)}. \tag{2.49b}$$

The part of the load of the hole boundary corresponding to the single-valued terms $\varphi^*(z)$, $\psi^*(z)$ in (2.47) is denoted f^*, i.e.

$$f^*(z) = \varphi^*(z) + z\overline{\frac{\mathrm{d}\varphi^*}{\mathrm{d}z}(z)} + \overline{\psi^*(z)} = f(z) - \left(A \ln z + \overline{A}\frac{z}{\overline{z}} + \overline{B} \ln \overline{z}\right). \tag{2.50}$$

The single-valued part of the solution $\varphi^*(z)$ and $\psi^*(z)$ is given by

$$\varphi^*(z) = -\frac{1}{2\pi i}\int_\gamma \frac{f^*(\sigma)}{\sigma - z}\,\mathrm{d}\sigma, \tag{2.51a}$$
$$\psi^*(z) = -\frac{1}{2\pi i}\int_\gamma \frac{\overline{f}^*(\sigma)}{\sigma - z}\,\mathrm{d}\sigma - \frac{\varphi'(z)}{z}. \tag{2.51b}$$

If the load can be expressed in form of a complex Fourier series

$$f^*(\theta) = \sum_{k=-\infty}^{\infty} g_k e^{ik\theta}, \tag{2.52}$$

this solution becomes

$$\varphi^*(z) = \sum_{k=1}^{\infty} g_{-k} z^{-k}, \tag{2.53a}$$
$$\psi^*(z) = \sum_{k=1}^{\infty} \left(\overline{g}_k + \delta_{k>2}(k-2)g_{2-k}\right) z^{-k}. \tag{2.53b}$$

The solution of the first fundamental problem for the lower half-plane in the case of zero resultant force is

$$\varphi(z) = -\frac{1}{2\pi i}\int_{-\infty}^{\infty} \frac{f(x)}{x - z}\,\mathrm{d}x, \tag{2.54a}$$
$$\psi(z) = -\frac{1}{2\pi i}\int_{-\infty}^{\infty} \frac{\overline{f}(x)}{x - z}\,\mathrm{d}x - z\varphi'(z). \tag{2.54b}$$

Should the integrals in the above equations not exist, the following formulae can be used instead:

$$\varphi'(z) = -\frac{1}{2\pi i}\int_{-\infty}^{\infty}\frac{f'(x)}{x-z}\,\mathrm{d}x, \tag{2.55a}$$

$$\psi'(z) = -\frac{1}{2\pi i}\int_{-\infty}^{\infty}\frac{\overline{f'}(x)}{x-z}\,\mathrm{d}x - \varphi'(z) - z\varphi''(z). \tag{2.55b}$$

2.2.3 Plane stress and generalised plane stress in anisotropic plates

The structure of the solution of the fourth-order equation (2.29) is determined by the solutions of the corresponding characteristic equation

$$S_{11}\mu^4 - 2S_{16}\mu^3 + (2S_{12} + S_{66})\mu^2 - 2S_{26}\mu + S_{22} = 0. \tag{2.56}$$

It can be shown that for finite and nonzero elastic moduli, this equation has nonreal roots. Since the coefficients of the equation are real, the roots must be pairwise complex conjugate. Therefore, only the following two cases are possible:

1. The roots of the characteristic equation are all different and can be denoted μ_1, μ_2, $\overline{\mu}_1$, $\overline{\mu}_2$.
2. The roots of the characteristic equation are pairwise equal and can be denoted $\mu_1 = \mu_2$, $\overline{\mu}_1 = \overline{\mu}_2$.

The roots μ_1 and μ_2 are called the complex parameters.

For isotropic materials, $\mu_1 = \mu_2 = i$ holds. Otherwise, the second case occurs rarely and can be converted by a linear transformation of variables to the isotropic formulation. Therefore, without loss of generality, attention can be restricted to unequal complex parameters. In this case, the general solution of the equation (2.29) reads

$$U = \mathrm{Re}\sum_{j=1}^{2}\chi_j(z_j), \tag{2.57}$$

where $\chi_j(z_j)$, $j = 1, 2$, are two holomorphic functions of the complex variables z_j which are defined by the affine transformation of the z-plane

$$z_j = x + \mu_j y. \tag{2.58}$$

With $\varphi_j(z) = \chi_j'(z_j)$, the in-plane stress components in a Cartesian coordinate system are related to the complex potentials by the equations

$$\sigma_x = 2\,\mathrm{Re}\sum_{j=1}^{2}\mu_j^2\varphi_j'(z_j), \tag{2.59a}$$

$$\sigma_y = 2\,\mathrm{Re}\sum_{j=1}^{2}\varphi_j'(z_j), \tag{2.59b}$$

$$\tau_{xy} = -2\,\mathrm{Re}\sum_{j=1}^{2}\mu_j\varphi_j'(z_j), \tag{2.59c}$$

and the in-plane displacements up to a rigid-body motion by

$$u = 2\,\mathrm{Re}\sum_{j=1}^{2} p_j \varphi_j(z_j), \tag{2.60a}$$

$$v = 2\,\mathrm{Re}\sum_{j=1}^{2} q_j \varphi_j(z_j), \tag{2.60b}$$

where the constants p_j and q_j, $j = 1, 2$, are given as

$$p_j = S_{11}\mu_j^2 + S_{12} - S_{16}\mu_j, \tag{2.61a}$$

$$q_j = S_{12}\mu_j + \frac{S_{22}}{\mu_j} - S_{26}. \tag{2.61b}$$

In polar coordinates, these equations become

$$\sigma_r = 2\,\mathrm{Re}\sum_{j=1}^{2} (\sin\theta - \mu_j \cos\theta)^2 \varphi_j'(z_j), \tag{2.62a}$$

$$\sigma_\theta = 2\,\mathrm{Re}\sum_{j=1}^{2} (\cos\theta + \mu_j \sin\theta)^2 \varphi_j'(z_j), \tag{2.62b}$$

$$\tau_{r\theta} = 2\,\mathrm{Re}\sum_{j=1}^{2} (\sin\theta - \mu_j \cos\theta)(\cos\theta + \mu_j \sin\theta)\varphi_j'(z_j) \tag{2.62c}$$

and

$$u_r = 2\,\mathrm{Re}\sum_{j=1}^{2} (p_j \cos\theta + q_j \sin\theta)\varphi_j(z_j), \tag{2.63a}$$

$$u_\theta = 2\,\mathrm{Re}\sum_{j=1}^{2} (q_j \cos\theta - p_j \sin\theta)\varphi_j(z_j). \tag{2.63b}$$

The total force acting on an arbitrary boundary arc up to a constant is given by

$$f_x = \pm 2\,\mathrm{Re}\sum_{j=1}^{2} \mu_j \varphi_j(z_j), \tag{2.64a}$$

$$f_y = \mp 2\,\mathrm{Re}\sum_{j=1}^{2} \varphi_j(z_j), \tag{2.64b}$$

where the upper sign holds for an outer boundary contour whereas the lower sign for an inner one. These functions are used for the formulation of the boundary conditions in the first boundary value problem. Note that the notation of the forces in the anisotropic case follows that of Lekhnitskii [56] and therefore differs slightly from the notation of the forces in the isotropic case which follows that of Muskhelishvili [71].

The complex potentials corresponding to the homogeneous state of stress σ_x, σ_y, τ_{xy} are

$$\varphi_j(z_j) = C_j z_j, \tag{2.65}$$

where the contants $C_j \in \mathbb{C}$, $j = 1, 2$, are determined as the solution of the system of linear equations

$$2\,\mathrm{Re}\sum_{j=1}^{2}\mu_j^2 C_j = \sigma_x, \tag{2.66a}$$

$$2\,\mathrm{Re}\sum_{j=1}^{2} C_j = \sigma_y, \tag{2.66b}$$

$$-2\,\mathrm{Re}\sum_{j=1}^{2}\mu_j C_j = \tau_{xy}, \tag{2.66c}$$

$$C_1 = \overline{C}_1. \tag{2.66d}$$

The solution of the first fundamental problem for the infinite plane weakened by an ellipse with major semi-axis 1 and minor semi-axis m has the structure

$$\varphi_j(z_j) = A_j \ln(z_j) + \hat{\varphi}_j^*(z_j), \tag{2.67}$$

where $\hat{\varphi}_j^*(z_j)$ is a function holomorphic and single-valued on the exterior of the hole and the constants A_j are related to the resultant

$$F = F_x + iF_y = [f_x(\theta) + if_y(\theta)]_0^{2\pi} \tag{2.68}$$

by the system of linear equations

$$\sum_{j=1}^{2}\left(A_j - \overline{A}_j\right) = \frac{F_y}{2\pi i}, \tag{2.69a}$$

$$\sum_{j=1}^{2}\left(\mu_j A_j - \overline{\mu}_j \overline{A}_j\right) = -\frac{F_x}{2\pi i}, \tag{2.69b}$$

$$\sum_{j=1}^{2}\left(\mu_j^2 A_j - \overline{\mu}_j^2 \overline{A}_j\right) = -\frac{S_{16}}{S_{11}}\frac{F_x}{2\pi i} - \frac{S_{12}}{S_{11}}\frac{F_y}{2\pi i}, \tag{2.69c}$$

$$\sum_{j=1}^{2}\left(\frac{A_j}{\mu_j} - \frac{\overline{A}_j}{\overline{\mu}_j}\right) = \frac{S_{12}}{S_{22}}\frac{F_x}{2\pi i} + \frac{S_{26}}{S_{22}}\frac{F_y}{2\pi i}. \tag{2.69d}$$

The part of the traction on the boundary of the hole corresponding to the single-valued terms $\varphi_j^*(z_j)$ in (2.67) is denoted as f_x^*, f_y^*:

$$f_x^* = \pm 2\,\mathrm{Re}\sum_{j=1}^{2}\mu_j \varphi_j^*(z_j) = f_x \mp 2\,\mathrm{Re}\sum_{j=1}^{2}\mu_j A_j \ln z_j, \tag{2.70a}$$

$$f_y^* = \mp 2\,\mathrm{Re}\sum_{j=1}^{2}\varphi_j^*(z_j) = f_y \pm 2\,\mathrm{Re}\sum_{j=1}^{2} A_j \ln z_j. \tag{2.70b}$$

The single-valued part of the solution $\varphi_j^*(z_j)$ is given by

$$\varphi_1^*(z_1) = \frac{1}{\mu_1 - \mu_2} \frac{1}{2\pi i} \int_\gamma \frac{f_x(\sigma) + \mu_2 f_y(\sigma)}{\sigma - w(z_1)} \, \mathrm{d}\sigma, \tag{2.71a}$$

$$\varphi_2^*(z_2) = -\frac{1}{\mu_1 - \mu_2} \frac{1}{2\pi i} \int_\gamma \frac{f_x(\sigma) + \mu_1 f_y(\sigma)}{\sigma - w(z_2)} \, \mathrm{d}\sigma. \tag{2.71b}$$

In these equations, w denotes the conformal mapping of the exterior of the ellipse in the z_j-plane onto the exterior of the unit circle and is given by the relation

$$w = \frac{z_j \pm \sqrt{z_j^2 - 1 - m^2 \mu_j^2}}{1 - mi\mu_j}, \tag{2.72}$$

where the sign of the square root has to be chosen according to the condition $|w| \geq 1$. If the load can be expressed in form of the Fourier series

$$f_x^* = \sum_{k=-\infty}^{\infty} g_{xk} e^{ik\theta}, \quad f_y^* = \sum_{k=-\infty}^{\infty} g_{yk} e^{ik\theta}, \tag{2.73}$$

the solution (2.71) becomes

$$\varphi_1^*(z_1) = -\frac{1}{\mu_1 - \mu_2} \sum_{k=1}^{\infty} \left(g_{x,-k} + \mu_2 g_{y,-k} \right) w(z_1)^{-k}, \tag{2.74a}$$

$$\varphi_2^*(z_2) = \frac{1}{\mu_1 - \mu_2} \sum_{k=1}^{\infty} \left(g_{x,-k} + \mu_1 g_{y,-k} \right) w(z_2)^{-k}. \tag{2.74b}$$

The solution of the first fundamental problem for the lower half-plane in the case of zero resultant force is

$$\varphi_1(z_1) = -\frac{1}{\mu_1 - \mu_2} \frac{1}{2\pi i} \int_{-\infty}^{\infty} \frac{f_x(x) + \mu_2 f_y(x)}{x - z_1} \, \mathrm{d}x, \tag{2.75a}$$

$$\varphi_2(z_2) = \frac{1}{\mu_1 - \mu_2} \frac{1}{2\pi i} \int_{-\infty}^{\infty} \frac{f_x(x) + \mu_1 f_y(x)}{x - z_2} \, \mathrm{d}x. \tag{2.75b}$$

Should the integrals in the above equations not exist, the following formulae can be used instead:

$$\varphi_1'(z_1) = -\frac{1}{\mu_1 - \mu_2} \frac{1}{2\pi i} \int_{-\infty}^{\infty} \frac{f_x'(x) + \mu_2 f_y'(x)}{x - z_1} \, \mathrm{d}x, \tag{2.76a}$$

$$\varphi_2'(z_2) = \frac{1}{\mu_1 - \mu_2} \frac{1}{2\pi i} \int_{-\infty}^{\infty} \frac{f_x'(x) + \mu_1 f_y'(x)}{x - z_2} \, \mathrm{d}x. \tag{2.76b}$$

2.3 Asymptotic analysis

The investigated boundary value problem often involves some parameter, say ϵ, whose influence on the solution has to be studied. This parameter might be involved in the partial

differential equation itself (e.g. a material parameter), in the domain (some geometric quantity) or in the boundary conditions. In such a situation, the solution of the boundary value problem can be thought of as a function of two variables: the spatial coordinates $\vec{r}$ and the parameter ϵ. The dependence of the solution on the parameter ϵ can be emphasised by adding it to the list of arguments of the solution: $\boldsymbol{\sigma} = \boldsymbol{\sigma}(\vec{r}; \epsilon)$.

The involved parameter is often very small in magnitude. In such cases, sufficient information about the influence of the parameter on the solution is contained in the behaviour of the function $\boldsymbol{\sigma}(\vec{r}; \epsilon)$ in the vicinity of $\epsilon = 0$. The description of the asymptotic behaviour of a function in the neighbourhood of a point is explained in Section 2.3.1. If a closed-form solution of the underlying boundary value problem is available, such an asymptotics can be constructed directly, for example by performing a Taylor series expansion. However, in many situations, the closed-form solution is unknown. The asymptotic expansion must then be constructed by appropriate techniques directly from the underlying boundary value problem.

A technique for the construction of an asymptotic expansion of a solution to a linear-elastic boundary value problem perturbed by a small hole is introduced in Section 2.3.2. The small parameter in this case is the relative radius of the hole. The technique relies on the method of compound asymptotic expansions. Several methods for improvement of the convergence of the asymptotic series are summarised in Section 2.3.4.

For a general introduction to asymptotic analysis, the reader is referred to the classical textbooks of Hinch [31], Johnson [41], Kevorkian and Cole [43] or Dyke [16]. The main reference for the method of compound asymptotic expansions is the monograph Maz'ya et al. [64], additional information can also be found in the monograph Kozlov et al. [44]. An introduction to the asymptotic analysis of strongly anisotropic plates is given in Christensen [12]. An informal, popular-scientific introduction to asymptotic methods can be found in Andrianov and Manevitch [4].

2.3.1 Basic concepts

The behaviour of a function $f(\epsilon)$ in the limit $\epsilon \to \epsilon_0$ can be characterised by comparing it to some (typically simpler) gauge function $g(\epsilon)$. For this purpose, the following Landau symbols are commonly used. It is said that

- $f(\epsilon) = o[g(\epsilon)]$ as $\epsilon \to \epsilon_0$ if $\lim\limits_{\epsilon \to \epsilon_0} \frac{f(\epsilon)}{g(\epsilon)} = 0$,
- $f(\epsilon) = O[g(\epsilon)]$ as $\epsilon \to \epsilon_0$ if $\lim\limits_{\epsilon \to \epsilon_0} \frac{f(\epsilon)}{g(\epsilon)}$ is finite and nonzero and
- $f(\epsilon) \sim g(\epsilon)$ as $\epsilon \to \epsilon_0$ if $\lim\limits_{\epsilon \to \epsilon_0} \frac{f(\epsilon)}{g(\epsilon)} = 1$.

To achieve a progressively better characterisation, the function $f(\epsilon)$ can be compared to a set of gauge functions. Such a set $\{g_n(\epsilon)\}_{n=0}^{\infty}$ is called an asymptotic sequence as $\epsilon \to \epsilon_0$ if

$$g_{n+1}(\epsilon) = o[g_n(\epsilon)] \quad \text{as } \epsilon \to \epsilon_0 \text{ for every } n. \tag{2.77}$$

In this text, the asymptotic sequence $\{\epsilon^n\}_{n=0}^{\infty}$ plays the central role. An approximation of the form

$$f(\epsilon) = \sum_{n=0}^{N} a_n g_n(\epsilon) + O[g_{N+1}(\epsilon)] \text{ as } \epsilon \to \epsilon_0 \tag{2.78}$$

is called an asymptotic expansion of the function $f(\epsilon)$ with respect to the asymptotic sequence $\{g_n(\epsilon)\}$ if

$$f(\epsilon) - \sum_{n=0}^{N} a_n g_n(\epsilon) = o[g_N(\epsilon)] \text{ as } \epsilon \to \epsilon_0. \tag{2.79}$$

Besides the parameter ϵ, the considered function often depends on another variable x, which can be a scalar, a vector or a complex number. Then the asymptotic expansion of such a function $f(x;\epsilon)$ is called separable if it has the form

$$f(x;\epsilon) = \sum_{n=0}^{N} a_n(x) g_n(\epsilon) + O[g_{N+1}(\epsilon)] \text{ as } \epsilon \to \epsilon_0. \tag{2.80}$$

If this expansion holds for all x in some domain of interest, then the expansion is said to be uniformly valid, otherwise it is not uniformly valid.

2.3.2 Method of compound asymptotic expansions

Although the method of compound asymptotic expansions can be applied to arbitrary elliptic equations and various types of singular perturbations of the domain, this section is limited to the explanation of the basic principle on the example of a linear-elastic boundary value problem perturbed by a single small hole.

Consider a two- or three-dimensional elastic body occupying a simply connected domain $\Omega \subset \mathbb{R}^n, n = 2$ or 3, which contains the origin 0. The domain is perturbed by a small hole of arbitrary shape also containing the origin. The hole's diameter is denoted ϵ. The perturbed domain is denoted Ω_ϵ, its outer boundary Γ_0 and the boundary of the hole Γ_1 (cf. Figure 2.1). The first boundary value problem is considered, the stress vectors prescribed on Γ_0 and Γ_1 are denoted $\vec{t}_0$ and $\vec{t}_1$, respectively. First, it is assumed that the total resultant force on each part of the boundary is zero.

It is intuitively clear that at a sufficient distance of the hole, its presence can be neglected and the solution of the perturbed problem is approximately equal to the solution of the unperturbed one. On the other hand, when the neighbourhood of the hole is appropriately scaled, the outer boundary tends to infinity, its presence can be neglected and the hole can thus be considered as a single hole in an infinite plane under the state of stress at infinity equal to the state of stress in the unperturbed domain at the point where the hole lies. The scaling is achieved by introducing a scaled position vector

$$\vec{\rho} = \frac{\vec{r}}{\epsilon}, \tag{2.81}$$

its norm being $\rho = \frac{r}{\epsilon}$ and its direction being $\vec{e} = \frac{\vec{\rho}}{\rho} = \frac{\vec{r}}{r}$. This intuitive observation gives an insight how the leading term of the asymptotic in the far- and the near-field

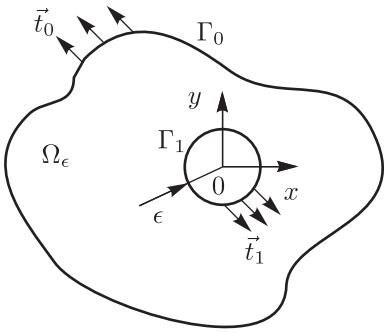

Figure 2.1: Explanation of the method of compound asymptotic expansions.

should look like. In the following, a composite asymptotic expansion is constructed, which approximates the solution in the far- and near-field at the same time.

The function $\boldsymbol{\sigma}_0^0(\vec{r})$, satisfying the field equations and the boundary condition on the outer boundary Γ_0, is taken as the principal term of the asymptotics of the solution of the perturbed boundary value problem as $\epsilon \to 0$. This function obviously violates the boundary condition on the hole boundary Γ_1. It is assumed that the principal term allows the expansion

$$\boldsymbol{\sigma}_0^0(\vec{r}) = \sum_{k=0}^{\infty} \mathbf{S}_{0k}^0(\vec{e}) r^k \tag{2.82}$$

at the origin, where $\mathbf{S}_{0k}^0(\vec{e})$ are functions not depending on the distance r. Since $r = O(\epsilon)$ on the hole boundary, it holds there

$$\boldsymbol{\sigma}_0^0(\vec{r}) \cdot \vec{n} = \mathbf{S}_{00}^0(\vec{e}) \cdot \vec{n} + O(\epsilon) \tag{2.83}$$

and thus the leading term of the discrepancy in the boundary condition on the hole is $\vec{t}_1 - \boldsymbol{S}_{00}^0(\vec{e}) \cdot \vec{n}$. It can be corrected by adding the function $\boldsymbol{\sigma}_1^0(\vec{\rho})$, satisfying the field equations and the boundary condition $\boldsymbol{\sigma}_1^0(\vec{\rho}) \cdot \vec{n} = \vec{t}_1(\vec{e}) - \mathbf{S}_{00}^0(\vec{e}) \cdot \vec{n}$ on Γ_1, to the principal term. Doing so and assuming that the correction allows the expansion

$$\boldsymbol{\sigma}_1^0(\vec{\rho}) = \sum_{k=1}^{\infty} \mathbf{S}_{1k}^0(\vec{e}) \rho^{-k} \tag{2.84}$$

at infinity, the stress vector on the outer boundary Γ_0 then becomes

$$\left[\boldsymbol{\sigma}_0^0(\vec{r}) + \boldsymbol{\sigma}_1^0\left(\frac{\vec{r}}{\epsilon}\right)\right] \cdot \vec{n} = \vec{t}_0(\vec{e}) + \underbrace{\epsilon r^{-1} \boldsymbol{S}_{11}^0(\vec{e}) \cdot \vec{n} + O(\epsilon^2)}_{\text{discrepancy}}. \tag{2.85}$$

Hence, both boundary conditions are satisfied up to the order $O(\epsilon)$.

In order to obtain the second-order approximation of the solution, the term $O(\epsilon)$ in the discrepancy (2.85) is corrected by adding $\epsilon \boldsymbol{\sigma}_0^1(\vec{r})$, where $\boldsymbol{\sigma}_0^1(\vec{r})$ satisfies the field equations and the boundary condition $\boldsymbol{\sigma}_0^1(\vec{r}) \cdot \vec{n} = -r^{-1} \boldsymbol{S}_{11}^0(\vec{e}) \cdot \vec{n}$ on Γ_0. Assuming again that this function can be expressed as

$$\boldsymbol{\sigma}_0^1(\vec{r}) = \sum_{k=0}^{\infty} \boldsymbol{S}_{0k}^1(\vec{e}) r^k, \tag{2.86}$$

the stress vector on Γ_1, expressed in terms of the scaled vector $\vec{\rho}$, becomes

$$\left[\boldsymbol{\sigma}_0^0(\epsilon\vec{\rho}) + \boldsymbol{\sigma}_1^0(\vec{\rho}) + \epsilon\boldsymbol{\sigma}_0^1(\vec{\rho})\right] \cdot \vec{n} = \vec{t}_1(\vec{e}) + \underbrace{\epsilon\left[\rho\boldsymbol{S}_{01}^0(\vec{e}) + \boldsymbol{S}_{00}^1(\vec{e})\right] \cdot \vec{n} + O(\epsilon^2)}_{\text{discrepancy}}. \tag{2.87}$$

Correcting the discrepancy by adding a function $\epsilon\boldsymbol{\sigma}_1^1(\vec{\rho})$, where $\boldsymbol{\sigma}_1^1(\vec{\rho})$ fulfils the field equations as well as the boundary condition $\boldsymbol{\sigma}_1^1(\vec{\rho}) \cdot \vec{n} = -\left[\rho\boldsymbol{S}_{01}^0(\vec{e}) + \boldsymbol{S}_{00}^1(\vec{e})\right] \cdot \vec{n}$ on Γ_1 leads to an expression which satisfies both boundary conditions up to the order $O(\epsilon^2)$.

A further iterative application of these steps leads to the result that the stress tensor can be expressed in the form

$$\boldsymbol{\sigma}(\vec{r}) = \sum_{n=0}^{N} \epsilon^n \left[\boldsymbol{\sigma}_0^n(\vec{r}) + \boldsymbol{\sigma}_1^n\left(\frac{\vec{r}}{\epsilon}\right)\right] \tag{2.88}$$

which satisfies both boundary conditions up to $O(\epsilon^{N+1})$. Here, $\boldsymbol{\sigma}_0^n(\vec{r})$, $n \in \mathbb{N}_0$ are called outer auxiliary functions. They depend on the unscaled variable r and are determined as solutions to certain boundary value problems on the unperturbed domain. On the other hand, $\boldsymbol{\sigma}_1^n(\vec{\rho})$, $n \in \mathbb{N}_0$ are inner auxiliary functions which depend on the scaled variable $\vec{\rho} = \vec{r}/\epsilon$ and are determined as solutions to boundary value problems on the infinite plane or space weakened by the hole.

The described procedure works only if the problems for the auxiliary functions $\boldsymbol{\sigma}_k^n$ arising during the iteration possess a unique solution that allows an asymptotic expansion of the form (2.82) or (2.84). Especially important is the question whether the solution of the inner auxiliary problem vanishes at infinity, as assumed in (2.84). In two-dimensional problems, it follows from the complex potential theory that this is the case if the total resultant of forces acting on the hole is zero. A problem with a nonzero total resultant can be converted to one with zero resultant by subtracting the trace of the logarithmic terms from the boundary conditions. This is always possible since the logarithmic terms are a priori given by the resultant force.

The constructed solution is uniformly valid in the whole domain and satisfies all boundary conditions up to the order $O(\epsilon^{N+1})$. It can be further simplified by specialisation either for the far-field where $r = O(\epsilon^0)$ or for the near-field of the hole where $\rho = O(\epsilon^0)$. For this purpose, two kinds of operators are introduced. The first of them, denoted as P^n, generates the first n terms of the asymptotic expansion of a field quantity as $\epsilon \to 0$ for $r = O(\epsilon^0)$. The second operator, denoted as Q^n, generates the first n terms of the asymptotic expansion of the field quantity as $\epsilon \to 0$ for $\rho = O(\epsilon^0)$. Thus, if the solution $\boldsymbol{\sigma}$ is valid in the whole domain, then $P^n\boldsymbol{\sigma}$ is valid only in the far-field and has a singularity at the origin whereas $Q^n\boldsymbol{\sigma}$ is valid only in the near-field and has a singularity at infinity. The function $P^n\boldsymbol{\sigma}$ then only satisfies the boundary condition in the far-field whereas the function $Q^n\boldsymbol{\sigma}$ only satisfies the boundary condition on the boundary of the hole.

Note that these operators also represent the relation of the method of compound asymptotic expansions to the possibly more common method of matched asymptotic expansions. In the method of matched asymptotic expansions, a separate ansatz is made for each of the functions $P^n\boldsymbol{\sigma}$ and $Q^n\boldsymbol{\sigma}$. The unknown coefficients or functions in the ansatz are then determined from the following conditions:

1. $P^n\boldsymbol{\sigma}$ must fulfil the boundary condition on the outer boundary Γ_0,

2. $Q^n\boldsymbol{\sigma}$ must fulfil the boundary condition on the inner boundary Γ_1,

3. $P^n\boldsymbol{\sigma}$ and $Q^n\boldsymbol{\sigma}$ must be asymptotic expansions of the same function $\boldsymbol{\sigma}$ in the far- and near-field, respectively.

Condition 3 is expressed by the so called matching principle (see Dyke [16]). With the expansions $P^n\boldsymbol{\sigma}$ and $Q^n\boldsymbol{\sigma}$ valid only in the far- or near-field, the solution valid uniformly in the whole domain can be constructed by the method of composite additive expansion.

Since the method of compound asymptotic expansions generally leads to a simpler algorithm than the method of matched asymptotics, it has been chosen as the main tool within this thesis.

2.3.3 Strong orthotropy

Many materials exhibit highly anisotropic elastic behaviour in the sense that one of the elastic moduli is significantly higher than the others. This property can be utilised to simplify the analysis of the anisotropic body. Three common combinations of elastic moduli of an orthotropic material are listed below. For each of the combinations, the order of magnitude of the complex parameters is given. In the listing, η always denotes a small parameter accounting to the strength of orthotropy of the considered material.

1. $E_1 \gg E_2, G_{12}$; $\eta = \frac{E_2}{E_1}$

$$\mu_1 = i\sqrt{\frac{G_{12}}{E_2}} + O(\eta), \quad \mu_2 = i\sqrt{\frac{E_2}{\eta G_{12}}} + O(\sqrt{\eta}) \tag{2.89}$$

2. $E_2 \gg E_1, G_{12}$; $\eta = \frac{E_1}{E_2}$

$$\mu_1 = i\sqrt{\eta\frac{G_{12}}{E_1}} + O(\eta\sqrt{\eta}), \quad \mu_2 = i\sqrt{\frac{E_1}{G_{12}}} + O(\eta) \tag{2.90}$$

3. $E_1, E_2 \gg G_{12}$; $\eta = \frac{G_{12}}{E_1}$

$$\mu_1 = i\sqrt{\eta\frac{E_1}{E_2}} + O(\eta\sqrt{\eta}), \quad \mu_2 = i\frac{1}{\sqrt{\eta}} + O(\sqrt{\eta}) \tag{2.91}$$

Thus, for a strongly orthotropic material, at least one of the complex parameters is either large or small. The solution can be represented as an asymptotic series in terms of this parameter or directly in terms of η. It has been shown (see Manevitch and Pavlenko [59]) that such series exhibit fast convergence even for moderately anisotropic materials.

2.3.4 Convergence of asymptotic series

The series obtained by perturbation methods sometimes exhibit slow convergence. There exist several techniques to improve the convergence of the asymptotic series. Two of them used in this thesis are sketched below. For more details, the reader is referred to e.g. Dyke [16].

The Euler transformation

The Euler transformation of the small parameter ϵ has the form

$$\bar{\epsilon} = \frac{\epsilon}{1+\epsilon}. \tag{2.92}$$

Recasting the original series $S(\epsilon)$ in powers of the new parameter $\bar{\epsilon}$ according to

$$S_{\text{Euler}}(\bar{\epsilon}) = S\big(\epsilon(\bar{\epsilon})\big) \tag{2.93}$$

improves the convergence of the series especially if the original series had a singularity close to zero.

Padé approximants

The Padé approximant of the function $S(\epsilon)$ of the order $[m/n]$, $m, n \in \mathbb{N}$, is the rational function

$$S_{\text{Pade}}(\epsilon) = \frac{\sum_{k=0}^{m} a_k \epsilon^k}{1 + \sum_{k=1}^{n} b_k \epsilon^k} \tag{2.94}$$

whose derivatives at $\epsilon = 0$ agree with $S(\epsilon)$ to the highest possible order, which amounts to

$$\frac{\mathrm{d}^k S}{\mathrm{d}\epsilon^k}(0) = \frac{\mathrm{d}^k S_{\text{Pade}}}{\mathrm{d}\epsilon^k}(0) \quad \text{for } k = 0, \ldots, m+n. \tag{2.95}$$

The disadvantage of the Padé approximants is that they may lead to spurious singularities that are not present in the original function. More details can be found in Baker and Graves-Morris [6].

Chapter 3

Modelling of bolted joints

In this chapter, the present approach to the mathematical modelling of bolted joints is described. First, the reduction of the original problem from a three-dimensional setting to a two-dimensional problem is explained. Then, the modelling of the contact between the bolt and the plate is discussed. In Section 3.3, a precise definition of the joint compliance is given and finally, in Section 3.4, the compatibility conditions for the determination of the load distribution on the bolts are presented.

3.1 Reduction to a two-dimensional problem

The geometry of a single- and double-lap bolted joint is schematically shown in the upper part of Figure 3.1. The free-body diagram of the bolted joint is shown in the lower part of this figure. The joint consists of two or three plates connected by either a finite number or an infinite array of bolts.

The bolts can be modelled as Euler-Bernoulli beams loaded by concentrated or piece-wise constant distributed forces. Since the modelling of the bolt deformations has already been discussed sufficiently in the literature, it is not be treated here. Instead, the reader is referred to e.g. Kradinov et al. [47].

Since the main topic of this thesis is the investigation of in-plane deformations in the connected plates, only symmetric double-lap configurations are considered where the tilting of the bolt can be neglected and the state of stress in each of the plates is essentially two-dimensional. Therefore, the plates are modelled as being in the state of plane stress or generalised plane stress. The outer plates denoted by indices 1 and 3 are assumed to be identical, the middle plate is denoted by index 2. The thicknesses of the plates are denoted $t^{(1)}$ and $t^{(2)}$. The number of the holes in each plate (equal to the number of the bolts) is denoted N_H. In the case of infinite arrays of holes the number of holes in one periodic cell is denoted N_C.

The plates are loaded by bearing stresses and possibly by a by-pass load. In the case of a finite number of bolts, the overall force transmitted over the joint is denoted $F^{(\mathrm{J})}$. In the case of infinite rows of bolts, $F^{(\mathrm{J})}$ denotes the force transmitted over one periodic cell.

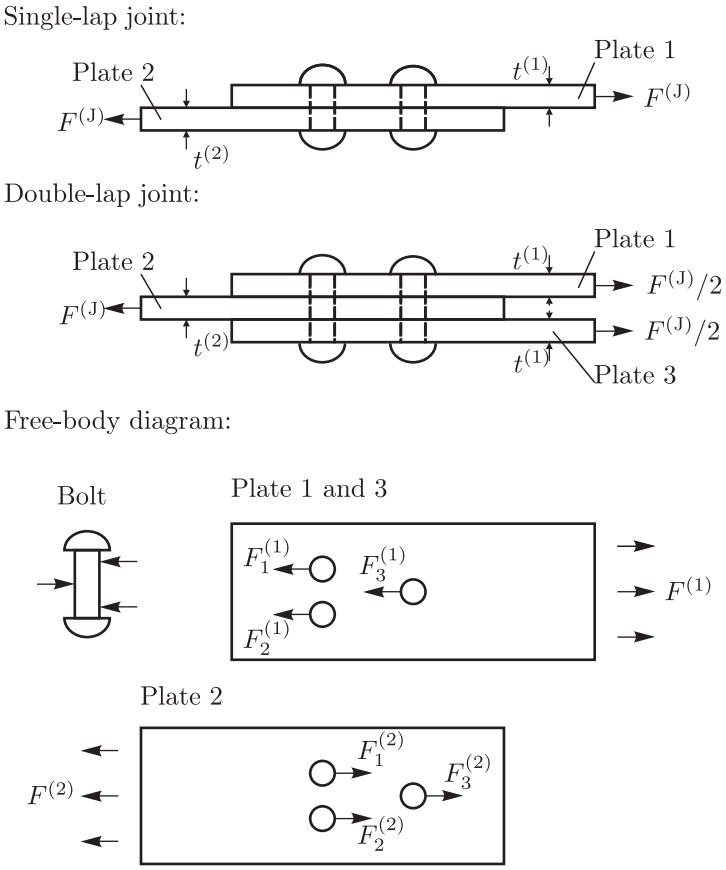

Figure 3.1: Bolted single- and double-lap joints and the corresponding free body diagram.

Within the framework of the plane stress theory, the forces are always normalised by the plate thickness. They are denoted

$$F^{(1)} = \frac{F^{(J)}/2}{t^{(1)}}, \quad F^{(2)} = \frac{F^{(J)}}{t^{(2)}}. \tag{3.1}$$

Each bolt transmits an a priori unknown part of this load. The force transmitted over the pth hole in the kth plate is denoted $F_k^{(p)}$. Assuming that all bolts are loaded in the same direction, the partition of the force satisfies

$$\sum_p F_p^{(k)} = F^{(k)}, \tag{3.2}$$

where in the case of a finite number of bolts, the index p runs from one to the number of holes whereas in the case of an infinite array, it runs from one to the number of categories of holes.

In this section, the upper index (k) denotes quantities related to the kth plate whereas the superscript (J) denotes quantities related to the whole joint. Later, when only a single plate is considered at a time, this designation is dropped.

3.2 Stress distribution in a pin-to-hole contact

The distribution of the radial and shear stresses in a pin-to-hole contact is a priori unknown. It depends on many factors, the most important of them are

1. elastic properties of the plate and of the bolt,
2. the geometry of the joint,
3. the clearance (difference between hole and bolt radius),
4. the magnitude of the transmitted force,
5. the friction between the plate and the bolt,
6. the degradation or plastification of the plate and the bolt.

A contact condition for a conforming contact of two elastic cylinders which captures the influence of factors 1–4 has been derived by Persson [74] (see also Johnson and Johnson [40]). It follows from the sketch in the left part of Figure 3.2 and in the present notation, it reads

$$\begin{cases} u_r - u_r^{(\mathrm{P})} = V\sin\theta - \Delta r(1-\sin\theta) & \text{inside the contact area,} \\ t_r = t_\theta = 0 & \text{outside the contact area,} \end{cases} \tag{3.3}$$

where u_r and $u_r^{(\mathrm{P})}$ are radial displacements on the boundary of the hole and the pin, respectively, $\Delta r = r - r^{(\mathrm{P})}$ is the clearance, V the displacement of the centre of the pin in the direction of the applied force and the angle θ is defined as in Figure 3.2. Note that since the radii of the hole and the bolt are typically similar in magnitude, the size of the contact area is comparable to the hole dimensions and therefore, the contact cannot be treated by the classical Hertz theory.

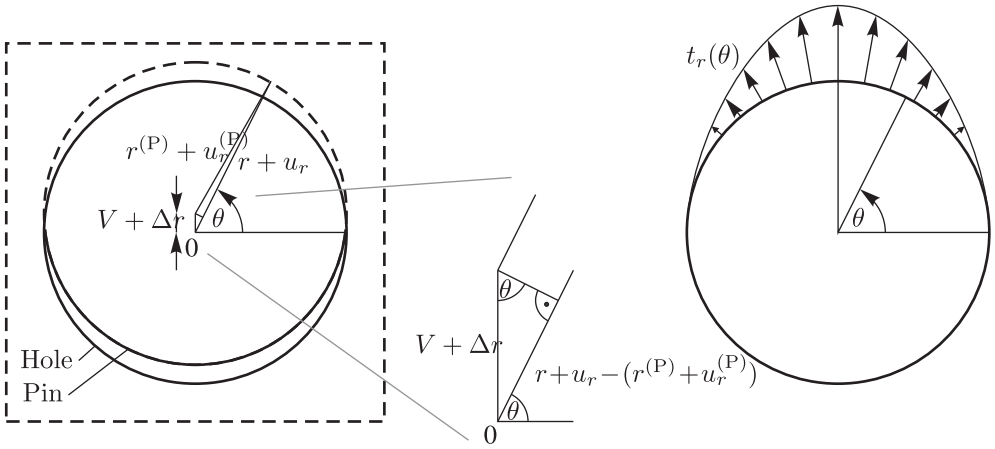

Figure 3.2: Left: Derivation of the contact condition (3.3). Right: Approximation of the contact pressure in a pin-to-hole contact.

Unfortunately, a closed-form solution of a pin-to-hole contact problem with the contact condition (3.3) is not possible even in the simplest case of a single hole in an infinite plate.

Several formulae for the contact stress distributions have therefore been proposed in the literature that lead at least to an approximate satisfaction of the contact condition. The simplest of them is a sinusoidal distribution of the normal stress over the upper part of the hole

$$t_r = \begin{cases} \dfrac{2F}{\pi r}\sin(\theta), & 0 \le \theta \le \pi, \\ 0, & \text{otherwise}, \end{cases} \qquad t_\theta = 0. \tag{3.4}$$

A more general approximation of the contact pressure with the contact angle 180° which comprises one free parameter m is

$$t_r = \begin{cases} \dfrac{2F}{\pi r}\big(\sin(\theta) + m\sin(3\theta)\big), & 0 \le \theta \le \pi, \\ 0, & \text{otherwise}, \end{cases} \qquad t_\theta = 0. \tag{3.5}$$

These formulae describe approximately the stress distribution in the case of zero clearance, a rigid bolt and vanishing friction.

In the isotropic case, the function $f^*(\theta)$ defined in (2.50) is periodic and can be expressed as a Fourier series

$$f^*(\theta) = \sum_{k=-\infty}^{\infty} g_k e^{ik\theta}. \tag{3.6}$$

The Fourier coefficients g_k corresponding to the load distribution (3.4) are given as

$$g_k = \frac{1-(-1)^k}{\pi^2 k^2(k-2)}F - \tilde{g}_k, \tag{3.7}$$

where $\tilde{g}_k$ are Fourier coefficients corresponding to the logarithmic terms defined by

$$\tilde{g}_k = \begin{cases} \dfrac{iF}{2\pi(1+\kappa)}, & k = 2, \\ 0, & k \ne 2, \end{cases} \tag{3.8}$$

and $g_0 = 0$ can be set without loss of generality.

In the anisotropic case, the functions $f_x^*(\theta)$ and $f_y^*(\theta)$ can be expressed as Fourier series

$$f_x^*(\theta) = \sum_{k=-\infty}^{\infty} g_{xk} e^{ik\theta}, \quad f_y^*(\theta) = \sum_{k=-\infty}^{\infty} g_{yk} e^{ik\theta}. \tag{3.9}$$

The Fourier coefficients are given as

$$g_{xk} = \frac{i\big(1-(-1)^k\big)}{\pi^2 k(k^2-4)}F - \tilde{g}_{xk}, \quad g_{yk} = \frac{2\big(1-(-1)^k\big)}{\pi^2 k(k^2-4)}F - \tilde{g}_{yk}, \tag{3.10}$$

where $\tilde{g}_{xk}$ and $\tilde{g}_{yk}$ are Fourier coefficients corresponding to the logarithmic terms defined by the expansions

$$\sum_{j=1}^{2} \mu_j A_j \ln(\cos\theta + \mu_j \sin\theta) = \sum_{k=-\infty}^{\infty} \tilde{g}_{xk} e^{ik\theta}, \tag{3.11}$$

$$\sum_{j=1}^{2} A_j \ln(\cos\theta + \mu_j \sin\theta) = \sum_{k=-\infty}^{\infty} \tilde{g}_{yk} e^{ik\theta} \tag{3.12}$$

and the constants A_j, $j = 1, 2$, are related to the resultant force F by equations (2.69).

For the purpose of both numerical and analytical calculations, the Fourier series of the boundary load must be truncated after a finite number of terms N_g:

$$f^*(\theta) = \sum_{k=-N_g}^{N_g} g_k e^{ik\theta}, \quad f_x^*(\theta) = \sum_{k=-N_g}^{N_g} g_{xk} e^{ik\theta}, \quad f_y^*(\theta) = \sum_{k=-N_g}^{N_g} g_{yk} e^{ik\theta}. \tag{3.13}$$

The Fourier coefficients of the assumed contact stress distribution drop cubically as $k \to \pm\infty$ which is demonstrated in Figure 3.3 where the absolute value of the Fourier coefficients (3.7) is plotted as a function of k. It is shown in Chapter 5 that for the

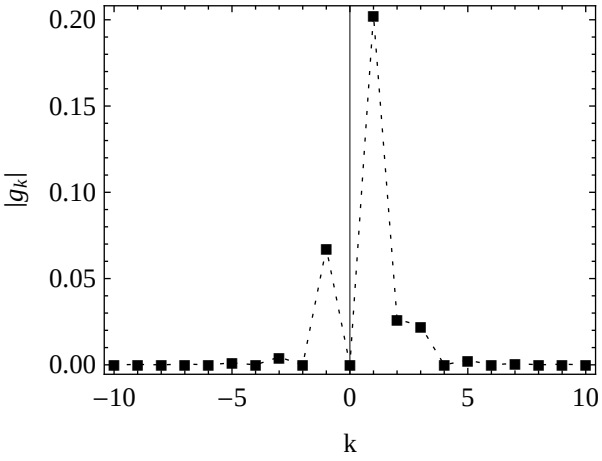

Figure 3.3: Absolute value of the Fourier coefficients g_k as a function of k.

computation of the compliance of an infinite row of loaded holes and the load distribution among bolts, only a few terms of this series actually have to be considered in order to get sufficiently accurate results. For $N_g = 1$, the first series in (3.13) becomes

$$f^*(\theta) = \sum_{k=-1}^{1} g_k e^{ik\theta} = \left(-\frac{2e^{-i\theta}}{3\pi^2} - \frac{2e^{i\theta}}{\pi^2} \right) F \tag{3.14}$$

and the corresponding stress vector on the boundary of the hole is

$$t_r(\theta) = \frac{-12(1+\kappa) + 4(1+\kappa)\cos(2\theta) - 3 + \pi(3+\kappa)\sin(\theta)}{6\pi^2(1+\kappa)} F, \tag{3.15a}$$

$$t_\theta(\theta) = -\frac{3\pi(-1+\kappa)\cos(\theta) + 4(1+\kappa)\sin(2\theta))}{6\pi^2(1+\kappa)} F. \tag{3.15b}$$

For $N_g = 2$, it becomes

$$f^*(\theta) = \sum_{k=-2}^{2} g_k e^{ik\theta} = \left(-\frac{2e^{-i\theta}}{3\pi^2} - \frac{2e^{i\theta}}{\pi^2} + \frac{ie^{2i\theta}}{4\pi} - \frac{ie^{2i\theta}}{2\pi(1+\kappa)} \right) F \tag{3.16}$$

and the corresponding stress vector on the boundary of the hole reads

$$t_r(\theta) = -\frac{6 - 2\cos(2\theta) + 3\pi\sin(\theta)}{3\pi^2} F, \tag{3.17a}$$

$$t_\theta(\theta) = -\frac{2\sin(2\theta)}{3\pi^2} F. \tag{3.17b}$$

Note that the shear stress on the boundary of the hole resulting from the sum (3.13) is not identically zero but it converges quickly to zero with increasing number of terms N_g. The solution of the problem of an infinite isotropic plane weakened by a single unit circular hole which is loaded by the load $f^*(\theta)$ corresponding to (3.4) with $F = 1$ (truncated after N_g terms) is given by formulae (2.51) and is be denoted $\hat{\varphi}_{\mathrm{BL}}(\zeta)$ and $\hat{\psi}_{\mathrm{BL}}(\zeta)$ in the subsequent text. Its analogon in the anisotropic case obtained by (2.71) is denoted $\hat{\varphi}_{j\mathrm{BL}}(\zeta_j)$, $j = 1, 2$.

It has to be pointed out that by choosing the above described simple form of the contact stress, only effects of plate geometry and material can be captured. All other effects listed in the beginning of this section are neglected in the present modelling.

3.3 Compliance of a pin-loaded hole

In this section, the definition of the joint compliance used in this work is given. It is based on the analysis of the in-plane deformation in the plates. The explanation assumes either a single pin-loaded hole or an infinite row of pin-loaded holes in which each hole carries the same load.

Roughly speaking, the compliance of a pin-loaded hole is the difference between the displacement of the hole and the extension of a comparative homogeneously deformed plate subject to the same load, divided by the transmitted force. This definition is explained more precisely in the following. For the purpose of the explanation, it is assumed that a total force F is transmitted over the plate in the direction of the positive y-axis and that the plate extends to infinity in the direction of the negative y-axis (see the left part of Figure 3.4).

According to the contact condition (3.3), the displacement of the bolt V is equal to the displacement of the centre of the contact area ($\theta = \pi/2$), i.e.

$$V = v(0, r). \tag{3.18}$$

The comparative plate is in the state of homogeneous deformation, its strain ε_x^*, ε_y^*, γ_{xy}^* being equal to the strain in the plate as $y \to -\infty$:

$$\lim_{y\to-\infty} \varepsilon_x(x, y) = \varepsilon_x^*, \quad \lim_{y\to-\infty} \varepsilon_y(x, y) = \varepsilon_y^*, \quad \lim_{y\to-\infty} \gamma_{xy}(x, y) = \gamma_{xy}^* = 0. \tag{3.19}$$

Define the displacement relative to the hole

$$\tilde{v}(x, y) = v(x, y) - V. \tag{3.20}$$

The function $\tilde{v}(x, y)$ tends to $-\infty$ as $y \to -\infty$ with an asymptote whose slope is equal to the strain ε_y^* in the comparative plate

$$\lim_{y\to-\infty} \frac{\tilde{v}(x, y)}{y} = \varepsilon_y^* \tag{3.21}$$

The compliance of a pin-loaded hole is defined as the difference between the displacement in the plate with joint and in the comparative plate under homogeneous deformation ε_x^*,

ε_y^* as $y \to -\infty$, divided by the force F transferred over the joint

$$C = \lim_{y \to -\infty} \frac{\tilde{v}(x,y) - (y+r)\varepsilon_y^*}{F}. \tag{3.22}$$

The meaning of the definition is illustrated in the right part of Figure 3.4.

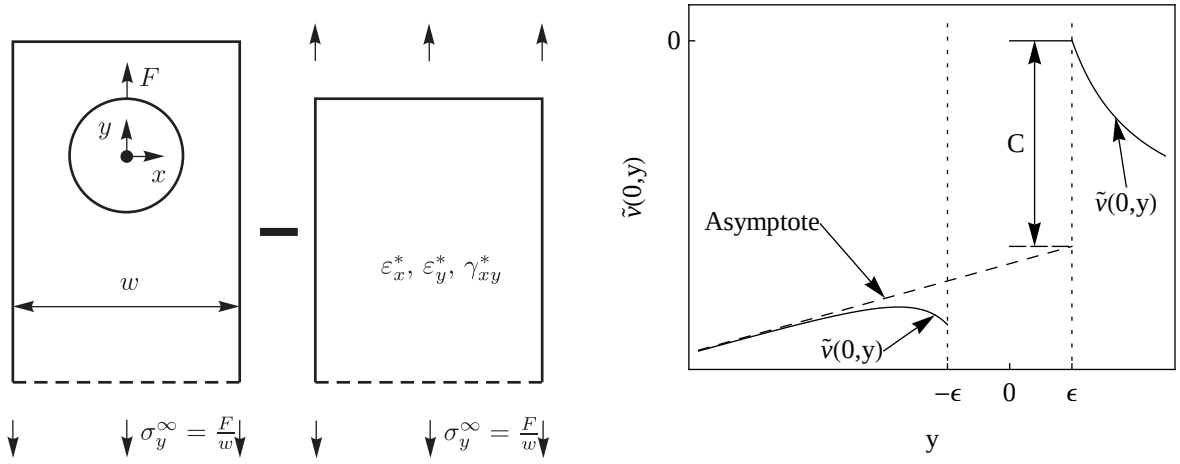

Figure 3.4: Definition of the compliance of a pin-loaded hole. Left: A plate containing a pin-loaded hole and the comparative plate. Right: A typical behaviour of the displacement in the plate containing a pin-loaded hole. The solid line represents the vertical displacement $\tilde{v}(0,y)$ along the line $x = 0$, the dashed line its asymptote as $y \to -\infty$. The displacement is undefined within the hole (interval $[-\epsilon, \epsilon]$).

Having defined the compliance of a pin-loaded hole in a single plate, the compliance of a double-lap joint can be defined as the ratio between the displacement in the above sense and the force $F^{(\mathrm{J})}$ transmitted over the joint. It equals to a weighted sum of compliances of the bolt $C^{(\mathrm{P})}$ and each of the plates $C^{(1)}$ and $C^{(2)}$

$$C^{(\mathrm{J})} = C^{(\mathrm{P})} + \frac{C^{(1)}}{2t^{(1)}} + \frac{C^{(2)}}{t^{(2)}}. \tag{3.23}$$

3.4 Load distribution on bolts

The load distribution on several bolts under the assumption of zero clearance and equal direction of load transmitted on each of the bolts can be determined in the following manner. First, the unknown transmitted forces over respective bolts in each of the plates are expressed using nondimensional coefficients $\lambda_p^{(k)}$, $p = 1, \ldots, N_A$, $k = 1, 2$, as

$$F_p^{(k)} = \lambda_p^{(k)} F^{(k)} \quad \text{for } p = 1, \ldots, N_A - 1, \tag{3.24a}$$

$$F_{N_A}^{(k)} = \left(1 - \sum_{p=1}^{N_A - 1} \lambda_p^{(k)}\right) F^{(k)}, \tag{3.24b}$$

where $N_A = N_H$ for a finite number of holes and $N_A = N_C$ for an infinite system of holes. Then, the plane problem is solved for each of the plates using one of the Algorithms 4.2

or 4.3 presented later in Chapter 4 under the assumptions on stress distribution in the pin-to-hole contact made in Section 3.2. Finally, the unknown coefficients λ_p, $p = 1, \ldots, N_A - 1$ are determined from the following compatibility conditions formulated in terms of the bolt displacements $V_p^{(k)}$:

$$V_p^{(1)} - V_{p+1}^{(1)} = V_p^{(2)} - V_{p+1}^{(2)} \quad \text{for } p = 1, \ldots, N_A - 1, \tag{3.25}$$

where $V_p^{(k)}$ is the vertical displacement of the central point in the contact area of the pth hole in the kth plate.

Two important special cases of the compatibility conditions should be mentioned explicitly:

1. If only one of the plates, say (1), is elastic, the rest being rigid, the compatibility condition reduces to

$$V_p^{(1)} - V_{p+1}^{(1)} = 0 \quad \text{for } p = 1, \ldots, N_A - 1. \tag{3.26}$$

2. If the double-lap configuration has a point symmetry (with respect to both the material and the geometry), then the same must hold for the load distribution on the bolts which allows to formulate the compatibility conditions in terms of displacements in only one of the plates, say (1), as

$$V_p^{(1)} - V_{p+1}^{(1)} = V_{N_A-p}^{(1)} - V_{N_A-p-1}^{(1)} \quad \text{for } p = 1, \ldots, N_A - 1, \tag{3.27a}$$

$$F_p^{(1)} = F_{N_A-p}^{(1)}. \tag{3.27b}$$

Chapter 4

Asymptotic analysis of the first fundamental problem for an infinite plane or half-plane weakened by small holes

In this chapter, a general asymptotic solution of the first fundamental problem for an infinite plane or half-plane weakened by arbitrarily located small holes is derived. The solution is based on the complex potential method and the method of compound asymptotic expansions, both introduced in Chapter 2. In Section 4.1, a full plane or half-plane containing a finite number of holes is considered. Results of this section are extended to infinite symmetric arrays of holes in Section 4.2. Three different underlying equations are discussed separately in each section, namely the potential equation (2.16) describing antiplane strain, the bipotential equation (2.31) describing plane stress and strain in isotropic plates and a more general elliptic fourth-order equation with constant coefficients (2.29) describing plane stress and generalised plane stress in anisotropic plates. Although only the latter two are relevant for the problem of bolted joints considered in this thesis, the Laplace equation is discussed at this place because its solution involves only a single complex potential which makes it a simple model for more complex equations of fourth order. At the end of this chapter, the solution is summarised in form of algorithms for a computer algebra system and a finite element model for the verification of the solution is presented. Part of the results of this chapter were published in Kratochvil and Becker [50, 52].

As a preliminary step towards the asymptotic analysis, the problem geometry has to be converted to a nondimensional form. In the physical geometry, the hole radii are denoted r_p and the distances between the holes w_k. The conversion of all geometric quantities to a nondimensional form is achieved by dividing them by one of the distances, say w_0. Taking into consideration the assumption of small holes, the dimensionless radii are denoted $\rho_p \epsilon = \frac{r_p}{w_0}$ and the dimensionless distances $h_k = \frac{w_k}{w_0}$. This process is schematically shown in Figure 4.1. It would be possible to express all other quantities such as stresses, displacements or forces in a nondimensional form as well. However, due to the linearity of the underlying field equations, this process does not lead to a significant simplification.

Therefore, in agreement with the conventions used in the literature on structural mechanics, all other quantities are left in the dimensional form.

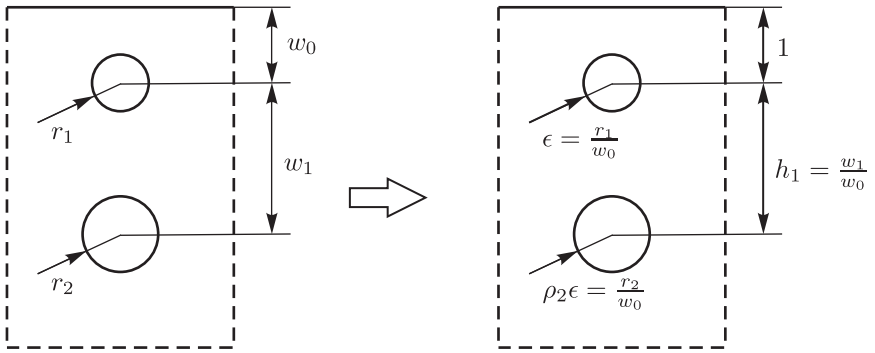

Figure 4.1: The conversion of the geometrical quantities to a nondimensional form.

4.1 Full plane or half-plane containing a finite number of holes

In this section, an infinite plane or half-plane weakened by a finite number of holes is considered. Since the solution of the boundary value problems is based on the complex potential method, the geometry of the problem has to be described in terms of complex coordinates $z = x + iy$. The problem geometry comprises an infinite plane or half-plane $\operatorname{Im} z < 0$ weakened by a finite number N_H of holes located at points $c_p \in \mathbb{C}$, $p = 1, \ldots, N_H$ (see Figure 4.2). The key assumption is that the holes are much smaller than their respective distances and the distances between each hole and the edge. Therefore, the hole radii can be denoted by $\epsilon\rho_p$, where ϵ is a small number and ρ_p is of the same order of magnitude as the respective distances of the holes. Besides the global complex coordinates z, the local coordinates

$$\zeta_p = \frac{z - c_p}{\epsilon\rho_p} \tag{4.1}$$

related to the pth hole are introduced. The inverse relation is

$$z = c_p + \epsilon\rho_p\zeta_p \tag{4.2}$$

and the relation between coordinates corresponding to two different holes p and q reads

$$\zeta_q = \frac{\rho_p}{\rho_q}\zeta_p + \frac{c_p - c_q}{\epsilon\rho_q}. \tag{4.3}$$

Sometimes, local polar coordinates ρ, θ are used for the description of field quantities in the vicinity of the holes. The definition of these coordinates is shown in Figure 4.3.

The solution procedure has a similar structure for all considered governing equations: It starts with an ansatz motivated by the solution for one hole presented in Section 2.3.2.

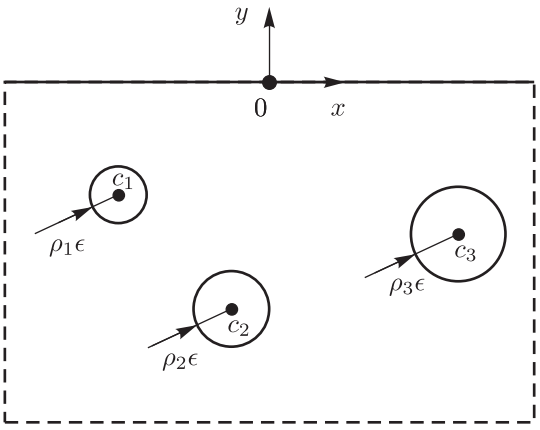

Figure 4.2: A half-plane weakened by a finite number of circular holes ($N_H = 3$).

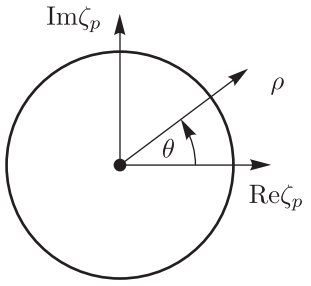

Figure 4.3: Local polar coordinates r, θ related to the pth hole.

Instead of stresses, this ansatz is formulated in terms of the complex potential(s). It involves a set of outer auxiliary functions, one set of inner auxiliary functions for each hole and the logarithmic terms which are known a priori from the boundary conditions. The outer auxiliary functions are defined on the full plane or half-plane without holes whereas the inner auxiliary functions are defined on an infinite plane weakened by a single unit hole. The splitting of the logarithmic terms from the auxiliary functions is necessary in order to guarantee existence, uniqueness and the required behaviour at infinity of the solutions to the auxiliary subproblems.

The ansatz for the complex potentials is first expanded in the powers of ϵ in the vicinity of each of the holes where $\zeta_p = O(\epsilon^0)$ as well as in the far-field where $z = O(\epsilon^0)$. The series obtained in this way are substituted into the corresponding boundary conditions, which leads to boundary value problems for the unknown auxiliary functions comprised in the ansatz. Since the auxiliary functions are defined in simpler geometries than the original one, the original complex problem is in this way splitted into several simpler subproblems (see Figure 4.4). Solving these subproblems thus completes the solution of the original problem.

All boundary conditions, including the state of stress at infinity, are assumed to have the form of a formal asymptotic series in terms of powers of ϵ. In most examples considered in Chapter 5, only one term of this formal infinite series is nonzero. Only for the determination of the load distribution on multiple holes considered in Section 5.3, boundary conditions involving terms of different order of magnitude appear.

It should be stressed that only a formal asymptotic solution is constructed in this chapter. Therefore, it is assumed that operations such as rearrangement of infinite sums or change of the order of infinite summation and differentiation or integration can always be carried out as needed.

Finally, to keep the equations in the following as compact as possible, it is convenient to

introduce the notation

$$\delta_{\text{condition}} = \begin{cases} 1 & \text{if condition holds,} \\ 0 & \text{if condition does not hold} \end{cases} \quad \text{and} \quad \delta_{kn} = \delta_{k=n}. \tag{4.4}$$

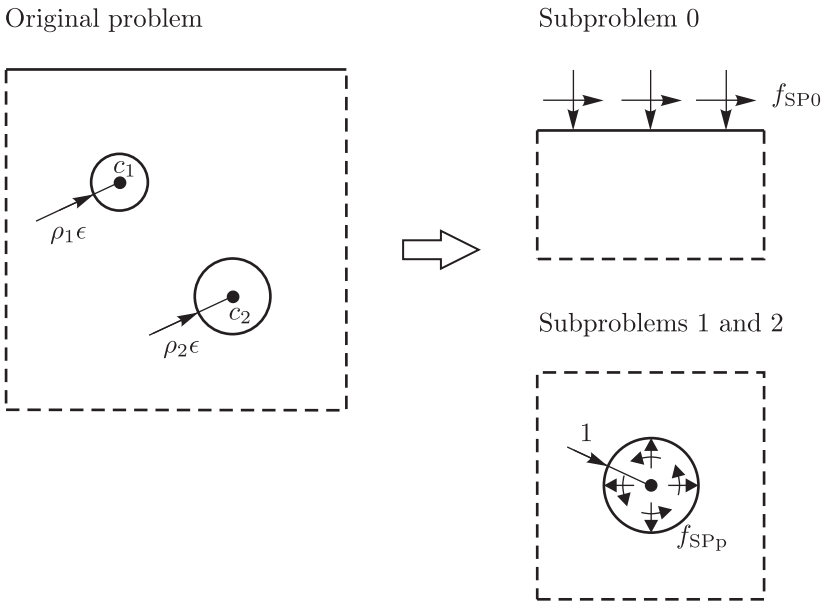

Figure 4.4: Asymptotic splitting of the original problem into subproblems.

4.1.1 Antiplane strain

Boundary conditions

The condition on the boundary of the pth hole is prescribed in the form of an asymptotic series in terms of ϵ as

$$\frac{\partial w}{\partial n} = f_p(\theta) = \sum_{n=0}^{\infty} f_p^n(\theta)\epsilon^n. \tag{4.5}$$

The functions $f_p^{*n}(\theta)$ are defined in analogy to (2.38) as

$$f_p^{*n}(\theta) = f_p^n(\theta) - \frac{\partial}{\partial\theta} A_p^n \ln\zeta_p = f_p^n(\theta) - A_p^n, \tag{4.6}$$

where

$$A_p^n = \frac{1}{2\pi}\int_0^{2\pi} f_p^n(\theta)\,\mathrm{d}\theta. \tag{4.7}$$

The solution of the first boundary value problem for an infinite plane weakened by a single unit circular hole under the boundary condition $f_p^{*n}(\theta)$ is denoted $\hat{\varphi}_p^n(\zeta_p)$.

In the case of a half-plane, the load

$$\frac{\partial w}{\partial y} = f_0(x) = \sum_{n=0}^{\infty} f_0^n(x)\epsilon^n \tag{4.8}$$

on the x-axis and the shear stresses at infinity

$$\tau_{xz}^{\infty} = \sum_{n=0}^{\infty} \tau_{xz}^{n} \epsilon^n, \quad \tau_{yz}^{\infty} = \sum_{n=0}^{\infty} \tau_{yz}^{n} \epsilon^n \tag{4.9}$$

are prescribed. The solution of the problem for a half-plane without holes under the load $f_0^n(x)$ and shear stresses at infinity τ_{xz}^n,τ_{yz}^n is denoted $\hat{\varphi}_0^n(z)$. In the case of a full plane, only the stresses at infinity are given.

The question considered in this chapter may thus be formulated as in what way the functions $\hat{\varphi}_0^n(z)$ are modified by the presence of the holes and conversely, how the functions $\hat{\varphi}_p^n(\zeta_p)$ are affected by other holes and the edge of the half-plane.

Ansatz for the complex potential

The complex potential is searched for in the form

$$\varphi = \sum_{n=0}^{\infty} \epsilon^n \left[\varphi_0^n(z) + \sum_{q=1}^{N_H} \Big(\varphi_q^n(\zeta_q) + A_q^n \ln \zeta_q \Big) \right], \tag{4.10}$$

where $\varphi_q^n(\zeta_q)$, $q = 1, \ldots, N_H$, $n \in \mathbb{N}_0$, are inner auxiliary functions defined on the exterior of the unit circle in the ζ_q-plane and $\varphi_0^n(z)$, $n \in \mathbb{N}_0$, are outer auxiliary functions defined on the full plane or the lower half-plane. All auxiliary functions are holomorphic and single-valued in their domain of definition. They are defined up to a constant that can be fixed by forcing the auxiliary functions to vanish at infinity. Therefore, the inner auxiliary functions allow the following Laurent series expansions at infinity:

$$\varphi_q^n(\zeta_q) = \sum_{k=1}^{\infty} a_{qk}^n \zeta_q^{-k} \tag{4.11}$$

and the outer auxiliary functions can be expanded at points c_p as follows:

$$\varphi_0^n(z) = \sum_{k=0}^{\infty} d_{pk}^n (z - c_p)^k. \tag{4.12}$$

Subproblems for the auxiliary functions

In this paragraph, boundary value problems for the auxiliary functions are derived from the boundary conditions of the original problem. The discussion starts with the boundary condition on the pth hole. Substituting the expansions (4.11) and (4.12) together with (4.2) and (4.3) into the ansatz (4.10) and using the expansions

$$\zeta_q^{-k} = \sum_{l=0}^{\infty} \binom{-k}{l} \rho_p^l \rho_q^k \zeta_p^l \epsilon^{k+l} (c_p - c_q)^{-k-l}, \tag{4.13}$$

$$\ln \zeta_q = \ln \left(\frac{c_p - c_q}{\epsilon \rho_q} \right) + \sum_{l=1}^{\infty} \frac{(-1)^{l+1}}{l} \left(\frac{\rho_p \zeta_p \epsilon}{c_p - c_q} \right)^l, \tag{4.14}$$

the complex potential becomes

$$\varphi(\zeta_p) = \sum_{n=0}^{\infty} \epsilon^n \left[\sum_{k=0}^{\infty} d_{pk}^n (\epsilon \rho_p \zeta_p)^k + \varphi_p^n(\zeta_p) + \sum_{\substack{q=1 \\ q\neq p}}^{N_H} \sum_{k=1}^{\infty} a_{qk}^n \sum_{l=0}^{\infty} \binom{-k}{l} \rho_p^l \rho_q^k \zeta_p^l \epsilon^{k+l} (c_p - c_q)^{-k-l} \right.$$
$$\left. + A_p^n \ln \zeta_p + \sum_{\substack{q=1 \\ q\neq p}}^{N_H} A_q^n \sum_{l=1}^{\infty} \frac{(-1)^{l+1}}{l} \left(\rho_p \zeta_p \epsilon\right)^l (c_p - c_q)^{-l} \right]. \quad (4.15)$$

Further, by using the substitution $n' = n + k$ in the first and $n' = n + k + l$ in the third term and dropping the apostrophes for convenience, the equation becomes

$$\varphi(\zeta_p) = \sum_{n=0}^{\infty} \epsilon^n \left[\sum_{k=0}^{\infty} d_{pk}^{n-k} \rho_p^k \zeta_p^k + \varphi_p^n(\zeta_p) + \sum_{\substack{q=1 \\ q\neq p}}^{N_H} \sum_{k=1}^{\infty} a_{qk}^{n-k-l} \sum_{\substack{l=0 \\ k+l\leq n}}^{\infty} \binom{-k}{l} \rho_p^l \rho_q^k \zeta_p^l (c_p - c_q)^{-k-l} \right.$$
$$\left. + \sum_{\substack{q=1 \\ q\neq p}}^{N_H} \sum_{k=1}^{n} A_q^{n-k} \frac{(-1)^{k+1}}{n} \rho_p^k \zeta_p^k (c_p - c_q)^{-k} + A_p^n \ln \zeta_p \right] \quad (4.16)$$

and by applying the rearrangement

$$\sum_{k=1}^{\infty} \sum_{\substack{l=0 \\ k+l\leq n}}^{\infty} (..)_{kl} = \sum_{k=0}^{n-1} \sum_{l=1}^{n-k} (..)_{lk} \quad (4.17)$$

finally

$$\varphi(\zeta_p) = \sum_{n=0}^{\infty} \epsilon^n \left[\varphi_p^n(\zeta_p) + \sum_{k=1}^{n} K_{pk}^n \zeta_p^k + A_p^n \ln \zeta_p \right], \quad (4.18)$$

where the coefficients K_{pk}^n are given as

$$K_{pk}^n = \rho_p^k \left[d_{pk}^{n-k} + \sum_{\substack{q=1 \\ q\neq p}}^{N_H} \sum_{l=1}^{n-k} a_{ql}^{n-k-l} \binom{-l}{k} \rho_q^l (c_p - c_q)^{-k-l} \right.$$
$$\left. + \sum_{\substack{q=1 \\ q\neq p}}^{N_H} A_q^{n-k} \frac{(-1)^{k+1}}{k} (c_p - c_q)^{-k} \right]. \quad (4.19)$$

Substituting the equation (4.18) into the boundary condition on the pth hole (4.5) and carrying out the differentiation according to (2.33), one obtains

$$\sum_{n=0}^{\infty} \epsilon^n \left[\frac{\partial}{\partial \nu_p} \operatorname{Re} \varphi_p^n(\zeta_p) + \operatorname{Re} \sum_{k=1}^{n} k K_{pk}^n \zeta_p^k \right] = \epsilon \rho_p \sum_{n=0}^{\infty} f_p^{*n}(\theta) \epsilon^n \quad \text{on } \zeta_p = e^{i\theta}, \quad (4.20)$$

where $\frac{\partial}{\partial \nu_p}$ denotes the normal derivative in the scaled ζ_p-plane related to the normal derivative in the unscaled z-plane by

$$\frac{\partial}{\partial \nu_p} = \epsilon \rho_p \frac{\partial}{\partial n}. \tag{4.21}$$

Comparing the same powers of ϵ on both sides of the equation, finally for $p = 1, \ldots, N_H$, $n \in \mathbb{N}$, one finds :

$$\frac{\partial}{\partial \nu_p} \operatorname{Re} \varphi_p^n(\zeta_p) = \rho_p f_p^{*n-1}(\theta) - \operatorname{Re} \sum_{k=1}^{n} k K_{pk}^n \zeta_p^k \quad \text{on } \zeta_p = e^{i\theta}. \tag{4.22}$$

In view of their definitions, the functions $\varphi_p^n(\zeta_p)$ are uniquely determined as the solution of the problem of an infinite plane weakened by a single unit hole under the boundary condition (4.22) and the condition $\varphi_p^n(\zeta_p) \to 0$ as $\zeta_p \to \infty$. This boundary value problem is solved in the next paragraph.

In the case of the half-plane, the boundary condition on the line $y = 0$ is treated in an analogous manner. Substituting (4.11) and (4.1) into the ansatz (4.10), one obtains

$$\varphi(z) = \sum_{n=0}^{\infty} \epsilon^n \left[\varphi_0^n(z) + \sum_{q=1}^{N_H} \left(\sum_{k=1}^{\infty} a_{qk}^n \epsilon^k \rho_q^k (z - c_q)^{-k} + A_q^n \ln(z - c_q) \right) \right] \tag{4.23}$$

and by using the substitution $n' = n + k$ in the second term and dropping the apostrophe for convenience

$$\varphi(z) = \sum_{n=0}^{\infty} \epsilon^n \left[\varphi_0^n(z) + \sum_{q=1}^{N_H} \left(\sum_{k=1}^{n} a_{qk}^{n-k} \rho_q^k (z - c_q)^{-k} + A_q^n \ln(z - c_q) \right) \right]. \tag{4.24}$$

Substituting the equation (4.24) into the boundary condition (4.8) and carrying out the differentiation according to (2.34), on $z = x$ one obtains

$$\sum_{n=0}^{\infty} \epsilon^n \left[\frac{\partial}{\partial y} \left(\operatorname{Re} \varphi_0^n(z) \right) + \operatorname{Im} \sum_{q=1}^{N_H} \left(\sum_{k=1}^{n} a_{qk}^{n-k} \rho_q^k k (z - c_q)^{-k-1} - \frac{A_q^n}{z - c_q} \right) \right] = \sum_{n=0}^{\infty} f_0^n(x) \epsilon^n. \tag{4.25}$$

Equating terms involving the same powers of ϵ, this equation finally for each $n \in \mathbb{N}$ becomes

$$\frac{\partial}{\partial y} \operatorname{Re} \varphi_0^n(z) = f_0^n(x) - \operatorname{Im} \sum_{q=1}^{N_H} \left(\sum_{k=1}^{n} a_{qk}^{n-k} \rho_q^k k (z - c_q)^{-k-1} - A_q^n (z - c_q)^{-1} \right) \quad \text{on } z = x. \tag{4.26}$$

As before, the functions $\varphi_0^n(z)$ are uniquely determined as the solution of the Neumann problem on the half-plane with the boundary condition (4.26).

Solution of the subproblems

In this paragraph, the auxiliary functions are determined by explicitly solving the corresponding subproblems. The solution starts with the boundary value problems for the inner auxiliary functions. The right-hand side of the boundary condition (4.22) is a linear combination of the functions $f_p^{*n}(\theta)$ and of functions of the form

$$f_{\mathrm{SPp}}(\zeta_p) = \operatorname{Re} \alpha \zeta_p^k, \tag{4.27}$$

where $\alpha \in \mathbb{C}$ and $k \in \mathbb{N}_0$ are constants. The solution of the problem with the boundary condition $f_p^{*n}(\theta)$ is $\hat{\varphi}_p^n(\zeta_p)$ and the solution of the problem with the boundary condition (4.27) can be obtained as follows. Substituting this function into the general formula (2.39) and using the fact that on γ the relation $\overline{\sigma} = 1/\sigma$ holds, one finds

$$\varphi'_{\mathrm{SPp}}(\zeta_p) = -\frac{1}{\pi i \zeta_p} \int_\gamma \frac{\frac{1}{2}(\alpha \sigma^k + \overline{\alpha} \sigma^{-k})}{\sigma - \zeta_p} \, \mathrm{d}\sigma. \tag{4.28}$$

Since $\zeta \in \operatorname{Ext}(\gamma)$, the function $F(\sigma) = \frac{\sigma^n}{\sigma - \zeta_p}$ for $n \geq 0$ is holomorphic on $\operatorname{Int}(\gamma)$ whereas for $n < 0$ it is holomorphic on $\operatorname{Ext}(\gamma) \setminus \{\zeta_p\}$ and has a simple pole at ζ_p. From the residue theorem

$$\frac{1}{2\pi i} \int_\gamma \frac{\sigma^n}{\sigma - \zeta_p} \mathrm{d}\sigma = \begin{cases} 0 & \text{if } n \geq 0, \\ -\zeta_p^n & \text{if } n < 0. \end{cases} \tag{4.29}$$

Applying this relation to the contour integral in (4.28), one obtains

$$\varphi'_{\mathrm{SPp}}(\zeta_p) = \overline{\alpha} \zeta_p^{-k-1}$$

and after integration

$$\varphi_{\mathrm{SPp}}(\zeta_p) = -\frac{\overline{\alpha} \zeta_p^{-k}}{k}. \tag{4.30}$$

Superposing the solutions (4.30) with coefficients from (4.22) and the function $\hat{\varphi}_p^n(\zeta_p)$, one finally obtains for the inner auxiliary functions

$$\varphi_p^n(\zeta_p) = \hat{\varphi}_p^n(\zeta_p) + \sum_{k=1}^{n} \overline{K}_{pk}^n \zeta_p^{-k}. \tag{4.31}$$

Similarly, in the case of the half-plane, the right-hand side of the boundary condition (4.26) is a superposition of the functions $f_0^n(x)$ and of functions of the form

$$f_{\mathrm{SP0}}(z) = \operatorname{Im} \alpha (z - c)^{-k-1}, \tag{4.32}$$

where $\alpha, c \in \mathbb{C}$, $k \in \mathbb{N}$ and $\operatorname{Im} c < 0$. Substituting this function into the general formula (2.40) and using the fact that $x = \overline{x}$, one obtains

$$\varphi'_{\mathrm{SP0}}(z) = \frac{1}{\pi} \int_{-\infty}^{\infty} \frac{\frac{1}{2i}\big(\alpha (x - c)^{-k-1} - \overline{\alpha} (x - \overline{c})^{-k-1}\big)}{x - z} \, \mathrm{d}x. \tag{4.33}$$

Since $\operatorname{Im} z \leq 0$ and $\operatorname{Im} c < 0$, the function $F_1(x) = \frac{(x-c)^{-n}}{x-z}$ is for $n > 0$ holomorphic on the upper half-plane whereas the function $F_2(x) = \frac{(x-\overline{c})^{-n}}{x-z}$ is holomorphic on the lower

half-plane with the exception of the point z where it has a simple pole. From the residue theorem for $n > 0$ thus follows

$$\frac{1}{2\pi i}\int_{-\infty}^{\infty}\frac{(x-c)^{-n}}{x-z}\mathrm{d}x = 0, \tag{4.34a}$$

$$\frac{1}{2\pi i}\int_{-\infty}^{\infty}\frac{(x-\overline{c})^{-n}}{x-z}\mathrm{d}x = -(z-\overline{c})^{-n}. \tag{4.34b}$$

By application of these formulae to (4.33), this equation becomes

$$\varphi'_{\mathrm{SP0}}(z) = \overline{\alpha}(z-\overline{c})^{-k-1}$$

and after carrying out the integration finally

$$\varphi_{\mathrm{SP0}}(z) = \begin{cases} -\frac{\overline{\alpha}(z-\overline{c})^{-k}}{k} & \text{if } k > 0, \\ \overline{\alpha}\ln(z-\overline{c}) & \text{if } k = 0. \end{cases} \tag{4.35}$$

Superposing the function $\hat{\varphi}_0^n(z)$ and the solutions (4.35) with the corresponding coefficients, one obtains the final expression for the inner auxiliary functions

$$\varphi_0^n(z) = \hat{\varphi}_0^n(z) + \sum_{q=1}^{N_H}\left(\sum_{k=1}^{n}\overline{a}_{qk}^{n-k}\rho_q^k(z-\overline{c}_q)^{-k} + \overline{A}_q^{\,n}\ln(z-\overline{c}_q)\right). \tag{4.36}$$

In the case of the full plane, the outer auxiliary functions only have to fulfil the condition at infinity from which it immediately follows

$$\varphi_0^n(z) = \hat{\varphi}_0^n(z). \tag{4.37}$$

Final form of the complex potentials

In equations (4.31) and (4.36), each of the auxiliary functions $\varphi_0^n(z)$ and $\varphi_p^n(\zeta_p)$ of the order n only depends on coefficients obtained by Laurent series expansions of the functions $\varphi_0^m(z)$ and $\varphi_p^m(\zeta_p)$ of order $m < n$. Thus, these formulae represent an iterative algorithm for successive determination of the auxiliary functions.

Once these auxiliary functions are known for $n = 0, \ldots, N$ where N is a chosen order of approximation, they are substituted into the ansatz (4.10) delivering a solution

$$\varphi(z) = \sum_{n=0}^{N}\epsilon^n\left[\varphi_0^n(z) + \sum_{q=1}^{N_H}\left(\varphi_q^n\left(\frac{z-c_q}{\epsilon\rho_q}\right) + A_q^n\ln(z-c_q)\right)\right] \tag{4.38}$$

which is valid in the whole domain and satisfies all boundary conditions up to the order $N-1$. This result can be further simplified by specialisation either for the far-field where $z = O(\epsilon^0)$ or for the near-field of each hole where $\zeta_p = O(\epsilon^0)$. The potentials in the far-field can be obtained by truncating the series (4.24)

$$P^N\varphi(z) = \sum_{n=0}^{N}\epsilon^n\left[\varphi_0^n(z) + \sum_{q=1}^{N_H}\left(\sum_{k=1}^{n}a_{qk}^{n-k}\rho_q^k(z-c_q)^{-k} + A_q^n\ln(z-c_q)\right)\right]. \tag{4.39}$$

Similarly, in the vicinity of the pth hole, by truncating (4.18) one obtains

$$Q_p^N \varphi(\zeta_p) = \sum_{n=0}^{N} \epsilon^n \left[\varphi_p^n(\zeta_p) + \sum_{k=1}^{n} K_{pk}^n \zeta_p^k + A_p \ln \zeta_p \right]. \tag{4.40}$$

4.1.2 Plane stress and strain in isotropic plates

Boundary conditions

The boundary condition on the pth hole is formulated in terms of the resultant force (2.45) as an asymptotic series

$$f_p(\theta) = \sum_{n=0}^{\infty} f_p^n(\theta) \epsilon^n, \tag{4.41}$$

the total resultant force corresponding to the term $f_p^n(\theta)$ being

$$F_p^n = F_{px}^n + i F_{py}^n = -i[f_p^n(\theta)]_0^{2\pi}. \tag{4.42}$$

Note that the term $f_p^n(\theta)\epsilon^n$ produces a resultant force of the order $O(\epsilon^n)$ and stresses of the order $O(\epsilon^{n-1})$. Specially, $f_p^0(\theta)$ produces a resultant force of the order $O(\epsilon^0)$ and stresses of the order $O(1/\epsilon)$. The functions $f_p^{*n}(\theta)$ are in analogy to (2.50) defined as

$$f_p^{*n}(\theta) = f_p^n(\theta) - \left(A_p^n \ln \zeta_p + \overline{A}_p^n \frac{\zeta_p}{\overline{\zeta}_p} + \overline{B}_p^n \right), \qquad \zeta_p = e^{i\theta}, \tag{4.43}$$

where the constants $A_p^n, B_p^n \in \mathbb{C}$ are determined by the resultant forces F_p^n via the relation (2.49). The solution of the problem of a single hole in an infinite plate under zero stresses at infinity and boundary condition $f_p^n(\theta)$ is denoted $\hat{\varphi}_p^n(\zeta_p), \hat{\psi}_p^n(\zeta_p)$.

Furthermore, the state of stress at infinity

$$\sigma_x^\infty = \sum_{n=0}^{\infty} \sigma_x^n \epsilon^n, \quad \sigma_y^\infty = \sum_{n=0}^{\infty} \sigma_y^n \epsilon^n, \quad \tau_{xy}^\infty = \sum_{n=0}^{\infty} \tau_{xy}^n \epsilon^n \tag{4.44}$$

and in the case of the half-plane also the load on its edge formulated again in terms of the resultant force (2.45)

$$f_0(x) = \sum_{n=0}^{\infty} f_0^n(x) \epsilon^n \tag{4.45}$$

have to be prescribed. For simplicity it is assumed that the total resultant of forces acting on the edge of the half-plane is zero.

Ansatz for the complex potentials

The complex potentials are searched for in the form

$$\varphi = \sum_{n=0}^{\infty} \epsilon^n \left[\varphi_0^n(z) + \sum_{q=1}^{N_H} \Big(\varphi_q^n(\zeta_q) + A_q^n \ln \zeta_q \Big) \right], \tag{4.46a}$$

$$\psi = \sum_{n=0}^{\infty} \epsilon^n \left[\psi_0^n(z) + \sum_{q=1}^{N_H} \left(\psi_q^n(\zeta_q) - \frac{\overline{c}_q}{\epsilon \rho_q} \frac{\mathrm{d}\varphi_q^n}{\mathrm{d}\zeta_q} + B_q^n \ln \zeta_q - \frac{A_q^n \overline{c}_q}{\epsilon \rho_q \zeta_q} \right) \right]. \tag{4.46b}$$

Similarly as in the previous paragraph, $\varphi_q^n(\zeta_q)$ and $\psi_q^n(\zeta_q)$, $q = 1, \ldots, N_H$, $n \in \mathbb{N}_0$, are inner auxiliary functions defined on the exterior of the unit circle in the ζ_q-plane and $\varphi_0^n(z)$ and $\psi_0^n(z)$, $n \in \mathbb{N}_0$, are outer auxiliary functions defined on the lower half-plane. All auxiliary functions are holomorphic and single-valued in their domains of definition and produce zero stresses at infinity. Note that the logarithmic terms correspond to the general structure of the complex potentials in a multiply connected domain and the two extra terms in the equation (4.46b) are due to the noninvariance of the potential ψ with respect to the translation of the coordinate system to the point c_q.

In the following, the fact is used that the inner auxiliary functions allow the following Laurent series expansions at infinity:

$$\varphi_q^n(\zeta_q) = \sum_{k=1}^{\infty} a_{qk}^n \zeta_q^{-k}, \tag{4.47a}$$

$$\psi_q^n(\zeta_q) = \sum_{k=1}^{\infty} b_{qk}^n \zeta_q^{-k} \tag{4.47b}$$

and the outer auxiliary functions can be expanded at points c_p as follows:

$$\varphi_0^n(z) = \sum_{k=0}^{\infty} d_{pk}^n (z - c_p)^k, \tag{4.48a}$$

$$\psi_0^n(z) = \sum_{k=0}^{\infty} e_{pk}^n (z - c_p)^k. \tag{4.48b}$$

Subproblems for the auxiliary functions

The boundary condition on the pth hole is treated first. Substituting the expansions (4.47) and (4.48) together with (4.2) and (4.3) into the ansatz (4.46), rearranging the sums in the same way as in the previous paragraph, using the expansions (4.13) and omitting the constant terms which do not contribute to the resulting stresses, for $p = 1, \ldots, N_H$ one gets

$$\varphi(\zeta_p) = \sum_{n=0}^{\infty} \epsilon^n \left[\varphi_p^n(\zeta_p) + \sum_{k=1}^{n} K_{pk}^n \zeta_p^k + A_p^n \ln \zeta_p \right], \tag{4.49a}$$

$$\psi(\zeta_p) = \sum_{n=0}^{\infty} \epsilon^n \left[\psi_p^n(\zeta_p) - \frac{\overline{c}_p}{\epsilon \rho_p} \frac{\mathrm{d}\varphi_p^n}{\mathrm{d}\zeta_p} + \sum_{k=1}^{n} L_{pk}^n \zeta_p^k + B_p^n \ln \zeta_p - \frac{A_p^n \overline{c}_p}{\epsilon \rho_p \zeta_p} \right], \tag{4.49b}$$

where the coefficients K_{pk}^n and L_{pk}^n are given as

$$K_{pk}^n = \rho_p^k \left[d_{pk}^{n-k} + \sum_{\substack{q=1 \\ q\neq p}}^{N_H} \sum_{l=1}^{n-k} a_{ql}^{n-k-l} \binom{-l}{k} \rho_q^l (c_p - c_q)^{-k-l} + \sum_{\substack{q=1 \\ q\neq p}}^{N_H} A_q^{n-k} \frac{(-1)^{k+1}}{k} (c_p - c_q)^{-k} \right], \quad (4.50a)$$

$$L_{pk}^n = \rho_p^k \left[e_{pk}^{n-k} + \sum_{\substack{q=1 \\ q\neq p}}^{N_H} \sum_{l=1}^{n-k} \binom{-l}{k} \rho_q^l (c_p - c_q)^{-k-l} \left(b_{ql}^{n-k-l} + a_{ql}^{n-k-l}(k+l) \frac{\overline{c}_q}{c_p - c_q} \right) + \sum_{\substack{q=1 \\ q\neq p}}^{N_H} (-1)^{k+1} \left(\frac{B_q^{n-k}}{k} + \frac{A_q^{n-k}\overline{c}_q}{c_p - c_q} \right) (c_p - c_q)^{-k} \right]. \quad (4.50b)$$

Substituting equations (4.49) into the boundary conditions on the pth hole, using (2.50) and comparing terms involving the same powers of ϵ, for each $n \in \mathbb{N}_0$ one finally finds

$$\varphi_p^n(\zeta_p) + \zeta_p \overline{\frac{\mathrm{d}\varphi_p^n}{\mathrm{d}\zeta_p}(\zeta_p)} + \overline{\psi_p^n(\zeta_p)} = f_p^{*n}(\theta) - \sum_{k=1}^{n} \left[K_{pk}^n \zeta_p^k + k\overline{K}_{pk}^n \zeta_p \overline{\zeta}_p^{k-1} + \left(\overline{L}_{pk}^n + \frac{c_p}{\rho_p}(k+1)\overline{K}_{p,k+1}^n \right) \overline{\zeta}_p^k \right] \quad \text{on } \zeta_p = e^{i\theta}. \quad (4.51)$$

In view of their definitions, the functions $\varphi_p^n(\zeta_p)$ and $\psi_p^n(\zeta_p)$ are uniquely determined as the solution of the problem of a single unit hole in an infinite plane with zero stresses at infinity and boundary condition (4.51) on the hole edge. This boundary value problem is solved in the next paragraph.

In the case of the half-plane, the boundary condition on the line $y = 0$ is treated in an analogous manner. Similarly as in the case of one complex potential, it can be shown that

$$\varphi(z) = \sum_{n=0}^{\infty} \epsilon^n \left[\varphi_0^n(z) + \sum_{q=1}^{N_H} \left(\sum_{k=1}^{n} a_{qk}^{n-k} \rho_q^k (z - c_q)^{-k} + A_q^n \ln(z - c_q) \right) \right], \quad (4.52a)$$

$$\psi(z) = \sum_{n=0}^{\infty} \epsilon^n \left[\psi_0^n(z) + \sum_{q=1}^{N_H} \left(\sum_{k=1}^{n} \rho_q^k \left(b_{qk}^{n-k} (z - c_q)^{-k} + \overline{c}_q a_{qk}^{n-k} k (z - c_q)^{-k-1} \right) + B_q^n \ln(z - c_q) - \frac{A_q^n \overline{c}_q}{z - c_q} \right) \right]. \quad (4.52b)$$

Substituting equations (4.52) into the boundary condition on the line $y = 0$ and comparing

the same powers of ϵ, for each $n \in \mathbb{N}_0$ one eventually gets

$$\begin{aligned}\varphi_0^n(z) + z\overline{\frac{\mathrm{d}\varphi_0^n}{\mathrm{d}z}(z)} + \overline{\psi_0^n(z)} &= f_0^n(x) \\ &- \sum_{q=1}^{N_H}\left[\sum_{k=1}^{n}\rho_q^k\Big(a_{qk}^{n-k}(z-c_q)^{-k} - k\overline{a}_{qk}^{n-k}(z-c_q)(z-\overline{c}_q)^{-k-1}\overline{b}_{qk}^{n-k}(z-\overline{c}_q)^{-k}\Big)\right. \\ &\left. - \left(A_q^n\ln(z-c_q) + \overline{B}_q^{\,n}\ln(z-\overline{c}_q) + \overline{A}_q^{\,n}\frac{\overline{c}_q - c_q}{z-\overline{c}_q}\right)\right] \text{ on } z = x. \quad (4.53)\end{aligned}$$

Again, it follows that the functions $\varphi_0^n(z)$ and $\psi_0^n(z)$ are uniquely determined as the solution of the problem of a half-plane with zero stresses at infinity and boundary condition (4.53) on the line $y = 0$. In the case of the full plane, the outer auxiliary functions only have to fulfil the stress conditions at infinity.

Solution of the subproblems

The inner auxiliary functions are determined as solution to the boundary value problem (4.51). The right-hand side of the boundary condition (4.51) is a linear combination of $f_p^n(\theta)$ and functions of the form

$$f_{\mathrm{SP_p}}(\zeta_p) = \alpha\zeta_p^k + \beta\zeta_p\overline{\zeta}_p^{k-1} + \gamma\overline{\zeta}_p^{\,k}, \quad (4.54)$$

where $\alpha, \beta, \gamma \in \mathbb{C}$ and $k \in \mathbb{N}$. The solution of the problem with the boundary condition $f_p^n(\theta)$ is $\hat{\varphi}_p^n(\zeta_p), \hat{\psi}_p^n(\zeta_p)$. The solution corresponding to the boundary condition (4.54) can be obtained in the following manner. Substituting (4.54) into the general solution of the first fundamental problem for an infinite plane weakened by a single circular hole (2.51) and using the fact that on γ the relation $\overline{\sigma} = 1/\sigma$ holds, one obtains

$$\varphi_{\mathrm{SP_p}}(\zeta_p) = -\frac{1}{2\pi i}\int_\gamma \frac{\alpha\sigma^k + \beta\sigma^{-k+2} + \gamma\sigma^{-k}}{\sigma - \zeta_p}\,\mathrm{d}\sigma, \quad (4.55a)$$

$$\psi_{\mathrm{SP_p}}(\zeta_p) = -\frac{1}{2\pi i}\int_\gamma \frac{\overline{\alpha}\sigma^{-k} + \overline{\beta}\sigma^{k-2} + \overline{\gamma}\sigma^{k}}{\sigma - \zeta_p}\,\mathrm{d}\sigma - \frac{\varphi'_{\mathrm{SP_p}}(\zeta_p)}{\zeta_p}. \quad (4.55b)$$

Both integrals may be evaluated using the formula (4.29) which yields

$$\varphi_{\mathrm{SP_p}}(\zeta_p) = \beta\zeta_p^{-k+2}\delta_{k>2} + \gamma\zeta_p^{-k}, \quad (4.56a)$$

$$\psi_{\mathrm{SP_p}}(\zeta_p) = \overline{\alpha}\zeta_p^{-k} + \beta(k-2)\zeta_p^{-k}\delta_{k>2} + \overline{\beta}\zeta_p^{k-2}\delta_{k<2} + \gamma k\zeta_p^{-k-2}. \quad (4.56b)$$

Superposing the solutions corresponding to each term on the right-hand side of the boundary condition (4.51) yields the following result for the inner auxiliary functions:

$$\varphi_p^n(\zeta_p) = \hat{\varphi}_p^n(\zeta_p) - \sum_{k=1}^{n}\left[k\overline{K}_{pk}^{\,n}\zeta_p^{-k+2}\delta_{k>2} + \left(\overline{L}_{pk}^{\,n} + \frac{c_p}{\rho_p}(k+1)\overline{K}_{p,k+1}^{\,n+1}\right)\zeta_p^{-k}\right], \quad (4.57a)$$

$$\begin{aligned}\psi_p^n(\zeta_p) = \hat{\psi}_p^n(\zeta_p) - \sum_{k=1}^{n}\Bigg[&\overline{K}_{pk}^{\,n}\zeta_p^{-k} + k(k-2)\overline{K}_{pk}^{\,n}\zeta_p^{-k}\delta_{k>2} \\ &+ kK_{pk}^n\zeta_p^{k-2}\delta_{k<2} + k\left(\overline{L}_{pk}^{\,n} + \frac{c_p}{\rho_p}(k+1)\overline{K}_{p,k+1}^{\,n+1}\right)\zeta_p^{-k-2}\Bigg]. \quad (4.57b)\end{aligned}$$

Similarly, in the case of the half-plane, the right-hand side of the boundary condition (4.53) is a superposition of $f_0^n(x)$ and functions of two different forms. The first one is

$$f_{\mathrm{SP0}}(z) = \alpha(z-c)^{-k} + \beta(z-c)(z-\overline{c})^{-k-1} + \gamma(z-\overline{c})^{-k}, \tag{4.58}$$

where $\alpha, \beta, \gamma, c \in \mathbb{C}$, $k \in \mathbb{N}$ and $\operatorname{Im} c < 0$. Substituting (4.58) into the general solution of the first fundamental problem for the half-plane (2.54), one obtains

$$\varphi_{\mathrm{SP0}}(z) = -\frac{1}{2\pi i}\int_{-\infty}^{\infty} \frac{\alpha(x-c)^{-k} + \beta(x-c)(x-\overline{c})^{-k-1} + \gamma(x-\overline{c})^{-k}}{x-z}\,\mathrm{d}x, \tag{4.59a}$$

$$\psi_{\mathrm{SP0}}(z) = -\frac{1}{2\pi i}\int_{-\infty}^{\infty} \frac{\overline{\alpha}(x-\overline{c})^{-k} + \overline{\beta}(x-\overline{c})(x-c)^{-k-1} + \overline{\gamma}(x-c)^{-k}}{x-z}\,\mathrm{d}x - z\varphi'_{\mathrm{SP0}}(z). \tag{4.59b}$$

The first and the last term in the integrand of both equations can be integrated using (4.34). The middle term in the first equation can be integrated by applying the residue theorem to the function $F_3(x) = \frac{(x-c)(x-\overline{c})^{-n}}{(x-z)}$, $n \in \mathbb{N}$ which is holomorphic on the lower half-plane except the point z where it has a simple pole. Similarly, form the application of the residue theorem to the function $F_4(x) = \frac{(x-\overline{c})(x-c)^{-n}}{(x-z)}$, $n \in \mathbb{N}$, which is holomorphic in the entire upper half-plane, follows that the integral of the middle term in the second equation vanishes. This gives

$$\varphi_{\mathrm{SP0}}(z) = \beta(z-c)(z-\overline{c})^{-k-1} + \gamma(z-\overline{c})^{-k}, \tag{4.60a}$$

$$\psi_{\mathrm{SP0}}(z) = \overline{\alpha}(z-\overline{c})^{-k} - \beta z(z-\overline{c})^{-k-1} + \beta(k+1)z(z-c)(z-\overline{c})^{-k-2} + \gamma k z(z-\overline{c})^{-k-1}. \tag{4.60b}$$

The second form comprised in the right-hand side of (4.53) is

$$f_{\mathrm{SPL}}(z) = A\ln(z-c) + \overline{B}\ln(z-\overline{c}) - \overline{A}\frac{c-\overline{c}}{z-\overline{c}}, \tag{4.61}$$

where $A, B, c \in \mathbb{C}$ and $\operatorname{Im} c < 0$. Analogously, substituting the function (4.61) into (2.55), one first obtains

$$\varphi'_{\mathrm{SPL}}(z) = -\frac{1}{2\pi i}\int_{-\infty}^{\infty} \frac{\frac{A}{x-c} + \frac{\overline{B}}{x-\overline{c}} + \overline{A}\frac{c-\overline{c}}{(x-\overline{c})^2}}{x-z}\,\mathrm{d}x, \tag{4.62a}$$

$$\psi'_{\mathrm{SPL}}(z) = -\frac{1}{2\pi i}\int_{-\infty}^{\infty} \frac{\frac{\overline{A}}{x-\overline{c}} + \frac{B}{x-c} - A\frac{c-\overline{c}}{(x-c)^2}}{x-z}\,\mathrm{d}x - \varphi'_{\mathrm{SPL}}(z) - z\varphi''_{\mathrm{SPL}}(z). \tag{4.62b}$$

By evaluating the integrals using the formulae (4.34), these equations become

$$\varphi'_{\mathrm{SPL}}(z) = \frac{\overline{B}}{z-\overline{c}} + \overline{A}\frac{c-\overline{c}}{(z-\overline{c})^2}, \tag{4.63a}$$

$$\psi'_{\mathrm{SPL}}(z) = \frac{A}{z-\overline{c}} + \varphi'_{\mathrm{SPL}}(z) + z\varphi''_{\mathrm{SPL}}(z) \tag{4.63b}$$

and carrying out the quadrature finally yields

$$\varphi_{\mathrm{SPL}}(z) = \overline{B}\ln(z-\overline{c}) - \overline{A}\frac{c-\overline{c}}{z-\overline{c}}, \tag{4.64a}$$

$$\psi_{\mathrm{SPL}}(z) = \overline{A}\ln(z-\overline{c}) - \overline{A}\frac{(c-\overline{c})z}{(z-\overline{c})^2} - \overline{B}\frac{\overline{c}}{z-\overline{c}}. \tag{4.64b}$$

Superposing the solutions (4.60) and (4.64) along with $\hat{\varphi}_0^n(z)$ and $\hat{\psi}_0^n(z)$, for the outer auxiliary functions one obtains

$$\begin{aligned}\varphi_0^n(z) = \hat{\varphi}_0^n(z) &- \sum_{q=1}^{N_H}\sum_{k=1}^{n}\left[-k\overline{a}_{qk}^{n-k}(z-c_q)(z-\overline{c}_q)^{-k-1} + \overline{b}_{qk}^{n-k}(z-\overline{c}_q)^{-k}\right] \\ &- \sum_{q=1}^{N_H}\left[\overline{B}_q^n\ln(z-\overline{c}_q) - \overline{A}_q^n\frac{c-\overline{c}_q}{z-\overline{c}_q}\right], \end{aligned}\tag{4.65a}$$

$$\begin{aligned}\psi_0^n(z) = \hat{\psi}_0^n(z) &- \sum_{q=1}^{N_H}\sum_{k=1}^{n}\left[\overline{a}_{qk}^{n-k}(z-\overline{c}_q)^{-k} + ka_{qk}^{n-k}z(z-\overline{c}_q)^{-k-1}\right. \\ &\left. - k(k+1)\overline{a}_{qk}^{n-k}z(z-c_q)(z-\overline{c}_q)^{-k-2} + k\overline{b}_{qk}^{n-k}z(z-\overline{c}_q)^{-k-1}\right] \\ &- \sum_{q=1}^{N_H}\left[\overline{A}_q^n\ln(z-\overline{c}_q) - \overline{A}_q^n\frac{(c-\overline{c}_q)z}{(z-\overline{c}_q)^2} - \overline{B}_q^n\frac{\overline{c}_q}{z-\overline{c}_q}\right]. \end{aligned}\tag{4.65b}$$

In the case of the full plane, the outer auxiliary functions only have to fulfil the stress conditions at infinity from which it follows immediately

$$\varphi_0^n(z) = \hat{\varphi}_0^n(z), \quad \psi_0^n(z) = \hat{\psi}_0^n(z). \tag{4.66}$$

Final form of the complex potentials

Once all auxiliary functions are determined for $n = 0, \ldots, N$ where N is a chosen order of approximation, they are substituted into the ansatz (4.46) delivering a solution

$$\varphi(z) = \sum_{n=0}^{N}\epsilon^n\left[\varphi_0^n(z) + \sum_{q=1}^{N_H}\left(\varphi_q^n\left(\frac{z-c_q}{\epsilon\rho_q}\right) + A_q^n\ln(z-c_q)\right)\right], \tag{4.67a}$$

$$\begin{aligned}\psi(z) = \sum_{n=0}^{N}\epsilon^n\Bigg[&\psi_0^n(z) + \sum_{q=1}^{N_H}\psi_q^n\left(\frac{z-c_q}{\epsilon\rho_q}\right) - \frac{\overline{c}_q}{\epsilon\rho_q}\frac{\mathrm{d}\varphi_q^n}{\mathrm{d}\zeta_q}\left(\frac{z-c_q}{\epsilon\rho_q}\right) \\ &+ \sum_{q=1}^{N_H}\left(B_q^n\ln(z-c_q) - \frac{A_q^n\overline{c}_q}{z-c_q}\right)\Bigg]\end{aligned}\tag{4.67b}$$

which is valid in the whole domain and satisfies all boundary conditions up to the order $N-1$. The potentials in the far-field can be obtained by truncating the series (4.52)

$$P^N\varphi(z) = \sum_{n=0}^{N} \epsilon^n \left[\varphi_0^n(z) + \sum_{q=1}^{N_H} \left(\sum_{k=1}^{n} a_{qk}^{n-k} \rho_q^k (z-c_q)^{-k} + A_q^n \ln(z-c_q) \right) \right], \tag{4.68a}$$

$$P^N\psi(z) = \sum_{n=0}^{N} \epsilon^n \left[\psi_0^n(z) + \sum_{q=1}^{N_H} \sum_{k=1}^{n} \rho_q^k \left(b_{qk}^{n-k} (z-c_q)^{-k} + \overline{c}_q a_{qk}^{n-k} k (z-c_q)^{-k-1} \right) + \sum_{q=1}^{N_H} \left(B_q^n \ln(z-c_q) - \frac{A_q^n \overline{c}_q}{z-c_q} \right) \right]. \tag{4.68b}$$

Similarly, in the vicinity of the pth hole, by truncating (4.49) and translating the potential ψ to the origin, one obtains

$$Q_p^N\varphi(\zeta_p) = \sum_{n=0}^{N} \epsilon^n \left[\varphi_p^n(\zeta_p) + \sum_{k=1}^{n} K_{pk}^n \zeta_p^k + A_p^n \ln \zeta_p \right], \tag{4.69a}$$

$$Q_p^N\psi(\zeta_p) = \sum_{n=0}^{N} \epsilon^n \left[\psi_p^n(\zeta_p) + \sum_{k=1}^{n} \left(L_{pk}^n \zeta_p^k + \frac{\overline{c}_p}{\rho_p} (k+1) K_{p,k+1}^{n+1} \right) \zeta_p^k + B_p^n \ln \zeta_p \right]. \tag{4.69b}$$

4.1.3 Plane stress in anisotropic plates

Boundary conditions

In the case of an anisotropic material, the problems of a circular and an elliptical hole in an infinite plane are equally difficult. Therefore, the more general problem of elliptic holes is considered in this section. The plane is weakened by N_H elliptical holes positioned at points c_p, $p = 1, \ldots, N_H$, see Figure 4.5. It is for simplicity assumed that the principal axes of all holes are parallel to each other. Due to the central assumption of small holes, the major and minor semi-axes of the pth hole can be designated by $\epsilon\rho_p$ and $\epsilon m_p \rho_p$, respectively, where ρ_p is the relative size of the hole and m_p its aspect ratio, both being of the order $O(\epsilon^0)$.

In addition to the variables z and ζ_p, introduced in the beginning of this section, their affine transformations z_j and

$$\zeta_{pj} = \frac{z_j - c_{pj}}{\epsilon\rho_p} \tag{4.70}$$

are used, where $c_{pj} = \operatorname{Re} c_p + \mu_j \operatorname{Im} c_p$ is the affine transformation of the centre of the pth hole. The relation between two local transformed coordinates corresponding to two different holes p and q is

$$\zeta_{qj} = \frac{\rho_p}{\rho_q} \zeta_{pj} + \frac{c_{pj} - c_{qj}}{\epsilon\rho_q}. \tag{4.71}$$

Furthermore, the conformal mapping w which maps the exterior of the pth ellipse in the ζ_{pj}-plane onto the exterior of the unit circle in the w-plane is defined by the equation

$$\zeta_{pj} = \frac{1 - m_p i \mu_j}{2} w + \frac{1 + m_p i \mu_j}{2} \frac{1}{w}. \tag{4.72}$$

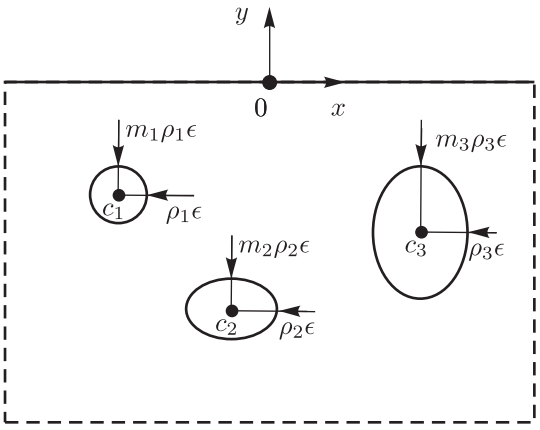

Figure 4.5: A half-plane weakened by a finite number of elliptical holes ($N_H = 3$).

Its inversion reads

$$w = \frac{\zeta_{pj} \pm \sqrt{\zeta_{pj}^2 - 1 - m_p^2\mu_j^2}}{1 - m_p i\mu_j}, \tag{4.73}$$

where the sign of the square root has to be chosen according to the condition $|w| \geq 1$.

The boundary condition on the pth hole is formulated in terms of the resultant force (2.64) as

$$f_{px}(\theta) = \sum_{n=0}^{\infty} f_{px}^n(\theta)\epsilon^n, \quad f_{py}(\theta) = \sum_{n=0}^{\infty} f_{py}^n(\theta)\epsilon^n, \tag{4.74}$$

the total resultant force corresponding to the term $f_{px}^n(\theta)$ and $f_{py}^n(\theta)$ being

$$F_p^n = F_{px}^n + iF_{py}^n = [f_{px}^n(\theta)]_0^{2\pi} + i[f_{py}^n(\theta)]_0^{2\pi}. \tag{4.75}$$

The functions f_{px}^{*n} and f_{py}^{*n} are defined analogously to (2.70) as

$$f_{px}^{*n}(\theta) = f_{px}^n(\theta) + 2\,\mathrm{Re}\sum_{j=1}^{2} \mu_j A_{pj}^n \ln\zeta_j, \tag{4.76a}$$

$$f_{py}^{*n}(\theta) = f_{py}^n(\theta) - 2\,\mathrm{Re}\sum_{j=1}^{2} A_{pj}^n \ln\zeta_j, \tag{4.76b}$$

where the constants $A_{pj}^n \in \mathbb{C}$, $p = 1, \ldots, N_H$, $n \in \mathbb{N}_0$, $j = 1, 2$, are determined by the resultant forces F_p^n via equations (2.69). The solution of the problem of a single hole in an infinite plate under zero stresses at infinity and boundary loads $f_{px}^n(\theta)$ and $f_{py}^n(\theta)$ are denoted $\hat{\varphi}_{pj}^n(\zeta_p)$.

Furthermore, in the case of the half-plane, the load

$$f_{x0}^n(x) = \sum_{n=0}^{\infty} f_{x0}^n(x)\epsilon^n, \quad f_{y0}^n(x) = \sum_{n=0}^{\infty} f_{y0}^n(x)\epsilon^n \tag{4.77}$$

of the line $y = 0$ and the state of stress at infinity are prescribed as in the isotropic case. The solution of the problem for a half-plane or a full plane without holes satisfying these conditions is denoted by $\hat{\varphi}_{0j}^n(z_j)$.

Ansatz for the complex potentials

The solution is searched for in the form

$$\varphi_j = \sum_{n=0}^{\infty} \epsilon^n \left[\varphi_{0j}^n(z_j) + \sum_{q=1}^{N_H} \Big(\varphi_{qj}^n(\zeta_{qj}) + A_{qj}^n \ln \zeta_{qj} \Big) \right], \tag{4.78}$$

where $\varphi_{qj}^n(\zeta_{qj})$, $n \in \mathbb{N}_0$, $q = 1, \ldots, N_H$, $j = 1, 2$, are inner auxiliary functions defined on the exterior of the qth ellipse and $\varphi_{0j}^n(z_j)$, $n \in \mathbb{N}_0$, $j = 1, 2$, are outer auxiliary functions defined on the full plane or the lower half-plane. All auxiliary functions are holomorphic and single-valued in their domains of definition and produce zero stresses at infinity. The logarithmic terms in (4.78) correspond to the general structure of the complex potentials in a multiply connected domain.

The inner auxiliary functions allow the following expansion at infinity:

$$\varphi_{qj}^n(\zeta_{qj}) = \sum_{k=1}^{\infty} a_{qjk}^n \zeta_{qj}^{-k}, \tag{4.79}$$

while the outer auxiliary functions allow the following expansions at the points c_{pj}:

$$\varphi_{0j}^n(z_j) = \sum_{k=0}^{\infty} d_{pjk}^n (z_j - c_{pj})^k. \tag{4.80}$$

Subproblems for the auxiliary functions

Similarly as in Section 4.1.1, it can be shown that

$$\varphi_j(\zeta_{pj}) = \sum_{n=0}^{\infty} \epsilon^n \left[\varphi_{pj}^n(\zeta_{pj}) + \sum_{k=1}^{n} K_{pjk}^n \zeta_{pj}^k + A_{pj}^n \ln \zeta_{pj} \right], \tag{4.81}$$

where the coefficients K_{pjk}^n are given by

$$K_{pjk}^n = \rho_p^k \left[d_{pjk}^{n-k} + \sum_{\substack{q=1 \\ q \neq p}}^{N_H} \sum_{l=1}^{n-k} a_{qjl}^{n-k-l} \binom{-l}{k} \rho_q^l (c_{pj} - c_{qj})^{-k-l} + \sum_{\substack{q=1 \\ q \neq p}}^{N_H} A_{qj}^{n-k} \frac{(-1)^{k+1}}{k} (c_{pj} - c_{qj})^{-k} \right]. \tag{4.82}$$

Substituting equations (4.81) into the boundary conditions on the pth hole (4.76) yields the conditions for the inner auxiliary functions on the boundary of the unit elliptical hole

$w(\zeta_{pj}) = e^{i\theta}$

$$2\,\mathrm{Re}\sum_{j=1}^{2}\mu_j\varphi_{pj}^{n}(\zeta_{pj}) = -f_{px}^{*n}(\theta) - 2\,\mathrm{Re}\sum_{j=1}^{2}\mu_j\sum_{k=1}^{n}K_{pjk}^{n}\zeta_{pj}^{k}, \tag{4.83a}$$

$$2\,\mathrm{Re}\sum_{j=1}^{2}\varphi_{pj}^{n}(\zeta_{pj}) = f_{py}^{*n}(\theta) - 2\,\mathrm{Re}\sum_{j=1}^{2}\sum_{k=1}^{n}K_{pjk}^{n}\zeta_{pj}^{k}. \tag{4.83b}$$

As for the condition on the boundary of the half-plane, it can be shown by a procedure analogous to that used in Section 4.1.1 that

$$\varphi_j(z_j) = \sum_{n=0}^{\infty}\epsilon^n\left[\varphi_{0j}^{n}(z_j) + \sum_{q=1}^{N_H}\left(\sum_{k=1}^{n}a_{qjk}^{n-k}\rho_q^k(z_j - c_{qj})^{-k} + A_{qj}^{n}\ln(z_j - c_{qj})\right)\right] \tag{4.84}$$

which after substitution into the boundary condition on the edge of the half-plane leads to the following boundary conditions on $z_j = x$:

$$\begin{aligned}2\,\mathrm{Re}\sum_{j=1}^{2}\mu_j\varphi_{0j}^{n}(z_j) &= f_{0x}^{n}(x)\\ &\quad - 2\,\mathrm{Re}\sum_{j=1}^{2}\mu_j\sum_{q=1}^{N_H}\left[\sum_{k=1}^{n}a_{qjk}^{n-k}\rho_q^k(z_j - c_{qj})^{-k} + A_{qj}^{n}\ln(z - c_{qj})\right],\end{aligned} \tag{4.85a}$$

$$\begin{aligned}2\,\mathrm{Re}\sum_{j=1}^{2}\varphi_{0j}^{n}(z_j) &= -f_{0y}^{n}(x)\\ &\quad - 2\,\mathrm{Re}\sum_{j=1}^{2}\sum_{q=1}^{N_H}\left[\sum_{k=1}^{n}a_{qjk}^{n-k}\rho_q^k(z_j - c_{qj})^{-k} + A_{qj}^{n}\ln(z - c_{qj})\right].\end{aligned} \tag{4.85b}$$

Solution of the subproblems

The right-hand side of the boundary condition (4.83) is a superposition of the functions $f_{px}^{*n}(\theta)$ and $f_{py}^{*n}(\theta)$ and functions of the form

$$f_{x,\mathrm{SPp}}(\zeta_{pj}) = -2\,\mathrm{Re}\sum_{j=1}^{2}\mu_j\alpha_j\zeta_{pj}^{k}, \qquad f_{y,\mathrm{SPp}}(\zeta_{pj}) = 2\,\mathrm{Re}\sum_{j=1}^{2}\alpha_j\zeta_{pj}^{k}, \tag{4.86}$$

where $\alpha_j \in \mathbb{C}$, j=1,2. Substituting this function into the general solution of the first boundary value problem for an ellipse (2.71) leads to

$$\varphi_{1,\mathrm{SPp}}(w) = \frac{1}{\mu_1 - \mu_2}\frac{1}{2\pi i}\sum_{j=1}^{2}\int_{\gamma}\frac{(\mu_2 - \mu_j)\alpha_j\zeta_{pj}^{k}(\sigma) + (\mu_2 - \overline{\mu}_j)\overline{\alpha}_j\overline{\zeta}_{pj}^{k}\left(\frac{1}{\sigma}\right)}{\sigma - w}\,\mathrm{d}\sigma, \tag{4.87a}$$

$$\varphi_{2,\mathrm{SPp}}(w) = -\frac{1}{\mu_1 - \mu_2}\frac{1}{2\pi i}\sum_{j=1}^{2}\int_{\gamma}\frac{(\mu_1 - \mu_j)\alpha_j\zeta_{pj}^{k}(\sigma) + (\mu_1 - \overline{\mu}_j)\overline{\alpha}_j\overline{\zeta}_{pj}^{k}\left(\frac{1}{\sigma}\right)}{\sigma - w}\,\mathrm{d}\sigma. \tag{4.87b}$$

Substituting the relation (4.72) into the above equations and expanding the powers by means of the binomial theorem, these equations become

$$\varphi_{1,\mathrm{SPp}}(w) = \frac{1}{\mu_1-\mu_2}\frac{1}{2\pi i}\sum_{j=1}^{2}\left[\int_\gamma \frac{(\mu_2-\mu_j)\alpha_j \sum_{l=0}^{k}\binom{k}{l}\left(\frac{1+m_p i\mu_j}{2}\right)^l\left(\frac{1-m_p i\mu_j}{2}\right)^{k-l}\sigma^{k-2l}}{\sigma-w}\,\mathrm{d}\sigma \right.$$
$$\left. + \int_\gamma \frac{(\mu_2-\overline{\mu}_j)\overline{\alpha}_j \sum_{l=0}^{k}\binom{k}{l}\left(\frac{1-m_p i\mu_j}{2}\right)^l\left(\frac{1+m_p i\mu_j}{2}\right)^{k-l}\sigma^{k-2l}}{\sigma-w}\,\mathrm{d}\sigma\right], \quad (4.88a)$$

$$\varphi_{2,\mathrm{SPp}}(w) = -\frac{1}{\mu_1-\mu_2}\frac{1}{2\pi i}\sum_{j=1}^{2}\left[\int_\gamma \frac{(\mu_1-\mu_j)\alpha_j \sum_{l=0}^{k}\binom{k}{l}\left(\frac{1+m_p i\mu_j}{2}\right)^l\left(\frac{1-m_p i\mu_j}{2}\right)^{k-l}\sigma^{k-2l}}{\sigma-w}\,\mathrm{d}\sigma \right.$$
$$\left. + \int_\gamma \frac{(\mu_1-\overline{\mu}_j)\overline{\alpha}_j \sum_{l=0}^{k}\binom{k}{l}\left(\frac{1-m_p i\mu_j}{2}\right)^l\left(\frac{1+m_p i\mu_j}{2}\right)^{k-l}\sigma^{k-2l}}{\sigma-w}\,\mathrm{d}\sigma\right]. \quad (4.88b)$$

Evaluating these integrals by means of the formula (4.34) yields

$$\varphi_{1,\mathrm{SPp}}(w) = -\frac{1}{2^k(\mu_1-\mu_2)}\sum_{j=1}^{2}\sum_{l=\lceil\frac{k+1}{2}\rceil}^{k}\binom{k}{l}\Big[(\mu_2-\mu_j)\alpha_j(1+m_p i\mu_j)^l(1-m_p i\mu_j)^{k-l}$$
$$+ (\mu_2-\overline{\mu}_j)\overline{\alpha}_j(1-m_p i\mu_j)^l(1+m_p i\mu_j)^{k-l}\Big]w^{k-2l}, \quad (4.89a)$$

$$\varphi_{2,\mathrm{SPp}}(w) = \frac{1}{2^k(\mu_1-\mu_2)}\sum_{j=1}^{2}\sum_{l=\lceil\frac{k+1}{2}\rceil}^{k}\binom{k}{l}\Big[(\mu_1-\mu_j)\alpha_j(1+m_p i\mu_j)^l(1-m_p i\mu_j)^{k-l}$$
$$+ (\mu_1-\overline{\mu}_j)\overline{\alpha}_j(1-m_p i\mu_j)^l(1+m_p i\mu_j)^{k-l}\Big]w^{k-2l}, \quad (4.89b)$$

where $\lceil..\rceil$ denotes the ceiling function. Superposing the solutions corresponding to each term of the right-hand side of the boundary condition (4.83) finally gives

$$\varphi_{p1}^n(w) = \hat{\varphi}_{p1}^n(w)$$
$$-\sum_{k=1}^{n}\frac{1}{2^k(\mu_1-\mu_2)}\sum_{j=1}^{2}\sum_{l=\lceil\frac{k+1}{2}\rceil}^{k}\binom{k}{l}\Big[(\mu_2-\mu_j)K_{pjk}^n(1+m_p i\mu_j)^l(1-m_p i\mu_j)^{k-l}$$
$$+ (\mu_2-\overline{\mu}_j)\overline{K}_{pjk}^{\,n}(1-m_p i\mu_j)^l(1+m_p i\mu_j)^{k-l}\Big]w^{k-2l}, \quad (4.90a)$$

$$\varphi_{p2}^n(w) = \hat{\varphi}_{p2}^n(w)$$
$$+\frac{1}{2^k(\mu_1-\mu_2)}\sum_{j=1}^{2}\sum_{l=\lceil\frac{k+1}{2}\rceil}^{k}\binom{k}{l}\Big[(\mu_1-\mu_j)K_{pjk}^n(1+m_p i\mu_j)^l(1-m_p i\mu_j)^{k-l}$$
$$+ (\mu_1-\overline{\mu}_j)\overline{K}_{pjk}^{\,n}(1-m_p i\mu_j)^l(1+m_p i\mu_j)^{k-l}\Big]w^{k-2l}. \quad (4.90b)$$

The right-hand side of the boundary condition (4.85) is a linear combination of functions $f_{0x}^n(x)$ and $f_{0y}^n(x)$ and of functions of two different kinds. The first of them is

$$f_{x,\mathrm{SP0}}(z_j) = 2\,\mathrm{Re}\sum_{j=1}^{2}\mu_j\alpha_j(z_j-c_j)^{-k}, \qquad f_{y,\mathrm{SP0}}(z_j) = -2\,\mathrm{Re}\sum_{j=1}^{2}\alpha_j(z_j-c_j)^{-k}, \quad (4.91)$$

where the constants $\alpha_j, c_j \in \mathbb{C}$ and $\mathrm{Im}\,c_j < 0$. Evaluating the general solution of the first fundamental problem for the half-plane (2.75) for the above right-hand side yields

$$\varphi_{1,\mathrm{SP0}}(z_1) = -\frac{1}{\mu_1-\mu_2}\frac{1}{2\pi i}\sum_{j=1}^{2}\left(\int_{-\infty}^{\infty}\frac{\mu_j\alpha_j(x-c_j)^{-k}+\overline{\mu}_j\overline{\alpha}_j(x-\overline{c}_j)^{-k}}{x-z_1}\,\mathrm{d}x \right.$$
$$\left. -\int_{-\infty}^{\infty}\frac{\mu_2\alpha_j(x-c_j)^{-k}+\mu_2\overline{\alpha}_j(x-\overline{c}_j)^{-k}}{x-z_1}\,\mathrm{d}x\right), \quad (4.92a)$$

$$\varphi_{2,\mathrm{SP0}}(z_2) = \frac{1}{\mu_1-\mu_2}\frac{1}{2\pi i}\sum_{j=1}^{2}\left(\int_{-\infty}^{\infty}\frac{\mu_j\alpha_j(x-c_j)^{-k}+\overline{\mu}_j\overline{\alpha}_j(x-\overline{c}_j)^{-k}}{x-z_2}\,\mathrm{d}x \right.$$
$$\left. -\int_{-\infty}^{\infty}\frac{\mu_1\alpha_j(x-c_j)^{-k}+\mu_1\overline{\alpha}_j(x-\overline{c}_j)^{-k}}{x-z_2}\,\mathrm{d}x\right) \quad (4.92b)$$

and evaluating the integrals involved in these equations by means of (4.34) leads to

$$\varphi_{1,\mathrm{SP0}}(z_1) = \sum_{j=1}^{2}\frac{\overline{\mu}_j-\mu_2}{\mu_1-\mu_2}\overline{\alpha}_j(z_1-\overline{c}_j)^{-k}, \quad (4.93a)$$

$$\varphi_{2,\mathrm{SP0}}(z_2) = -\sum_{j=1}^{2}\frac{\overline{\mu}_j-\mu_1}{\mu_1-\mu_2}\overline{\alpha}_j(z_2-\overline{c}_j)^{-k}. \quad (4.93b)$$

The second form involved in the boundary condition (4.85) is

$$f_{x,\mathrm{SPL}}(z_j) = 2\,\mathrm{Re}\sum_{j=1}^{2}\mu_jA_j\ln(z_j-c_j), \qquad f_{y,\mathrm{SPL}}(z_j) = -2\,\mathrm{Re}\sum_{j=1}^{2}A_j\ln(z_j-c_j), \quad (4.94)$$

where $A_j, c_j \in \mathbb{C}$ and $\mathrm{Im}\,c_j < 0$. The general solution of the first fundamental problem for the half-plane (2.76) gives

$$\varphi'_{1,\mathrm{SPL}}(z_1) = \frac{1}{\mu_1-\mu_2}\frac{1}{2\pi i}\sum_{j=1}^{2}\int_{-\infty}^{\infty}\frac{\frac{\mu_jA_j}{x-c_j}+\frac{\overline{\mu}_j\overline{A}_j}{x-\overline{c}_j}-\frac{\mu_2A_j}{x-c_j}-\frac{\mu_2\overline{A}_j}{x-\overline{c}_j}}{x-z_1}\,\mathrm{d}x, \quad (4.95a)$$

$$\varphi'_{2,\mathrm{SPL}}(z_2) = -\frac{1}{\mu_1-\mu_2}\frac{1}{2\pi i}\sum_{j=1}^{2}\int_{-\infty}^{\infty}\frac{\frac{\mu_jA_j}{x-c_j}+\frac{\overline{\mu}_j\overline{A}_j}{x-\overline{c}_j}-\frac{\mu_1A_j}{x-c_j}-\frac{\mu_1\overline{A}_j}{x-\overline{c}_j}}{x-z_2}\,\mathrm{d}x. \quad (4.95b)$$

Evaluating the integrals involved in these equations by means of (4.34) and integrating with respect to z leads to

$$\varphi_{1,\mathrm{SPL}}(z_1) = \sum_{j=1}^{2}\frac{\overline{\mu}_j-\mu_2}{\mu_1-\mu_2}\overline{A}_j\ln(z_1-\overline{c}_j), \quad (4.96a)$$

$$\varphi_{2,\mathrm{SPL}}(z_2) = -\sum_{j=1}^{2}\frac{\overline{\mu}_j-\mu_1}{\mu_1-\mu_2}\overline{A}_j\ln(z_2-\overline{c}_j). \quad (4.96b)$$

Superposing the solutions corresponding to each term on the right-hand side of the boundary condition (4.85) finally yields

$$\varphi_{01}^n(z_1) = \hat{\varphi}_{01}^n(z_1) - \sum_{j=1}^{2} \frac{\overline{\mu}_j - \mu_2}{\mu_1 - \mu_2} \sum_{q=1}^{N_H} \left[\sum_{k=1}^{n} \overline{a}_{qjk}^{n-k} \rho_q^k (z_1 - \overline{c}_{qj})^{-k} + \overline{A}_{qj}^{n} \ln(z_1 - \overline{c}_{qj}) \right], \quad (4.97a)$$

$$\varphi_{02}^n(z_2) = \hat{\varphi}_{02}^n(z_2) - \sum_{j=1}^{2} \frac{\overline{\mu}_j - \mu_1}{\mu_2 - \mu_1} \sum_{q=1}^{N_H} \left[\sum_{k=1}^{n} \overline{a}_{qjk}^{n-k} \rho_q^k (z_2 - \overline{c}_{qj})^{-k} + \overline{A}_{qj}^{n} \ln(z_2 - \overline{c}_{qj}) \right]. \quad (4.97b)$$

In the case of the full plane, the outer auxiliary functions are trivially given as

$$\varphi_{0j}^n(z_j) = \hat{\varphi}_{0j}^n(z_j). \quad (4.98)$$

The formulae (4.90) and (4.97) represent an explicit iterative algorithm to determine the auxiliary functions.

Final form of the complex potentials

The solution

$$\varphi_j(z_j) = \sum_{n=0}^{N} \epsilon^n \left[\varphi_{0j}^n(z_j) + \sum_{q=1}^{N_H} \left(\varphi_{qj}^n \left(\frac{z_j - c_{qj}}{\epsilon \rho_q} \right) + A_{qj}^n \ln(z_j - c_{qj}) \right) \right] \quad (4.99)$$

is valid in the whole domain and satisfies all boundary conditions up to the order $N-1$. The potentials in the far-field can be obtained by truncating the series (4.84)

$$P^N \varphi_j(z_j) = \sum_{n=0}^{N} \epsilon^n \left[\varphi_{0j}^n(z_j) + \sum_{q=1}^{N_H} \left(\sum_{k=1}^{n} a_{qjk}^{n-k} \rho_q^k (z_j - c_{qj})^{-k} + A_{qj}^n \ln(z_j - c_{qj}) \right) \right]. \quad (4.100)$$

In the vicinity of the pth hole by truncating (4.81) the following result is obtained:

$$Q^N \varphi_j(\zeta_{pj}) = \sum_{n=0}^{N} \epsilon^n \left[\varphi_{pj}^n(\zeta_{pj}) + \sum_{k=1}^{n} K_{pjk}^n \zeta_{pj}^k + A_{pj}^n \ln(\zeta_{pj}) \right]. \quad (4.101)$$

4.2 Full plane or half-plane containing an infinite array of holes

The results of the previous section can easily be extended to the case of an infinite symmetric array of holes. It is assumed that all the holes can be divided into a finite number N_C of categories, so that all inner auxiliary functions corresponding to holes of the same category are equal because of symmetry. Thus, despite the infinite number of holes, the number of unknown auxiliary functions remains finite. The number of holes in one category can be either finite or infinite. In this work, for simplicity, only the latter case is considered.

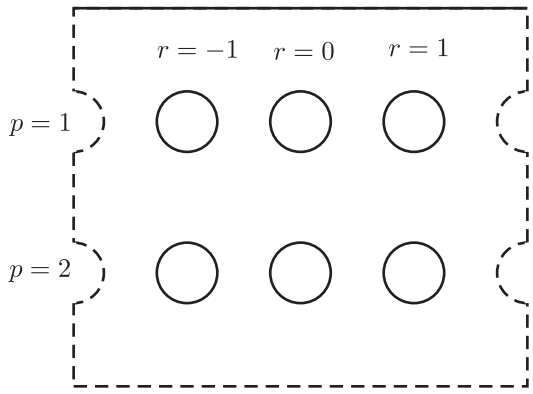

Figure 4.6: Numbering of the holes in an infinite array: index p denotes the number of the category, index r the position of the hole in the category.

The centres of the holes are denoted by c_{pr} where, in contrast to Section 4.1, the index p, $p = 1, \ldots, N_C$, refers to the category whereas the index r, $r \in \mathbb{Z}$, refers to the position of the hole in the category (see Figure 4.6).

Due to the given symmetry, the coefficients d^n_{pk}, e^n_{pk} and d^n_{pjk} can be defined by a Laurent series expansion of the outer auxiliary potentials at any hole of the pth category. Therefore, $r = 0$ can be chosen without loss of generality. For future use, the coefficients

$$S^1_{pqk} = \sum_{r=-\infty}^{\infty}{}' (c_{p0} - c_{qr})^{-k} \tag{4.102}$$

and functions

$$T^1_{qk}(z) = \sum_{r=-\infty}^{\infty}{}' (z - c_{qr})^{-k}, \tag{4.103a}$$

$$T^2_q(z) = \sum_{r=-\infty}^{\infty}{}' \ln(z - c_{qr}) \tag{4.103b}$$

are defined, where the doubly infinite sums denoted by an apostrophe are defined as

$$\sum_{r=-\infty}^{\infty}{}' a_r = a_0 + \sum_{r=1}^{\infty} (a_r + a_{-r}) \tag{4.104}$$

and all terms involving negative powers or a logarithm of zero are excluded from summation. Furthermore, the sums that do not converge in the classical sense are understood as

$$\sum_{r=-\infty}^{\infty}{}' a_r(z) = \int \left(\sum_{r=-\infty}^{\infty}{}' a'_r(z) \right) \mathrm{d}z. \tag{4.105}$$

The transition from finite systems of holes to infinite arrays is achieved by formally replacing the sum over all holes $\sum_{q=1}^{N_H}$ by the double sum $\sum_{q=1}^{N_C} \sum_{r=-\infty}^{\infty}$ in each equation of Section 4.1.

4.2.1 Antiplane strain

By means of the substitution described above, the equation (4.19) becomes

$$K_{pk}^{n} = \rho_p^k \left[d_{pk}^{n-k} + \sum_{q=1}^{N_C} \left(\sum_{l=1}^{n-k} a_{ql}^{n-k-l} \binom{-l}{k} \rho_q^l S_{pq,k+l}^1 + A_q^{n-k} \frac{(-1)^{k+1}}{k} S_{pqk}^1 \right) \right], \tag{4.106}$$

equation (4.36) transforms to

$$\varphi_0^n(z) = \hat{\varphi}_0^n(z) + \sum_{q=1}^{N_C} \left(\sum_{k=1}^{n} \overline{a}_{qk}^{n-k} \rho_q^k \overline{T}_{qk}^1(z) + \sum_{q=1}^{N_C} \overline{A}_q^n \overline{T}_q^2(z) \right) \tag{4.107}$$

and finally equation (4.39) takes the form

$$P^N \varphi(z) = \sum_{n=0}^{N} \epsilon^n \left[\varphi_0^n(z) + \sum_{q=1}^{N_C} \left(\sum_{k=1}^{n} a_{qk}^{n-k} \rho_q^k T_{qk}^1(z) + A_q^n T_q^2(z) \right) \right]. \tag{4.108}$$

In many practically relevant cases the Laurent series expansion of the inner auxiliary functions (4.11) only contains a finite number M of terms. In these cases, the equation (4.38) can be expressed as

$$\varphi(z) = \sum_{n=0}^{N} \epsilon^n \left[\varphi_0^n(z) + \sum_{q=1}^{N_C} \left(\sum_{k=1}^{M} a_{qk}^n (\epsilon \rho_q)^k T_{qk}^1(z) + A_q^n T_q^2(z) \right) \right]. \tag{4.109}$$

All other steps of the procedure described in Section 4.1.1 remain unchanged.

4.2.2 Plane stress and strain in isotropic plates

In addition to the definitions made in the beginning of this section, the following designations are used in this subsection:

$$S_{pqk}^2 = \sum_{r=-\infty}^{\infty}{}' \overline{c}_{qr} (c_{p0} - c_{qr})^{-k}, \tag{4.110a}$$

$$T_{qk}^3(z) = \sum_{r=-\infty}^{\infty}{}' (z - c_{qr})(z - \overline{c}_{qr})^{-k}, \tag{4.110b}$$

$$T_{qk}^4(z) = \sum_{r=-\infty}^{\infty}{}' (c_{qr} - \overline{c}_{qr})(z - \overline{c}_{qr})^{-k}, \tag{4.110c}$$

$$T_{qk}^5(z) = \sum_{r=-\infty}^{\infty}{}' \overline{c}_{qr} (z - \overline{c}_{qr})^{-k}, \tag{4.110d}$$

$$T_{qk}^6(z) = \sum_{r=-\infty}^{\infty}{}' \overline{c}_{qr} (z - c_{qr})^{-k}. \tag{4.110e}$$

Proceeding as described in the beginning of this section, equations (4.50) become

$$K_{pk}^n = \rho_p^k \left[d_{pk}^{n-k} + \sum_{q=1}^{N_C} \left(\sum_{l=1}^{n-k} a_{ql}^{n-k-l} \binom{-l}{k} \rho_q^l S_{pq,k+l}^1 + A_q^{n-k} \frac{(-1)^{k+1}}{k} S_{pqk}^1 \right) \right], \tag{4.111a}$$

$$L_{pk}^n = \rho_p^k \left[e_{pk}^{n-k} + \sum_{q=1}^{N_C} \sum_{l=1}^{n-k} \binom{-l}{k} \rho_q^l \left(b_{ql}^{n-k-l} S_{pq,k+l}^1 + a_{ql}^{n-k-l} (k+l) S_{pq,k+l+1}^2 \right) + \sum_{q=1}^{N_C} (-1)^{k+1} \left(\frac{B_q^{n-k}}{k} S_{pqk}^1 + A_q^{n-k} S_{pq,k+1}^2 \right) \right], \tag{4.111b}$$

equations (4.65) take the form

$$\varphi_0^n(z) = \hat{\varphi}_0^n(z) - \sum_{q=1}^{N_C} \sum_{k=1}^{n} \left[-k \overline{a}_{qk}^{n-k} T_{q,k+1}^3(z) + \overline{b}_{qk}^{n-k} \overline{T}_{qk}^1(z) \right] - \sum_{q=1}^{N_C} \left[\overline{B}_q^n \overline{T}_q^2(z) - \overline{A}_q^n T_{q1}^4(z) \right], \tag{4.112a}$$

$$\psi_0^n(z) = \hat{\psi}_0^n(z) - \sum_{q=1}^{N_C} \sum_{k=1}^{n} \left[\overline{a}_{qk}^{n-k} \overline{T}_{qk}^1(z) + k a_{qk}^{n-k} z \overline{T}_{q,k+1}^1(z) - k(k+1) \overline{a}_{qk}^{n-k} z T_{q,k+2}^3(z) + k \overline{b}_{qk}^{n-k} z \overline{T}_{q,k+1}^1(z) \right] - \sum_{q=1}^{N_C} \left[\overline{A}_q^n \overline{T}_{qk}^2(z) - \overline{A}_q^n z T_{q2}^4(z) - \overline{B}_q^n T_{q1}^5(z) \right]. \tag{4.112b}$$

and equations (4.68) become

$$P^N \varphi(z) = \sum_{n=0}^{N} \epsilon^n \left[\varphi_0^n(z) + \sum_{q=1}^{N_C} \left(\sum_{k=1}^{n} a_{qk}^{n-k} \rho_q^k T_{qk}^1(z) + A_q^n T_q^2(z) \right) \right], \tag{4.113a}$$

$$P^N \psi(z) = \sum_{n=0}^{N} \epsilon^n \left[\psi_0^n(z) + \sum_{q=1}^{N_C} \sum_{k=1}^{n} \rho_q^k \Big(b_{qk}^{n-k} T_{qk}^1(z) + k a_{qk}^{n-k} T_{q,k+1}^6(z) \Big) + \sum_{q=1}^{N_C} \Big(B_q^n T_q^2(z) - A_q^n T_{q1}^6(z) \Big) \right]. \tag{4.113b}$$

If the Laurent series expansion of the inner auxiliary functions (4.47) only comprises a finite number of terms M, equations (4.67) become

$$\varphi(z) = \sum_{n=0}^{N} \epsilon^n \left[\varphi_0^n(z) + \sum_{q=1}^{N_C} \left(\sum_{k=1}^{M} \epsilon^k \rho_q^k a_{qk}^n T_{qk}^1(z) + A_q^n T_q^2(z) \right) \right], \tag{4.114a}$$

$$\psi(z) = \sum_{n=0}^{N} \epsilon^n \left[\psi_0^n(z) + \sum_{q=1}^{N_C} \sum_{k=1}^{M} \epsilon^k \rho_q^k \Big(b_{qk}^n T_{qk}^1(z) + k a_{qk}^n T_{q,k+1}^6(z) \Big) + \sum_{q=1}^{N_C} \Big(B_q^n T_q^2(z) - A_q^n T_{q1}^6(z) \Big) \right]. \tag{4.114b}$$

All other steps described in Section 4.1.2 remain unchanged.

4.2.3 Plane stress in anisotropic plates

In addition to the definitions made in the beginning of this section, the affine transformations of the points c_{pr} denoted by c_{prj} and the sums

$$S^1_{pqjk} = \sum_{r=-\infty}^{\infty}{}' (c_{p0j} - c_{qrj})^{-k}, \tag{4.115a}$$

$$T^1_{qjk}(z_j) = \sum_{r=-\infty}^{\infty}{}' (z_j - c_{qrj})^{-k}, \tag{4.115b}$$

$$T^2_{qj}(z_j) = \sum_{r=-\infty}^{\infty}{}' \ln(z_j - c_{qrj}) \tag{4.115c}$$

are introduced, where the doubly infinite sums are defined as in the beginning of this section.

By formally replacing the sum over all holes $\sum_{q=1}^{N_H}$ by the double sum $\sum_{q=1}^{N_C}\sum_{r=-\infty}^{\infty}$, the equation (4.82) becomes

$$K^n_{pjk} = \rho_p^k \left[d^{n-k}_{pjk} + \sum_{q=1}^{N_C}\sum_{l=1}^{n-k} a^{n-k-l}_{qjl} \binom{-l}{k} \rho_q^l S^1_{pqj,k+l} + \sum_{q=1}^{N_C} \frac{(-1)^{k+1}}{k} A^{n-k}_{qj} S^1_{pqjk} \right], \tag{4.116}$$

equations (4.97) become

$$\varphi^n_{01}(z_1) = \hat{\varphi}^n_{01}(z_1) - \sum_{j=1}^{2} \frac{\overline{\mu}_j - \mu_2}{\mu_1 - \mu_2} \sum_{q=1}^{N_C} \left[\sum_{k=1}^{n} \overline{a}^{n-k}_{qjk} \rho_q^k \overline{T}^1_{qjk}(z_1) + \overline{A}^n_{qj} \overline{T}^2_{qj}(z_1) \right], \tag{4.117a}$$

$$\varphi^n_{02}(z_2) = \hat{\varphi}^n_{02}(z_2) - \sum_{j=1}^{2} \frac{\overline{\mu}_j - \mu_1}{\mu_2 - \mu_1} \sum_{q=1}^{N_C} \left[\sum_{k=1}^{n} \overline{a}^{n-k}_{qjk} \rho_q^k \overline{T}^1_{qjk}(z_2) + \overline{A}^n_{qj} \overline{T}^2_{qj}(z_2) \right], \tag{4.117b}$$

equation (4.100) can be expressed as

$$P^N \varphi_j(z_j) = \sum_{n=0}^{N} \epsilon^n \left[\varphi^n_{0j}(z_j) + \sum_{q=1}^{N_C} \left(\sum_{k=1}^{n} b^{n-k}_{qjk} \rho_q^k T^1_{qjk}(z_j) + A^n_{qj} T^2_{qj}(z_j) \right) \right]. \tag{4.118}$$

and finally equation (4.99) takes the form

$$\varphi_j(z_j) = \sum_{n=0}^{N} \epsilon^n \left[\varphi^n_{0j}(z_j) + \sum_{q=1}^{N_C} \left(\sum_{r=-\infty}^{\infty} \varphi^n_{qj} \left(\frac{z_j - c_{qrj}}{\epsilon \rho_q} \right) + A^n_{qj} T^2_{qj}(z_j) \right) \right]. \tag{4.119}$$

All other steps of Section 4.1.3 remain unchanged.

4.3 Implementation

The evaluation of the solutions for finite systems of holes described in Section 4.1 only involves simple operations such as substitution of one algebraic expression into another and evaluation of the Laurent series coefficients. The solutions for infinite arrays of holes described in Section 4.2 additionally require the evaluation of infinite sums S and T. The hole patterns discussed in Chapter 5 in the case of isotropic material behaviour lead to sums where the rth term is a rational function of the index r. They can always be evaluated as a finite combination of the so-called polygamma functions. The polygamma function of the order n, $n \in \mathbb{N}_0$, is defined as the $(n+1)$th derivative of the logarithm of the gamma function

$$\Psi_n(z) = \frac{\mathrm{d}^{n+1}}{\mathrm{d}z^{n+1}} \ln \Gamma(z). \tag{4.120}$$

Its relation to the sums of rational functions is given by the expansions

$$\Psi_n(z) = \begin{cases} -\gamma + \displaystyle\sum_{k=0}^{\infty} \left(\frac{1}{k+1} - \frac{1}{k+z} \right) & \text{for } n = 0, \\ (-1)^{n+1} n! \displaystyle\sum_{k=0}^{\infty} \frac{1}{(k+z)^{n+1}} & \text{for } n > 0, \end{cases} \tag{4.121}$$

where γ is the Euler-Mascheroni constant. Moreover, by using classical identities for the polygamma function such as the reflection and the recurrence formula, the sums involved in the examples of the next chapter can be expressed in a form involving only trigonometric functions. For more details on the properties of the polygamma function, the reader is referred to Abramowitz and Stegun [1]. Unfortunately, the anisotropic version of the problem leads to sums whose rth terms involve square roots and therefore cannot be evaluated in a closed-form using this elegant method.

Although both types of solutions can in principle be evaluated by hand, the number of required operations increases dramatically with the approximation order, making computer algebra systems the only possible way to obtain higher-order approximations in an explicit form. Therefore, the solutions described in Section 4.1 and 4.2 have been implemented in the commercial computer algebra system MATHEMATICA [94]. The implementations of each of the considered models follow the same scheme. It is a list of definitions related to each other. By invoking the result, the definitions are iteratively applied unless the result is obtained in an explicit form up to a given order of approximation. The procedure along with references to the defining equations for each considered model is given below.

The number of different inner auxiliary functions is denoted by N_A. In the case of a finite number of holes, this number is equal to the number of holes ($N_A = N_H$), in the case of infinite number of holes, it is equal to the number of categories ($N_A = N_C$). The procedure for the Laplace equation is summarised in Algorithm 4.1, for the biharmonic equation in Algorithm 4.2 and for the fourth-order partial differential equation with constant coefficients (2.29) in Algorithm 4.3.

1. Define the geometric configuration in terms of the variables N_H, c_p and ρ_p, $p = 1, \ldots, N_H$, in the case of a finite number of holes and N_C, c_{pr} and ρ_p, $p = 1, \ldots, N_C$, $r \in \mathbb{Z}$, in the case of an infinite array.

2. Define the applied loads in terms of the functions $\hat{\varphi}_0^n(z)$ and $\hat{\varphi}_p^n(\zeta_p)$, $p = 1, \ldots, N_A$, $n \in \mathbb{N}_0$, and the resultant forces F_p, $p = 1, \ldots, N_A$.

3. Calculate the constants A_p, $p = 1, \ldots, N_A$, from the resultant forces F_p using (4.7).

4. In the case of an infinite array,

   4.1 For $p, q = 1, \ldots, N_A$, $k = 1, \ldots, N$, calculate the infinite sum S_{pqk}^1 defined in (4.102).

   4.2 For $q = 1, \ldots, N_A$, $k = 1, \ldots, N$, calculate the infinite sums T_{qk}^1 and T_q^2 defined in (4.103a).

5. For $n = 0, \ldots, N + 2$ do

   5.1 For $k = 1, \ldots, n$, $p = 1, \ldots, N_A$, calculate the coefficients a_{qk}^n, d_{pk}^n by means of the equations (4.11) and (4.12).

   5.2 For $k = 1, \ldots, n$, $p = 1, \ldots, N_A$, calculate the coefficients K_{pk}^n by means of the equations (4.19).

   5.3 For $p = 1, \ldots, N_A$, calculate the inner auxiliary functions $\varphi_p^n(\zeta_p)$ from (4.31) and the outer auxiliary functions $\varphi_0^n(z)$ from (4.36).

6. Calculate the resulting potentials $\varphi(z)$ from (4.38) and their near- and far-field approximations $P^N\varphi(z)$ from (4.39) and $Q^N\varphi(\zeta_p)$ from (4.40), respectively.

7. Evaluate the stress and the displacements using the equations (2.14) and (2.32).

Algorithm 4.1: Solution of the first fundamental problem for the Laplace equation.

1. Define the geometric configuration in terms of the variables N_H, c_p and ρ_p, $p = 1, \ldots, N_H$, in the case of a finite number of holes and N_C, c_{pr} and ρ_p, $p = 1, \ldots, N_C$, $r \in \mathbb{Z}$, in the case of an infinite array.

2. Define the applied loads in terms of the functions $\hat{\varphi}_0^n(z)$, $\hat{\psi}_0^n(z)$ and $\hat{\varphi}_p^n(\zeta_p)$, $\hat{\psi}_p^n(\zeta_p)$, $p = 1, \ldots, N_A$, $n \in \mathbb{N}_0$, and the resultant forces F_p, $p = 1, \ldots, N_A$.

3. Calculate the constants A_p, B_p, $p = 1, \ldots, N_A$, from the resultant forces F_p using (2.49).

4. In the case of an infinite array,

4.1 For $m = 1, 2$, $p, q = 1, \ldots, N_A$, $k = 1, \ldots, N$, calculate the infinite sum S^m_{pqk} defined in (4.110a) and (4.102).

4.2 For $m = 1, \ldots, 6$, $q = 1, \ldots, N_A$, $k = 1, \ldots, N$, calculate the infinite sum T^m_{qk} defined in (4.110a) and (4.103a).

5. For $n = 0, \ldots, N + 2$ do

5.1 For $k = 1, \ldots, n$, $p = 1, \ldots, N_A$, calculate the coefficients $a^n_{qk}, b^n_{qk}, d^n_{pk}, e^n_{pk}$ by means of the equations (4.47) and (4.48).

5.2 For $k = 1, \ldots, n$, $p = 1, \ldots, N_A$, calculate the coefficients K^n_{pk}, L^n_{pk} by means of the equations (4.50).

5.3 For $p = 1, \ldots, N_A$, calculate the inner auxiliary functions $\varphi^n_p(\zeta_p)$, $\psi^n_p(\zeta_p)$ from (4.57) and the outer auxiliary functions $\varphi^n_0(z)$, $\psi^n_0(z)$ from (4.65).

6. Calculate the resulting potentials $\varphi(z)$, $\psi(z)$ from (4.67) and their near- and far-field approximations $P^N\varphi(z)$, $P^N\psi(z)$ from (4.68) and $Q^N\varphi(\zeta_p)$, $Q^N\psi(\zeta_p)$ from (4.69), respectively.

7. Evaluate the stress and the displacements using the Kolosov equations (2.42).

Algorithm 4.2: Solution of the first fundamental problem for the bipotential equation.

---

1. Define the geometric configuration in terms of the variables N_H, c_p, m_p and ρ_p, $p = 1, \ldots, N_H$, in the case of a finite number of holes and N_C, c_{pr}, ρ_p and m_p, $p = 1, \ldots, N_C$, $r \in \mathbb{Z}$, in the case of an infinite array.

2. Define the applied loads in terms of the functions $\hat{\varphi}^n_{0j}(z)$ and $\hat{\varphi}^n_{pj}(\zeta_p)$, $p = 1, \ldots, N_A$, $n \in \mathbb{N}_0$, $j = 1, 2$, and the resultant forces F_p, $p = 1, \ldots, N_A$.

3. Calculate the constants A_{pj}, $p = 1, \ldots, N_A$, $j = 1, 2$, from the resultant forces F_p using (2.69).

4. In the case of an infinite array,

4.1 For $p, q = 1, \ldots, N_A$, $k = 1, \ldots, N$, $j = 1, 2$, calculate the infinite sum S^1_{pqjk} defined in (4.115a).

4.2 For $q = 1, \ldots, N_A$, $k = 1, \ldots, N$, $j = 1, 2$, calculate the infinite sum T^1_{qjk} defined in (4.115b).

4.3 For $q = 1, \ldots, N_A$, $j = 1, 2$, calculate the infinite sum T^2_{qj} defined in (4.115c).

5. For $n = 0, \ldots, N + 2$ do

5.1 For $k = 1, \ldots, n$, $p, q = 1, \ldots, N_A$, $j = 1, 2$, calculate the coefficients a^n_{qjk}, d^n_{pjk} by means of the equations (4.79) and (4.80).

5.2 For $k = 1, \ldots, n$, $p = 1, \ldots, N_A$, $j = 1, 2$, calculate the coefficients K^n_{pjk} by means of the equations (4.82).

5.3 For $p = 1, \ldots, N_A$, $j = 1, 2$, calculate the inner auxiliary functions $\varphi^n_{pj}(\zeta_{pj})$ from (4.90) and the outer auxiliary functions $\varphi^n_{0j}(z)$ from (4.97).

6. Calculate the resulting potentials $\varphi_j(z_j)$, $j = 1, 2$, from (4.99) and their near- and far-field approximations $P^N\varphi_j(z_j)$ from (4.100) and $Q^N_p\varphi(\zeta_{pj})$ from (4.101), respectively.

7. Evaluate the stress and the displacements using the Lekhnitskii equations (2.59) and (2.60).

Algorithm 4.3: Solution of the first fundamental problem for the fourth-order partial differential equation with constant coefficients (2.29).

4.4 Verification of the results by means of the FEM

In order to verify the correctness of the presented results, they are compared to a numerical solution. For this purpose, a fully parametrised finite element model has been created in the commercial FE Software ABAQUS [13] using its PYTHON scripting interface. The model allows an arbitrary finite number of holes arbitrarily located within a rectangle. The infinite extension of the plate is modelled by a sufficiently large but finite domain. Infinite rows of holes are modelled by modelling only one cell of the periodic structure and imposing periodic boundary conditions. The model is based on quadratic quadrilateral elements with reduced integration (ABAQUS code CPS8R). The mesh is automatically generated, aiming for a fine discretisation in the neighbourhood of the holes and a relatively coarse discretisation in the regions corresponding to the infinite extension. Therefore, in the neighbourhood of each hole, a very fine regular sweep mesh with up to 600 elements on the hole edge is used, whereas in the far-field, a relatively coarse free mesh is generated. A typical mesh is shown in Figure 4.7.

Several different variants of boundary conditions are implemented. In the first variant, distributed boundary loads are prescribed exactly as in the analytical solution, i.e. loads corresponding to the state of stress at infinity are prescribed on the outer boundary of the domain and the same loads as in the analytical solution are prescribed on the boundary of loaded holes. To avoid rigid body motions, three displacement degrees of freedom of two different nodes are fixed. This variant verifies solely the correctness of the analytical solution and the convergence of the obtained asymptotic series. It is used to verify the results on the stress concentration factors of Sections 5.1 and on the compliance of an infinite row of pin-loaded holes in Section 5.2.

In order to verify the assumptions on the distribution of the stresses in a pin-to-hole contact, a contact variant of the model has been developed as well. In this variant shown in Figure 4.8, the bolts are modelled as fixed rigid bodies whose displacements are fixed. A surface-to-surface contact algorithm with small sliding without friction is chosen to model the interaction between bolts and the plate because it corresponds to the assumptions

made in the analytical solution. The clearance between the bolt and the hole is zero. The vertical displacement of the nodes on the bottom edge of the plate is constrained by a multi-point constraint and these nodes are loaded by a force corresponding to the overall force transmitted over the joint. This model is used to verify the results on the compliance of an infinite row of pin-loaded holes in Section 5.2 and on the load distribution among bolts in Section 5.3.

Finally, it should be stressed that the aim of the present finite element model is solely to verify the analytical results of this thesis within their scope of validity. More detailed finite element studies that investigate the influence of parameters not included in the present modelling have been sufficiently documented in the literature (cf. Section 1.2).

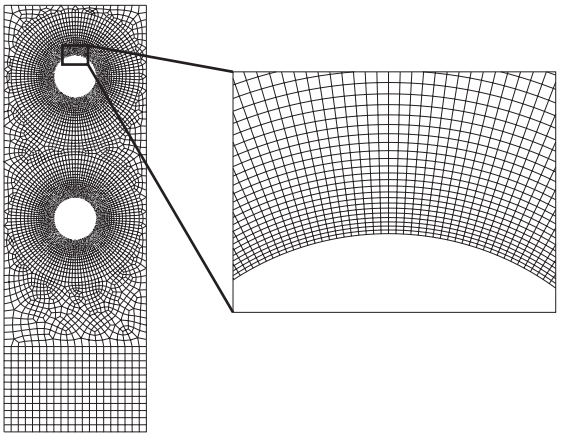

Figure 4.7: A typical medium mesh with 240 elements on the boundary of each hole.

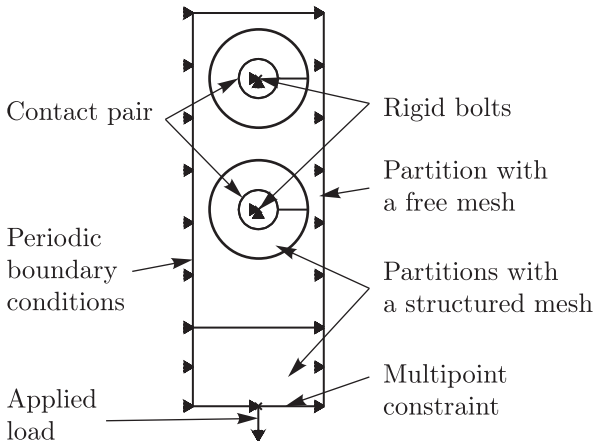

Figure 4.8: A scheme of the variant of the FEM model involving contact between the plate and two rigid bolts.

4.5 Discussion

In this chapter, a general formal asymptotic solution of the first fundamental problem for an infinite plane or half-plane weakened by a finite or infinite number of small holes for three types of underlying equations is given. The proposed asymptotic solution is uniformly valid in the whole domain, i.e. in the vicinity of each of the holes as well as in the far-field.

Apart from some trivial generalisations such as considering holes of different radii or elliptical holes in the anisotropic case, the solution is presented in a form as general as needed for the actual application. The given solution might be further generalised in a variety of ways. One possibility is to consider other types of boundary conditions such as displacement or contact conditions. In this case, the only change would be the formulation of the boundary value problems for the auxiliary functions and their solution. Another possible generalisation is by considering other types of unperturbed domains than a full plane or a half-plane. Although the presented method in principle works for an arbitrary unperturbed domain, the problem lies in the solution of the corresponding

outer subproblems. A closed-form solution could be obtained only for simple unbounded domains discussed in this chapter. In more complex domains, the subproblems would need to be solved numerically. Such an approach would lead to a representation of the solution as a series in terms of the relative hole radius with numerically determined coefficients.

Chapter 5

Applications

This chapter contains a collection of problems solved by the method introduced in Chapter 4. The presented examples can be divided into three classes. In Section 5.1, stress concentration on several configurations of unloaded holes is investigated. The purpose of this section is to investigate the capabilities of the present method by means of classical and relatively simple problems where a very high number of terms in the asymptotic series can be achieved. Then, in Section 5.2, the compliance of two configurations involving an infinite row of pin-loaded holes is investigated. Finally, in Section 5.3, the load distribution on a double-lap joint involving a finite number and two infinite rows of bolts is discussed.

All results of this chapter are obtained with the MATHEMATICA implementation of Algorithms 4.2 and 4.3. Theoretically, these algorithms can produce all results with an arbitrarily high order of approximation. From the practical point of view, the achievable order of approximation is limited by the complexity of formulae arising during the computation. There are two problems related to increasing complexity of the formulae:

1. Too complex formulae do not provide the engineer with much insight about the dependence of the quantities of interest on the involved parameters which breaks the main objective of this work.

2. Too complex formulae become unmanageable even with a computer algebra system within a reasonable time.

The order of approximation of formulae presented in this chapter is usually restricted by point 1. It should be noted that the order of approximation of the presented intermediate steps is sometimes lower than the order of the results following from them. Also, the order of approximation of results in the plots is often higher than that of the results presented in the text. This is necessary because the intermediate steps with an appropriate order of approximation are often too complex.

For some numerical examples, specific material parameters have to be chosen. The examples involving isotropic material behaviour are given for aluminium with $E = 70\,\mathrm{GPa}$, $\nu = 0.35$. The examples involving anisotropic material behaviour are given for laminates of T300/Epoxy with the material parameters $E_1 = 135\,000\,\mathrm{GPa}$, $E_2 = 8\,500\,\mathrm{GPa}$, $\nu_{12} = 0.35$, $G_{12} = 4\,200\,\mathrm{GPa}$. For a given laminate layup, the compliance coefficients and the

effective engineering constants are computed using the classical laminate theory (see Jones [42]). The corresponding complex parameters for a laminate with the layup $[\pm 45°]_S$ are $\mu_1 = -0.889 + 0.458i$ and $\mu_2 = 0.889 + 0.458i$, for $[0/90°]_S$ $\mu_1 = 0.242i$ and $\mu_2 = 4.13i$, for a $[0°]$ uni-directional layer they become $\mu_1 = 0.717i$ and $\mu_2 = 5.56i$ and for a $[90°]$ layer, they become $\mu_1 = 0.180i$ and $\mu_2 = 1.40i$.

An important question is the convergence of the derived asymptotic series. Chapter 4 is limited to the derivation of a formal asymptotic solution. A strict mathematical proof of the convergence of the series is not available. Therefore, numerical convergence studies for representative problems are presented in this chapter. Furthermore, in order to provide an independent check of the correctness of the presented results, some of them were verified by means of the finite element model described in Section 4.4.

5.1 Stress concentration on unloaded holes

5.1.1 A single hole in a half-plane

An isotropic half-plane contains a single hole of radius ϵ and edge distance 1 according to Figure 5.1. The plane is subject to uniaxial tension σ_x^∞ at infinity. This classical problem of plane theory of elasticity has already been treated by various methods (cf. Section 1.2). The purpose of this example is solely to test the present method on this 'benchmark' problem.

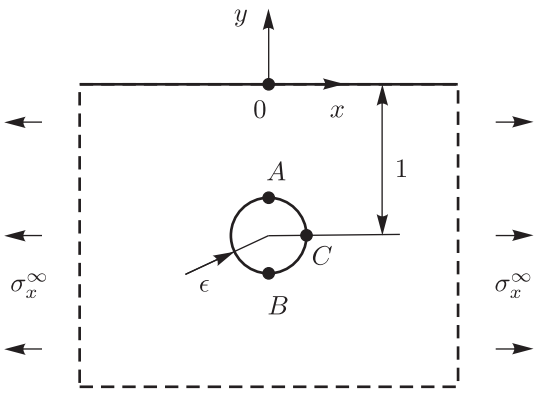

Figure 5.1: A single hole in a half-plane under uniaxial tension.

Algorithm 4.2 with the settings

$$N_H = 1, \quad c_1 = -i, \quad \rho_1 = 1, \tag{5.1a}$$

$$\hat{\varphi}_0^n(z) = \delta_{n0}\frac{\sigma_x^\infty}{4}z, \quad \hat{\psi}_0^n(z) = -\delta_{n0}\frac{\sigma_x^\infty}{2}z, \quad \hat{\varphi}_1^n(\zeta_1) = \hat{\psi}_1^n(\zeta_1) = 0, \quad F_1^n = 0 \tag{5.1b}$$

gives the complex potentials

$$\varphi(z) = \sigma_x^\infty \left[\frac{z}{4} + \frac{(-1+3z^2)\,\epsilon^2}{2(-i+z)^2(i+z)} + \frac{(i-5z-3iz^2+3z^3)\,\epsilon^4}{4(-i+z)^3(i+z)} \right] + O(\epsilon^6), \tag{5.2a}$$

$$\psi(z) = \sigma_x^\infty \left[-\frac{z}{2} + \frac{i\,(i-3z+5iz^2+9z^3)\,\epsilon^2}{2(-i+z)^3(i+z)^2} + \frac{i\,(i+5z+6iz^2-26z^3+13iz^4+9z^5)\,\epsilon^4}{4(-i+z)^4(i+z)^3} \right] + O(\epsilon^6). \tag{5.2b}$$

The hoop stress on the boundary of the hole is

$$\frac{\sigma_\theta}{\sigma_x^\infty} = 1 - 2\cos(2\theta) - \frac{3}{2}\cos(2\theta)\epsilon^2 - \frac{1}{2}\big(\sin(\theta) + 5\sin(3\theta)\big)\epsilon^3 + \frac{1}{8}\big(9\cos(2\theta) + 21\cos(4\theta)\big)\epsilon^4 + \frac{9}{4}\big(\sin(3\theta) + \sin(5\theta)\big)\epsilon^5 + \frac{1}{32}\big(-31\cos(2\theta) - 98\cos(4\theta) - 55\cos(6\theta)\big)\epsilon^6 + O(\epsilon^7) \tag{5.3}$$

and the tension along the x-axis

$$\frac{\sigma_x}{\sigma_x^\infty} = 1 - \frac{2\,(1-12x^2+3x^4)\,\epsilon^2}{(1+x^2)^3} - \frac{3\,(-1+7x^2-7x^4+x^6)\,\epsilon^4}{(1+x^2)^4} + \frac{(-11+181x^2-141x^4+3x^6)\,\epsilon^6}{4\,(1+x^2)^4} + O(\epsilon^8). \tag{5.4}$$

The stress concentration at distinguished points A, B, C and 0 is

$$k_A = 3 + \frac{3\epsilon^2}{2} + 2\epsilon^3 + \frac{3\epsilon^4}{2} - \frac{3\epsilon^6}{8} + \frac{3\epsilon^7}{8} + \frac{111\epsilon^8}{128} + \frac{11\epsilon^9}{16} + \frac{51\epsilon^{10}}{64} + O(\epsilon^{11}), \tag{5.5a}$$

$$k_B = 3 + \frac{3\epsilon^2}{2} - 2\epsilon^3 + \frac{3\epsilon^4}{2} - \frac{3\epsilon^6}{8} - \frac{3\epsilon^7}{8} + \frac{111\epsilon^8}{128} - \frac{11\epsilon^9}{16} + \frac{51\epsilon^{10}}{64} + O(\epsilon^{11}), \tag{5.5b}$$

$$k_C = -1 - \frac{3\epsilon^2}{2} + \frac{15\epsilon^4}{4} - \frac{23\epsilon^6}{4} + \frac{1143\epsilon^8}{128} - \frac{1203\epsilon^{10}}{128} + O(\epsilon^{12}), \tag{5.5c}$$

$$k_0 = 1 - 2\epsilon^2 + 3\epsilon^4 - \frac{11\epsilon^6}{4} + \frac{3\epsilon^8}{8} + \frac{9\epsilon^{10}}{16} + O(\epsilon^{12}). \tag{5.5d}$$

The convergence of the obtained series has been investigated numerically. It is discussed using the example of the series (5.5a). Note that in this example, admissible values of the parameter ϵ are $0 < \epsilon < 1$, the limiting value $\epsilon = 1$ corresponding to the situation when the hole boundary reaches the boundary of the half-plane. Figure 5.2 shows the convergence of the partial sums for relatively small values of ϵ whereas Figure 5.3 shows the convergence for ϵ close to the limiting value 1. In both cases, N denotes the highest power of ϵ involved in the partial sum. It can be observed that with a reasonable effort, the result can be constructed even for ϵ close to 1. Finally, Figure 5.4 shows the dependence of the first few partial sums on ϵ. The curve labelled 'FEM' has been obtained by the FEM model described in Section 4.4. It can be seen that e.g. for ϵ as high as 0.6, the first

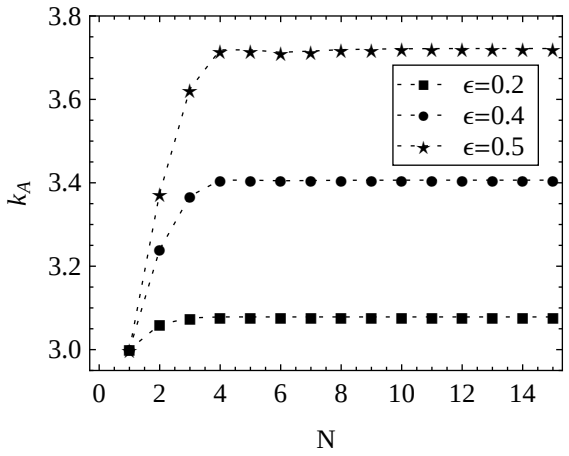

Figure 5.2: Convergence of the stress concentration factor (5.5a) for small values of the relative hole radius ϵ.

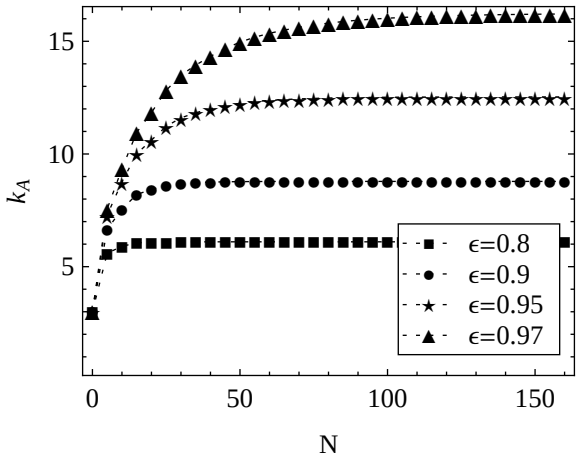

Figure 5.3: Convergence of the stress concentration factor (5.5a) for larger values of the relative hole radius ϵ.

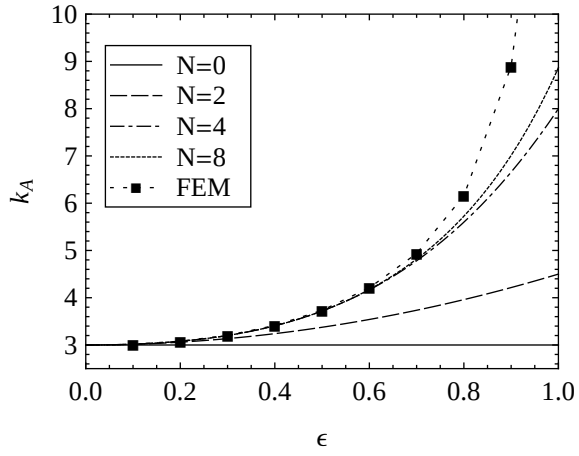

Figure 5.4: Dependence of the stress concentration factor (5.5a) on the relative hole radius.

four terms provide a sufficient accuracy. Other series in this and the following examples exhibit qualitatively the same behaviour.

Next, the influence of material anisotropy is investigated, the geometry and loading remaining unchanged. The solution of the problem is generated by Algorithm 4.3 with the settings

$$N_H = 1, \quad c_1 = -i, \quad \rho_1 = 1, \quad m_1 = 1, \tag{5.6a}$$

$$\hat{\varphi}^n_{0j}(z_j) = \delta_{n0} C_j z_j, \quad \hat{\varphi}^n_{1j}(\zeta_{1j}) = 0, \quad F^n_1 = 0, \tag{5.6b}$$

where the constants C_j are determined from equations (2.66). When numerical values are assigned to the complex parameters μ_1 and μ_2 before the algorithm is executed, the asymptotic solution involving coefficients in numerical form can easily be obtained for arbitrary material moduli. However, leaving the complex parameters in symbolic form, the coefficients in the asymptotic solution become very complex despite the simple geometry. A relatively compact closed-form representation of the solution can only be obtained by assuming strong orthotropy.

The properties of the solution are discussed by means of the stress concentration factor k_A. Below, k_A is given for the three cases of strong orthotropy listed in Section 2.3.3 in terms of the complex parameters μ_1 and μ_2. If one of the complex parameters is large (case 1), the stress concentration is

$$k_A\big|_{|\mu_2|\gg 1} = (1 - i\mu_1 - i\mu_2) + \frac{(i + 4\mu_1 - 5i\mu_1^2 - i\mu_1\mu_2)\,\epsilon^2}{8\mu_1} + \frac{(-1 + 3i\mu_1 + 6\mu_1^2 - 5i\mu_1^3 - i\mu_1^2\mu_2)\,\epsilon^3}{16\mu_1^2} + O(\epsilon^4) + O(\mu_2^{-1}), \quad (5.7)$$

if one of the complex parameters is small (case 2), it becomes

$$k_A\big|_{|\mu_1|\ll 1} = (1 - i\mu_1 - i\mu_2) + \left(\frac{i + 4\mu_1 - 5i\mu_1^2}{8\mu_1} - \frac{i\mu_1}{2\mu_2^2} + \frac{5i}{8\mu_2} - \frac{i\mu_2}{8}\right)\epsilon^2 + \left(\frac{\mu_1}{\mu_2^3} - \frac{i\mu_2}{16}\frac{-1 + 3i\mu_1 + 6\mu_1^2 - 5i\mu_1^3}{16\mu_1^2} - \frac{3i\,(-3i + 4\mu_1)}{16\mu_2^2} + \frac{-4 + 15i\mu_1 + 8\mu_1^2}{16\mu_1\mu_2}\right)\epsilon^3 + O(\epsilon^4) + O(\mu_1^2) \quad (5.8)$$

and finally if one of them is large and the other small (case 3), the stress concentration is

$$k_A\big|_{|\mu_1|\ll 1,|\mu_2|\gg 1} = (1 - i\mu_1 - i\mu_2) + \frac{(i + 4\mu_1 - 5i\mu_1^2 - i\mu_1\mu_2)\,\epsilon^2}{8\mu_1} + \frac{(-1 + 3i\mu_1 + 6\mu_1^2 - 5i\mu_1^3 - i\mu_1^2\mu_2)\,\epsilon^3}{16\mu_1^2} + O(\epsilon^4) + O(\mu_1^2). \quad (5.9)$$

The convergence of the series (5.9) is numerically investigated for a T300/Epoxy laminate with the $[0/90°]_S$ layup for whose effective material moduli it holds $E_1 = E_2 \gg G_{12}$. A convergence test shows that the radius of convergence is approximately $\epsilon_0 = 0.27$. This rather poor behaviour can be improved by using the Euler transformation or the Padé approximants, the latter giving better results. Figure 5.5 shows the convergence of the diagonal Padé approximants of the stress concentration factor k_A. It can be observed that the Padé approximants significantly improve the convergence. The dependence of the first several partial sums of series (5.9) on ϵ is shown in Figure 5.6. As can be seen, the approximation of strong orthotropy gives satisfactory results for the considered laminate.

5.1.2 Multiple holes in a half-plane

In this section, several geometrically more complex situations are discussed. Consider first a half-plane under uniaxial tension σ_x^∞ at infinity containing two holes of radius ϵ, respective distance 1 and edge distance h according to Figure 5.7. Algorithm 4.2 with

$$N_H = 2, \quad c_1 = -1/2 - ih, \quad c_2 = 1/2 - ih \quad (5.10)$$

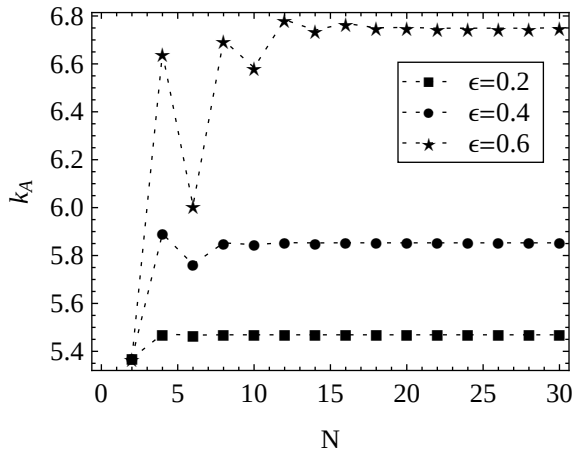

Figure 5.5: Convergence of the diagonal Padé approximants $[\frac{N}{2}/\frac{N}{2}]$ of the stress concentration factor (5.9).

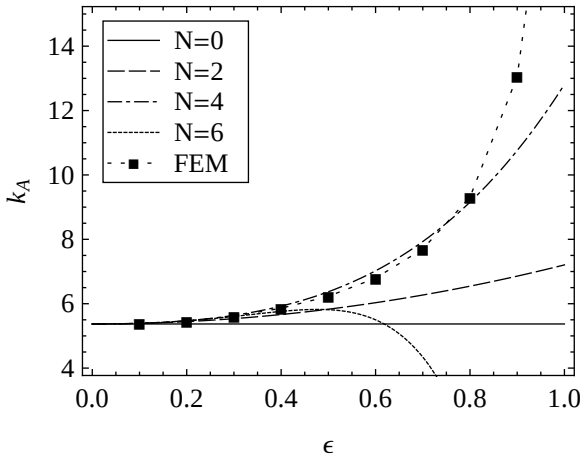

Figure 5.6: Dependence of the stress concentration factor (5.9) on the relative hole radius.

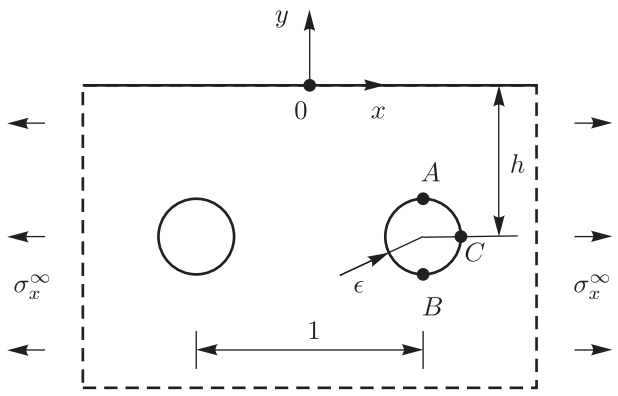

Figure 5.7: Two holes in a half-plane under uniaxial tension.

and other settings as in (5.1) yields the following stress concentration factors at selected points A, B, C and 0:

$$k_A = 3 + \frac{\left(3 + 12h^2 + 432h^4 - 1728h^6 - 2560h^8 - 4096h^{10}\right)\epsilon^2}{2h^2\left(1+4h^2\right)^4} + \frac{\left(4 + 80h^2 + 64h^4 + 8960h^6 - 8192h^8 + 8192h^{10}\right)\epsilon^3}{2h^3\left(1+4h^2\right)^5} + O(\epsilon^4), \quad (5.11a)$$

$$k_B = 3 + \frac{\left(3 + 12h^2 + 432h^4 - 1728h^6 - 2560h^8 - 4096h^{10}\right)\epsilon^2}{2h^2\left(1+4h^2\right)^4} - \frac{\left(4 + 80h^2 + 64h^4 + 8960h^6 - 8192h^8 + 8192h^{10}\right)\epsilon^3}{2h^3\left(1+4h^2\right)^5} + O(\epsilon^4), \quad (5.11b)$$

$$k_C = -1 + \frac{\left(-3 - 36h^2 - 432h^4 + 1728h^6 + 512h^8 + 2048h^{10}\right)\epsilon^2}{2h^2\left(1+4h^2\right)^4} + \frac{\left(48h^3 - 1152h^5 + 17280h^7 - 1536h^9 + 30720h^{11} + 24576h^{13}\right)\epsilon^3}{2h^3\left(1+4h^2\right)^5} + O(\epsilon^4), \quad (5.11c)$$

$$k_0 = 1 - \frac{16\left(3 - 12h^2 - 416h^4 - 1920h^6 - 2304h^8 + 1024h^{10}\right)\epsilon^2}{\left(1+4h^2\right)^6} + O(\epsilon^4). \quad (5.11d)$$

For $h = 1/2$, these stress concentration factors become

$$k_A = 3 - \epsilon^2 + 18\epsilon^3 + \frac{119\epsilon^4}{2} - 57\epsilon^5 - \frac{567\epsilon^6}{4} - 72\epsilon^7 - \frac{2247\epsilon^8}{8} + O(\epsilon^9), \quad (5.12a)$$

$$k_B = 3 - \epsilon^2 - 18\epsilon^3 + \frac{119\epsilon^4}{2} + 57\epsilon^5 - \frac{567\epsilon^6}{4} + 72\epsilon^7 - \frac{2247\epsilon^8}{8} + O(\epsilon^9), \quad (5.12b)$$

$$k_C = -1 - \epsilon^2 + 15\epsilon^3 + \frac{197\epsilon^4}{2} - 18\epsilon^5 - \frac{3119\epsilon^6}{4} + 114\epsilon^7 + \frac{27061\epsilon^8}{8} + O(\epsilon^9), \quad (5.12c)$$

$$k_0 = 1 + 16\epsilon^2 - 48\epsilon^4 - 56\epsilon^6 + 1104\epsilon^8 + O(\epsilon^9). \quad (5.12d)$$

The convergence of the series (5.12a) is investigated numerically in Figures 5.8 and 5.9. The admissible values of the parameter ϵ are $0 < \epsilon < 1/2$, the limiting value $1/2$ corresponding to the case when the holes touch each other and at the same time the boundary of the half-plane. Figure 5.8 shows the dependence of the partial sum of the series (5.12a) on the maximal power of ϵ involved in the sum for three different values of ϵ. It can be observed that the number of terms needed for convergence increases with increasing ϵ. To manifest the behaviour of the sum of the first few terms of the series, their dependence on ϵ is plotted in Figure 5.9. The solution labelled 'FEM' has been generated using the FE-Model described in Section 4.4. Further examples of the verification of the present results by means of the FEM can be found in the work of Schmidt [84].

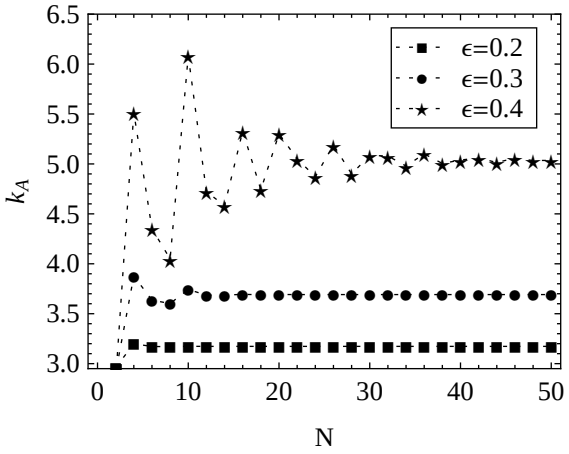

Figure 5.8: Convergence of the stress concentration factor (5.12a).

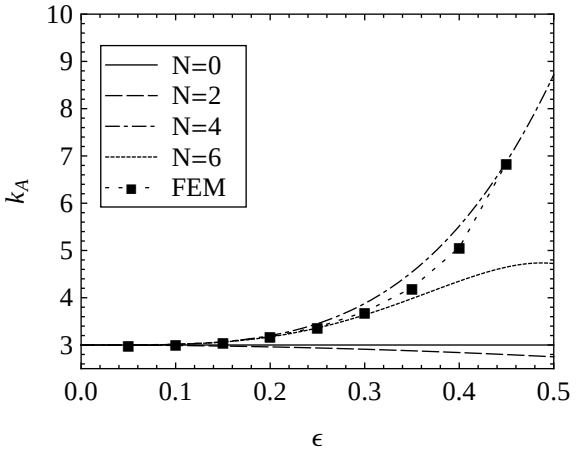

Figure 5.9: Dependence of the stress concentration factor (5.12a) on the relative hole radius.

Algorithm 4.2 can be applied to more complex configurations as well. As an example, consider a half-plane under uniaxial tension σ_x^∞ containing a zig-zag array of seven holes

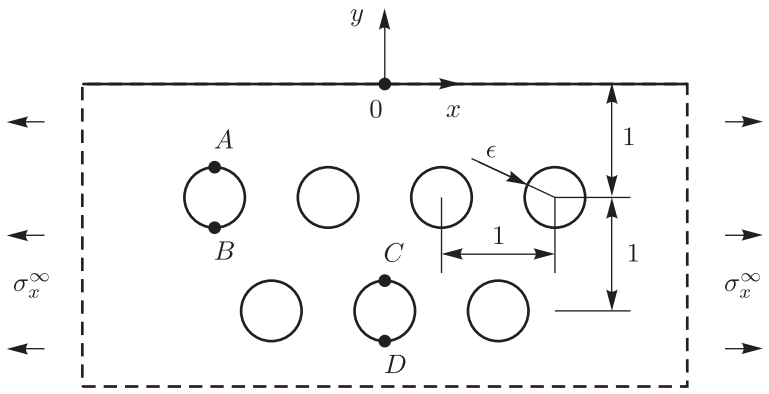

Figure 5.10: A zig-zag array of seven holes in a half-plane under uniaxial tension.

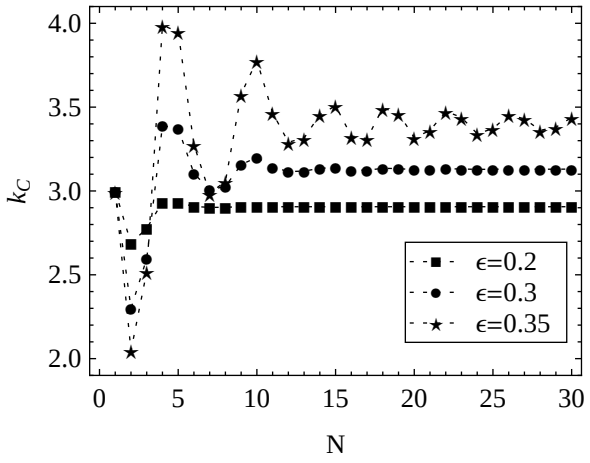

Figure 5.11: Convergence of the stress concentration factor (5.14c).

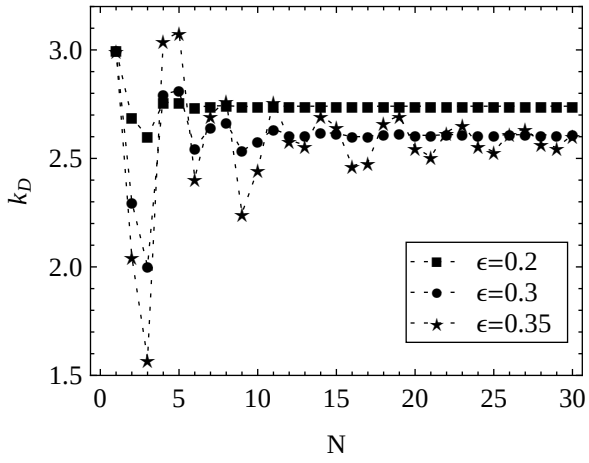

Figure 5.12: Convergence of the stress concentration factor (5.14d).

according to Figure 5.10. Algorithm 4.2 with

$$N_H = 7, \quad c_p = \begin{cases} p - 5/2 - i, & p = 1, \dots, 4, \\ p - 6 - 2i, & p = 5, \dots, 7, \end{cases} \tag{5.13}$$

other settings being the same as in (5.1), gives the following stress concentrations at distinguished points $A - D$ and 0 :

$$k_A = 3 - 5.40236\epsilon^2 - 2.28475\epsilon^3 + 87.0511\epsilon^4 + 2.83144\epsilon^5 - 509.926\epsilon^6 + O(\epsilon^7), \tag{5.14a}$$

$$k_B = 3 - 5.40236\epsilon^2 + 2.28475\epsilon^3 + 87.0511\epsilon^4 - 2.83144\epsilon^5 - 509.926\epsilon^6 + O(\epsilon^7), \tag{5.14b}$$

$$k_C = 3 - 7.78106\epsilon^2 + 11.0063\epsilon^3 + 97.9041\epsilon^4 - 7.23796\epsilon^5 - 366.3\epsilon^6 + O(\epsilon^7), \tag{5.14c}$$

$$k_D = 3 - 7.78106\epsilon^2 - 11.0063\epsilon^3 + 97.9041\epsilon^4 + 7.23796\epsilon^5 - 366.3\epsilon^6 + O(\epsilon^7), \tag{5.14d}$$

$$k_0 = 1 + 5.39990\epsilon^2 - 11.8424\epsilon^4 + 30.1005\epsilon^6 + O(\epsilon^8). \tag{5.14e}$$

Note that no numerical approximation is needed throughout the computation, except for the numerical approximation of rational coefficients in the final result. The convergence of the series (5.14c) and (5.14d) is investigated numerically in Figures 5.11 and 5.12. In this example, the admissible values of the parameter ϵ are $0 < \epsilon < 1/2$. It can be seen that especially for larger values of ϵ, the convergence is worse than in the previous examples. This demonstrates the fact that with increasing complexity of the geometry, the convergence of the asymptotic series generally worsens.

5.1.3 Infinite rows of holes

In this section, two configurations involving an infinite row of unloaded holes are discussed. The first of them is an infinite plane containing an infinite row of unloaded holes with radius ϵ distributed with spacing 1 along the x-axis according to Figure 5.13. The plane is subject to uniaxial tension σ_x^∞ at infinity.

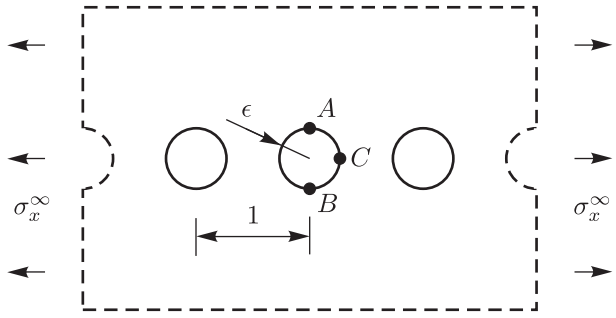

Figure 5.13: Infinite row of holes in an infinite plane under uniaxial tension.

Due to the periodicity in x-direction, all holes belong to the same category. Algorithm 4.2 with

$$N_H = \infty, \quad N_C = 1, \quad c_{1r} = r, \quad \rho_1 = 1, \tag{5.15a}$$

$$\hat{\varphi}_0^n(z) = \delta_{n0}\frac{\sigma_x^\infty}{4}z, \quad \hat{\psi}_0^n(z) = -\delta_{n0}\frac{\sigma_x^\infty}{2}z, \quad \hat{\varphi}_1^n(\zeta_1) = \hat{\psi}_1^n(\zeta_1) = 0, \quad F_1^n = 0 \tag{5.15b}$$

yields the following potentials:

$$\varphi(z) = \sigma_x^\infty\left[\frac{z}{4} + \frac{1}{2}\pi\cot(\pi z)\epsilon^2 - \frac{1}{2}\pi^3\cot(\pi z)\epsilon^4 + \frac{23}{45}\pi^5\cot(\pi z)\epsilon^6\right] + O(\epsilon^8), \tag{5.16a}$$

$$\begin{aligned}\psi(z) = \sigma_x^\infty\Bigg[&-\frac{z}{2} + \frac{1}{2}\left(-2\pi\cot(\pi z) + \pi^2 z\csc(\pi z)^2\right)\epsilon^2 \\ &+ \frac{1}{6}\left(5\pi^3\cot(\pi z) - 3\pi^4 z\csc(\pi z)^2 + 3\pi^3\cot(\pi z)\csc(\pi z)^2\right)\epsilon^4 \\ &+ \frac{1}{90}\left(-76\pi^5\cot(\pi z) + 46\pi^6 z\csc(\pi z)^2 - 45\pi^5\cot(\pi z)\csc(\pi z)^2\right)\epsilon^6\Bigg] + O(\epsilon^8).\end{aligned} \tag{5.16b}$$

The solution satisfies the following periodic boundary conditions on the vertical lines $x = \frac{1}{2} + k, k \in \mathbb{Z}$:

$$u(-1/2 + k, y) = u(1/2 + k, y), \quad t_y(1/2 + k, y) = 0. \tag{5.17}$$

The hoop stress on the border of each hole is

$$\frac{\sigma_\theta}{\sigma_x^\infty} = 1 - 2\cos(2\theta) + \frac{2}{3}\pi^2\big(-1 + 3\cos(2\theta)\big)\epsilon^2 + \frac{2}{45}\pi^4\cos(2\theta)\big(-49 + 30\cos(2\theta)\big)\epsilon^4 + \frac{2}{945}\pi^6\big(-322 + 1043\cos(2\theta) - 394\cos(4\theta) + 70\cos(6\theta)\big)\epsilon^6 + \frac{2\pi^8}{14175}\big(5005 - 16359\cos(2\theta) + 5994\cos(4\theta) - 1441\cos(6\theta) + 189\cos(8\theta)\big)\epsilon^8 + O(\epsilon^{10}). \quad (5.18)$$

The stress concentration factors at selected points A, B and C are

$$k_A = 3 - \frac{8\pi^2\epsilon^2}{3} + \frac{158\pi^4\epsilon^4}{45} - \frac{3658\pi^6\epsilon^6}{945} + \frac{57976\pi^8\epsilon^8}{14175} + O(\epsilon^{10}), \quad (5.19a)$$

$$k_B = 3 - \frac{8\pi^2\epsilon^2}{3} + \frac{158\pi^4\epsilon^4}{45} - \frac{3658\pi^6\epsilon^6}{945} + \frac{57976\pi^8\epsilon^8}{14175} + O(\epsilon^{10}), \quad (5.19b)$$

$$k_C = -1 + \frac{4\pi^2\epsilon^2}{3} - \frac{38\pi^4\epsilon^4}{45} + \frac{794\pi^6\epsilon^6}{945} - \frac{4408\pi^8\epsilon^8}{4725} + O(\epsilon^{10}). \quad (5.19c)$$

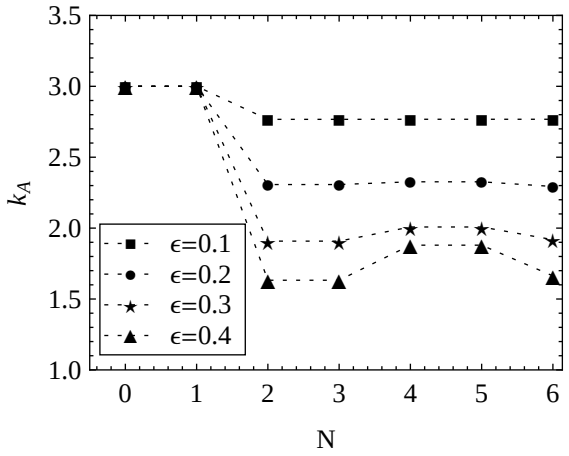

Figure 5.14: Convergence of the diagonal Padé approximants $[\frac{N}{2}/\frac{N}{2}]$ of the stress concentration factor (5.19a).

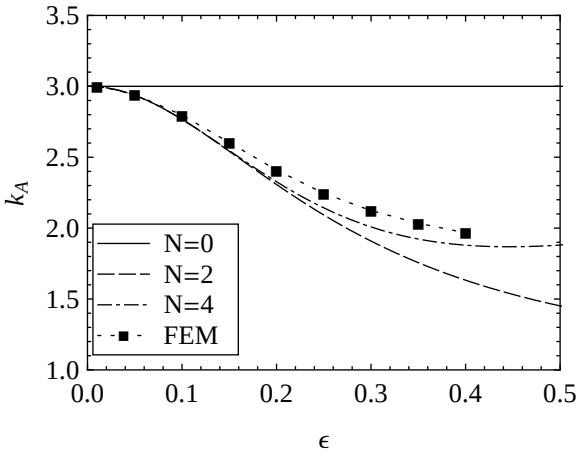

Figure 5.15: The dependence of the diagonal Padé approximants $[\frac{N}{2}/\frac{N}{2}]$ of the stress concentration factor (5.19a) on the relative hole radius.

A numerical investigation shows that the convergence of the above series is relatively poor for higher values of ϵ. Besides that, the computation of higher order approximations turns out to be much more complicated than in the previous examples because of the necessity to evaluate the infinite sums. It was found out that the convergence can be significantly improved using Padé approximants. Their performance is discussed by means of the example of the series (5.19a) in Figures 5.14 and 5.15. Diagonal Padé approximants were employed in both cases. Figure 5.14 shows the dependence of the stress concentration factor k_A on the order of the approximation N whereas Figure 5.15 shows the dependence of the stress concentration factor on ϵ. The points labelled 'FEM' were obtained using the FE model introduced in Section 4.4. It can be observed that for $N = 4$ the Padé approximants provide a sufficient approximation of the result in the whole admissible domain $0 < \epsilon < 1/2$.

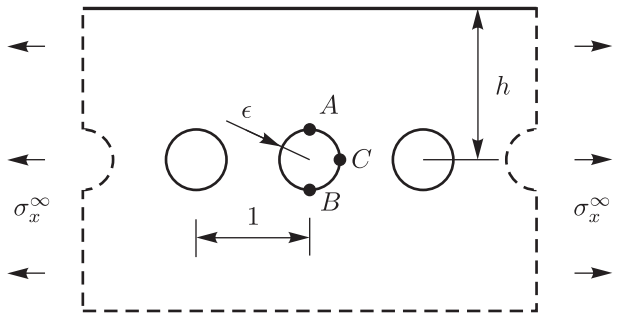

Figure 5.16: An infinite row of holes in a half-plane under uniaxial tension.

Next, the influence of the finite boundary is investigated by considering a half-plane containing an infinite row of holes with radius ϵ, spacing 1 and edge distance h according to Figure 5.16. The plate is subject to uniaxial tension σ_x^∞ at infinity. Algorithm 4.2 with

$$N_H = \infty, \quad N_C = 1, \quad c_{1r} = r - ih, \quad \rho_1 = 1 \tag{5.20}$$

and other settings as in (5.15) yields the following stress concentration factors at selected points A, B, C and 0:

$$\begin{aligned} k_A = 3 - \frac{1}{3}\pi^2 \operatorname{csch}(2h\pi)^4 \Big(&18 - 96h^2\pi^2 - 19\cosh(4h\pi) - 48h^2\pi^2\cosh(4h\pi) + \cosh(8h\pi) \\ &+ 48h\pi\sinh(4h\pi)\Big)\epsilon^2 + \pi^3 \operatorname{csch}(2h\pi)^5 \Big(176h^2\pi^2\cosh(2h\pi) - 7\cosh(2h\pi) + 7\cosh(6h\pi) \\ &+ 16h^2\pi^2\cosh(6h\pi) - 60h\pi\sinh(2h\pi) - 20h\pi\sinh(6h\pi)\Big)\epsilon^3 + O(\epsilon^4), \end{aligned} \tag{5.21a}$$

$$\begin{aligned} k_B = 3 - \frac{1}{3}\pi^2 \operatorname{csch}(2h\pi)^4 \Big(&18 - 96h^2\pi^2 - 19\cosh(4h\pi) - 48h^2\pi^2\cosh(4h\pi) + \cosh(8h\pi) \\ &+ 48h\pi\sinh(4h\pi)\Big)\epsilon^2 - \pi^3 \operatorname{csch}(2h\pi)^5 \Big(176h^2\pi^2\cosh(2h\pi) - 7\cosh(2h\pi) + 7\cosh(6h\pi) \\ &+ 16h^2\pi^2\cosh(6h\pi) - 60h\pi\sinh(2h\pi) - 20h\pi\sinh(6h\pi)\Big)\epsilon^3 + O(\epsilon^4), \end{aligned} \tag{5.21b}$$

$$\begin{aligned} k_C = -1 + \frac{1}{6}\pi^2 \operatorname{csch}(2h\pi)^4 \Big(&9 - 192h^2\pi^2 - 10\cosh(4h\pi) \\ &- 96h^2\pi^2\cosh(4h\pi) + \cosh(8h\pi) + 48h\pi\sinh(4h\pi)\Big)\epsilon^2 + O(\epsilon^4), \end{aligned} \tag{5.21c}$$

$$k_0 = 1 - 2\pi^2 \operatorname{csch}(h\pi)^3 \Big(4h\pi\cosh(h\pi) - 3\sinh(h\pi)\Big)\epsilon^2 + O(\epsilon^4). \tag{5.21d}$$

As expected, these results converge as $h \to \infty$ to the results (5.19) for the full plane. The convergence behaviour of the series is similar to that for an infinite plane.

Unfortunately, Algorithm 4.3 for anisotropic plates cannot be evaluated for infinite rows in the same manner as in the case of isotropic material behaviour because some of the infinite sums cannot be computed analytically.

5.2 Compliance of infinite rows of pin-loaded holes

The simplest model for the determination of the compliance of a pin-loaded hole within the framework of plane stress theory might seem to be that of a concentrated force. However, in the plane stress theory, the solution corresponding to the concentrated force has a logarithmic singularity in the displacements at the origin and thus the compliance of such a model would be infinite. The same holds for another model, a single pin-loaded hole or a finite number of pin-loaded holes in an infinite plane, which gives zero stresses and logarithmic displacements at infinity. On the other hand, a finite domain containing a hole gives a finite compliance but is much more difficult to treat analytically. Therefore, in the author's opinion, the simplest model is an infinite row of small pin-loaded holes in an infinite medium.

5.2.1 An infinite plane containing a single row of pin-loaded holes

An infinite plane contains an infinite row of holes with radius ϵ distributed with spacing 1 along the x-axis according to Figure 5.17. Each hole is loaded by the distribution of radial and tangential stresses (3.13) with total resultant F_y in the y-direction. The stress field at infinity is supposed to fulfil the conditions

$$\lim_{y\to\infty}\sigma_x(x,y)=0,\quad \lim_{y\to-\infty}\sigma_y(x,y)=\sigma_y^\infty,\quad \lim_{y\to\pm\infty}\tau_{xy}(x,y)=0, \tag{5.22}$$

where $\sigma_y^\infty = F_y/1$. In order to understand the influence of the infinite row of loaded holes on the global equilibrium, the stress field resulting from an infinite row of concentrated forces F_y distributed in the same way as the holes is briefly discussed first. The corresponding complex potentials are obtained by an infinite superposition of the solutions for a concentrated force as

$$\varphi(z)=\frac{-iF_y}{2\pi(1+\kappa)}\ln\sin(\pi z), \tag{5.23a}$$

$$\psi(z)=\frac{-i\kappa F_y}{2\pi(1+\kappa)}\ln\sin(\pi z)+\frac{i\pi F_y}{2\pi(1+\kappa)}z\cot(\pi z). \tag{5.23b}$$

These potentials produce stresses that are periodic in x-direction with period 1 and have the following limits as $y\to\pm\infty$:

$$\lim_{y\to\infty}\sigma_x(x,y)=\frac{-3+\kappa}{2(1+\kappa)}\sigma_y^\infty,\qquad \lim_{y\to-\infty}\sigma_x(x,y)=\frac{3-\kappa}{2(1+\kappa)}\sigma_y^\infty, \tag{5.24a}$$

$$\lim_{y\to\infty}\sigma_y(x,y)=-\frac{1}{2}\sigma_y^\infty,\qquad \lim_{y\to-\infty}\sigma_y(x,y)=\frac{1}{2}\sigma_y^\infty, \tag{5.24b}$$

$$\lim_{y\to\infty}\tau_{xy}(x,y)=0,\qquad \lim_{y\to-\infty}\tau_{xy}(x,y)=0. \tag{5.24c}$$

The only terms in the solution for an infinite row of loaded holes (4.114) that contribute to the stresses at infinity are the potentials $\hat\varphi_0^n(z),\hat\psi_0^n(z)$ and the potentials (5.23). Therefore, in order to obtain a solution satisfying (5.22), the potentials $\hat\varphi_0^n(z),\hat\psi_0^n(z)$ have to be chosen as

$$\hat\varphi_0^n(z)=\delta_{n0}\frac{\sigma_y^\infty}{2(1+\kappa)}z,\quad \hat\psi_0^n(z)=-\delta_{n0}\frac{(1-\kappa)\sigma_y^\infty}{2(1+\kappa)}z. \tag{5.25}$$

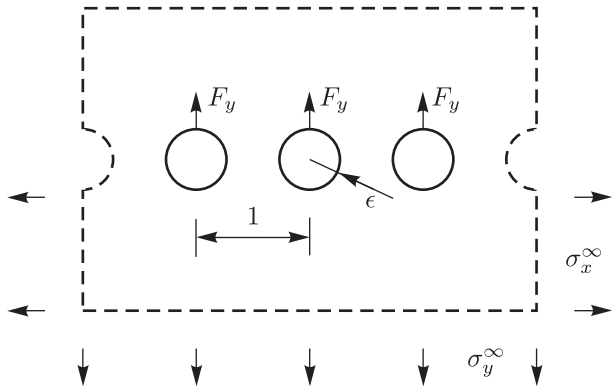

Figure 5.17: An infinite plane containing a single row of pin-loaded holes.

Then, applying Algorithm 4.2 with $N_g = 1$, (5.25) and

$$N_H = \infty, \quad N_C = 1, \quad c_{1r} = r, \quad \rho_1 = 1 \tag{5.26a}$$

$$\hat{\varphi}_1^n(\zeta_1) = \delta_{n0} F_y \hat{\varphi}_{\mathrm{BL}}(\zeta_1), \quad \hat{\psi}_1^n(\zeta_1) = \delta_{n0} F_y \hat{\psi}_{\mathrm{BL}}(\zeta_1), \quad F_1^n = \delta_{n0} i F_y, \tag{5.26b}$$

where the functions $\hat{\varphi}_{\mathrm{BL}}(\zeta)$ and $\hat{\psi}_{\mathrm{BL}}(\zeta)$ have been defined in Section 3.2, yields the complex potentials

$$\varphi(z) = F_y \left[\frac{\pi z - i \ln \sin(\pi z)}{2\pi(1+\kappa)} - \frac{2\cot(\pi z)\epsilon}{3\pi} + \frac{\pi(1-\kappa)\cot(\pi z)\epsilon^2}{2(1+\kappa)} - \frac{2}{9}\pi \cot(\pi z)\epsilon^3 \right] + O(\epsilon^4), \tag{5.27}$$

$$\psi(z) = F_y \left[-\frac{\pi z(1-\kappa) - i\pi z \cot(\pi z) + i\kappa \ln \sin(\pi z)}{2\pi(1+\kappa)} - \frac{2\big(\pi z + \sin(2\pi z)\big)\epsilon}{3\pi \sin(\pi z)^2} - \frac{\pi\big(4\pi z(-1+\kappa) + (6-2\kappa)\sin(2\pi z)\big)\epsilon^2}{8(1+\kappa)\sin(\pi z)^2} + \frac{\pi\big(-13\cos(\pi z) + \cos(3\pi z) - 4\pi z \sin(\pi z)\big)\epsilon^3}{18 \sin(\pi z)^3} \right] + O(\epsilon^4). \tag{5.28}$$

The stresses resulting from these potentials satisfy the conditions (5.22) at infinity and

$$\lim_{y \to -\infty} \sigma_x(x,y) = \frac{3-\kappa}{1+\kappa}\sigma_y^\infty, \quad \lim_{y \to \infty} \sigma_x(x,y) = 0. \tag{5.29}$$

The solution satisfies the periodic conditions on the vertical lines $x = \frac{1}{2} + k, k \in \mathbb{Z}$,

$$u(1/2 + k, y) = 0, \quad t_y(1/2 + k, y) = 0. \tag{5.30}$$

The strain in the comparative plate is

$$\varepsilon_x^* = \lim_{y \to -\infty} \varepsilon_x(x,y) = 0, \quad \varepsilon_y^* = \lim_{y \to -\infty} \varepsilon_y(x,y) = \frac{(\kappa-1)\sigma_y^\infty}{G(1+\kappa)}, \tag{5.31a}$$

$$\gamma_{xy}^* = \lim_{y \to -\infty} \gamma_{xy}(x,y) = 0. \tag{5.31b}$$

Finally, the compliance of the row of pin-loaded holes evaluated using (3.22) is

$$C = \frac{2(1+\kappa)(3+\kappa)+3\pi-3\pi\kappa\ln(2\pi\epsilon)}{6\pi^2(1+\kappa)G} + \frac{(8+12\pi+12\kappa-9\pi\kappa+4\kappa^2+3\pi\kappa^2)\,\epsilon}{12\pi(1+\kappa)G} + \frac{(16+63\pi+32\kappa-36\pi\kappa+16\kappa^2+15\pi\kappa^2)\,\epsilon^2}{72(1+\kappa)G} + \frac{(4\pi+9\pi^2+8\pi\kappa+6\pi^2\kappa+4\pi\kappa^2-3\pi^2\kappa^2)\,\epsilon^3}{36(1+\kappa)G} + O(\epsilon^4). \quad (5.32)$$

Under the assumption of plane stress, this expression can be written in terms of the engineering constants E and ν as

$$C = \frac{3\pi(1+\nu)^2+16(3+\nu)+3\pi\,(-3-2\nu+\nu^2)\ln(2\pi\epsilon)}{12\pi^2E} + \frac{(20+3\pi+4\nu-3\pi\nu+6\pi\nu^2)\,\epsilon}{6\pi E} + \frac{(128+45\pi-18\pi\nu+57\pi\nu^2)\,\epsilon^2}{72E} + \frac{2\,(4\pi+3\pi^2\nu)\,\epsilon^3}{9E} + O(\epsilon^4). \quad (5.33)$$

When an additional tension $\tilde{\sigma}_x = -\frac{3-\kappa}{1+\kappa}\sigma_x^\infty$ in the x-direction is prescribed at infinity so that instead of (5.29), the stresses at infinity satisfy the conditions

$$\lim_{y\to-\infty}\sigma_x(x,y) = 0, \quad \lim_{y\to\infty}\sigma_x(x,y) = -\frac{3-\kappa}{1+\kappa}\sigma_y^\infty, \quad (5.34)$$

the potentials $\hat{\varphi}_0(z), \hat{\psi}_0(z)$ have to be chosen as

$$\hat{\varphi}_0^n(z) = \delta_{n0}\frac{(\kappa-1)\sigma_y^\infty}{4(1+\kappa)}z, \quad \hat{\psi}_0^n(z) = \delta_{n0}\frac{\sigma_y^\infty}{1+\kappa}z \quad (5.35)$$

and the compliance becomes

$$C = \frac{2(1+\kappa)(3+\kappa)+3\pi-3\pi\kappa\ln(2\pi\epsilon)}{6\pi^2(1+\kappa)G} + \frac{(8+3\pi+12\kappa+3\pi\kappa+4\kappa^2)\,\epsilon}{12\pi(1+\kappa)G} + \frac{(16-45\pi+32\kappa+54\pi\kappa+16\kappa^2-3\pi\kappa^2)\,\epsilon^2}{72(1+\kappa)G} + \frac{(4\pi-9\pi^2+8\pi\kappa-6\pi^2\kappa+4\pi\kappa^2+3\pi^2\kappa^2)\,\epsilon^3}{36(1+\kappa)G} + O(\epsilon^4). \quad (5.36)$$

It can be observed that the first term remains unchanged and the tension affects the terms of the order $O(\epsilon)$ and higher.

Figure (5.18) shows the dependence of the partial sums of the series (5.32) on the relative hole radius ϵ. N denotes the highest power involved in the partial sum, $N = 0$ corresponding to the first term that involves a constant and a logarithmic part. The compliance in this and all subsequent plots is nondimensionalised by the inverse Young's modulus, i.e. the plotted quantity is CE. The points labelled 'FEM' were obtained using the contact variant of the FEM model described in Section 4.4. As can be seen, in the technically relevant domain $\epsilon < 0.2$, the the curve $N = 1$ agrees well with the numerical results. For higher values of ϵ, corrections of higher order are necessary. On the other hand, a small

discrepancy between the numerical and analytical solutions for small ϵ is caused by the inaccuracy of the assumed contact stress distribution.

Finally, assume that the holes are loaded with a general distribution of normal and tangential forces of the form (3.13) with $N_g = 5$. Then the compliance is given as

$$\begin{aligned} C = \frac{1}{2\pi(1+\kappa)G}\Big[&1 - \kappa\ln(2\pi\epsilon) - \pi\left(5+6\kappa+\kappa^2\right)\operatorname{Re} g_{-5} + \pi\left(4+5\kappa+\kappa^2\right)\operatorname{Im} g_{-4} \\ &+ \pi\kappa(1+\kappa)\operatorname{Re} g_{-3} - \pi\kappa(1+\kappa)\operatorname{Im} g_{-2} - \pi\kappa(1+\kappa)\operatorname{Re} g_{-1} - \pi(1+\kappa)\operatorname{Re} g_1 \\ &+ \pi(1+\kappa)\operatorname{Im} g_2 + \pi(1+\kappa)\operatorname{Re} g_3 - \pi(1+\kappa)\operatorname{Im} g_4 - \pi(1+\kappa)\operatorname{Re} g_5\Big] \\ &+ \frac{1}{4(1+\kappa)G}\Big[4 - 3\kappa + \kappa^2 + 2\pi(1-\kappa^2)\operatorname{Re} g_{-1} - 2\pi(1+\kappa)\operatorname{Re} g_1\Big]\epsilon \\ &+ \frac{1}{24(1+\kappa)G}\Big[21\pi - 12\pi\kappa + 5\pi\kappa^2 + 4\pi^2\left(-2-\kappa+\kappa^2\right)\operatorname{Im} g_{-2} \\ &+ 4\pi^2\left(1+2\kappa+\kappa^2\right)\operatorname{Re} g_{-1} - 4\pi^2\left(1+2\kappa+\kappa^2\right)\operatorname{Re} g_1 - 4\pi^2(1+\kappa)\operatorname{Im} g_2\Big]\epsilon^2 \\ &+ \frac{1}{12G}\Big[\pi^2(3-\kappa) + 4\pi^3(-2+\kappa)\operatorname{Re} g_{-1} + 2\pi^3(-2+\kappa)\operatorname{Re} g_1\Big]\epsilon^3 + O(\epsilon)^4. \end{aligned} \quad (5.37)$$

The influence of the number of terms N_g is investigated in the right part of Figure 5.18. It can be seen that $N_g = 0$ leads to a grossly inaccurate solution but starting from $N = 1$, the increasing number of terms has virtually no impact on the quality of the approximation in the whole domain of interest. Therefore, $N_g = 1$ has been chosen for this and subsequent applications.

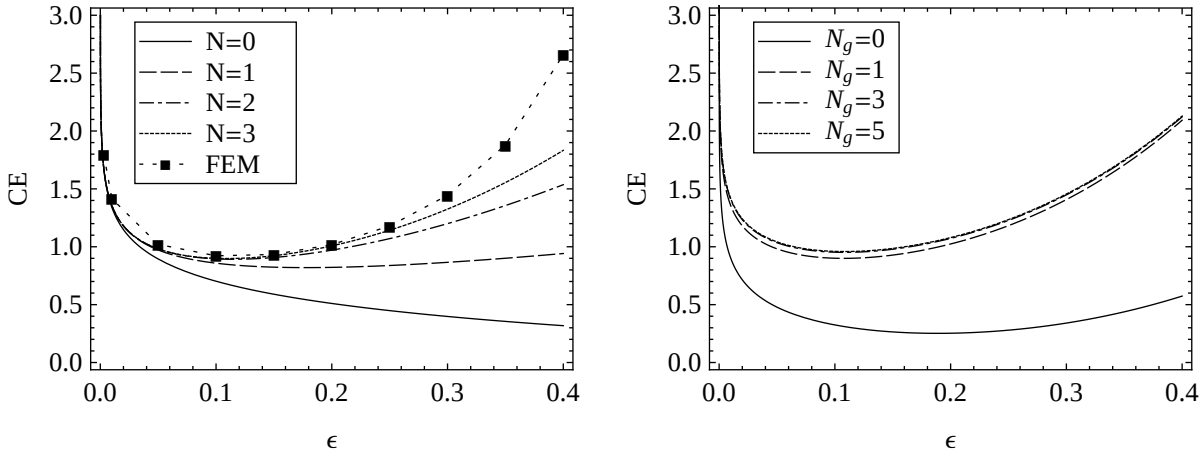

Figure 5.18: Dependence of the compliance of an infinite row of pin-loaded holes in an isotropic plane on the relative hole radius. Left: Convergence of (5.32) with respect to the approximation order N. Right: convergence of (5.37) with respect to the number N_g of the terms involved in the series (3.13).

Comparison to Huth's formula

Although the proposed formula (5.32) describes the compliance of an infinite row of pin-loaded holes, it is certainly interesting to compare it to some of the semi-empirical

formulae for the compliance of a joint involving a single bolt such as Huth's formula. Huth's formula in the present notation reads

$$C^{(\mathrm{J})} = \left(\frac{t^{(1)}+t^{(2)}}{2d}\right)^{a} \frac{b}{n}\left(\frac{1}{nt^{(1)}E^{(1)}}+\frac{1}{t^{(2)}E^{(2)}}+\frac{1}{2nt^{(1)}E^{(\mathrm{P})}}+\frac{1}{2t^{(2)}E^{(\mathrm{P})}}\right), \tag{5.38}$$

where $E^{(1)}$ and $E^{(2)}$ are the Young's moduli of the plates, $E^{(\mathrm{P})}$ is the Young's modulus of the bolt, d is the bolt diameter, $t^{(1)}$ and $t^{(2)}$ are the thicknesses of the plates, $n = 1$ for a single-shear and $n = 2$ for a double-shear configuration and the constants a and b depend on the type of joint:

- $a = 2/3, b = 3$ for bolted metallic joints,
- $a = 2/5, b = 2.2$ for riveted metallic joints,
- $a = 2/3, b = 4.2$ for bolted graphite/epoxy joints.

The joint compliance according to Huth's formula is clearly a sum of contributions of each of the plates and of the bolt. For a comparison to the present results on pin-loaded holes, only the part corresponding to plate compliance can be taken. A double-lap configuration is best suited for the comparison since the tilting of the bolt which is not taken into account in the present solution does not appear here. Setting $n = 2$, $t^{(1)} = t^{(2)} = t$, $E^{(1)} = E^{(2)} = E$, $a = \frac{2}{3}$, $b = 3$ in (5.38) and omitting the terms corresponding to the bolt compliance yields

$$C^{(\mathrm{J})} = \frac{9}{4}\left(\frac{t}{d}\right)^{2/3}\frac{1}{tE}. \tag{5.39}$$

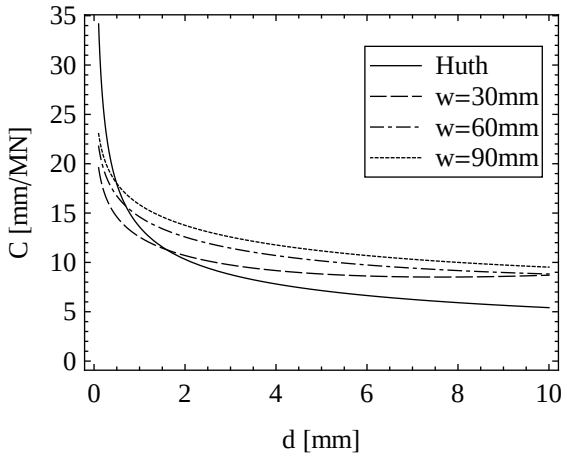

Figure 5.19: Comparison of the present result on the compliance of an infinite row of pin-loaded holes to Huth's formula.

The bolt diameter is nondimensionalised by the plate thickness in the Huht's formula. Therefore, in contrast to the proposed formula (5.32), Huth's formula does not possess the proper scaling $C \propto \frac{1}{Et}$ which is necessary to take into account the effects of plane deformations. For this reason, both formulae can be compared to each other only in terms of dimensioned quantities.

The present results are generated by combining the formula (3.23) with the first two terms of the asymptotic expansion (5.32). The comparison is shown in Figure 5.19. The dimensions used correspond roughly to the dimensions of specimens tested by Huth in his work [35]. Although the general run of both curves is similar, it can be seen that the numerical values differ by tens of percents.

5.2.2 A half-plane containing a single row of pin-loaded holes

Now, the influence of the finite edge distance on the results of the previous section is discussed. Therefore, consider a half-plane with a single row of holes with spacing 1 and edge distance h (see Figure 5.20). The holes are loaded by the distribution of radial and tangential load (3.13) with a total resultant F_y in the y-direction. The edge of the half-plane is free and as $y \to -\infty$, the following limits are expected:

$$\lim_{y\to-\infty} \sigma_x(x,y) = 0, \quad \lim_{y\to-\infty} \sigma_y(x,y) = \sigma_y^\infty. \tag{5.40}$$

The potentials $\hat{\varphi}_0(z)$ and $\hat{\psi}_0(z)$ are chosen according to (5.35).

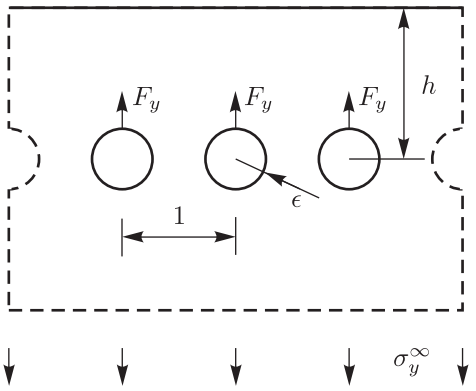

Figure 5.20: A half-plane containing an infinite row of pin-loaded holes.

Applying Algorithm 4.2 with

$$N_H = \infty, \quad N_C = 1, \quad c_{1r} = r - ih, \tag{5.41}$$

the potentials $\hat{\varphi}_0^n(z)$ and $\hat{\psi}_0^n(z)$ according to (5.35) and other settings as in (5.26) yields the following complex potentials:

$$\varphi(z) = F_y \left[-\frac{z}{4} - \frac{-4ih\pi \coth(\pi(h+iz)) + 2i \ln\sinh(\pi(h-iz)) + 2i\kappa \ln\sinh(\pi(h+iz))}{4\pi(1+\kappa)} \right.$$
$$\left. + \frac{2i}{3\pi}\big(\coth(\pi(h-iz)) + 2\coth(\pi(h+iz)) + 2h\pi \operatorname{csch}(\pi(h+iz))^2\big)\epsilon \right] + O(\epsilon^2), \tag{5.42a}$$

$$\psi(z) = F_y \left[\frac{1}{2\pi(1+\kappa)} \Big(\pi(1+\kappa)z - \pi z(-1+\kappa)\coth(h\pi) + 2ih\pi \coth(\pi(h-iz)) \right.$$
$$\left. - 2h\pi^2 z \operatorname{csch}(\pi(h+iz))^2 - i\kappa \ln\sinh(\pi(h-iz)) - i\ln\sinh(\pi(h+iz)) \right.$$

$$+ i\pi z \operatorname{csch}(h\pi)\operatorname{csch}(\pi(h-iz))\sin(\pi z) + i\pi z\kappa \operatorname{csch}(h\pi)\operatorname{csch}(\pi(h+iz))\sin(\pi z)\Big)$$
$$+ \frac{1}{3\pi}\Big(4i\coth(\pi(h-iz)) + 2\pi(2ih+z)\operatorname{csch}(\pi(h-iz))^2 - 4\pi z\operatorname{csch}(\pi(h+iz))^2$$
$$+ 2i\coth(\pi(h+iz)) - 8h\pi^2 z\operatorname{csch}(\pi(h+iz))^2\coth(\pi(h+iz))\Big)\epsilon\Big] + O(\epsilon^2). \quad (5.42b)$$

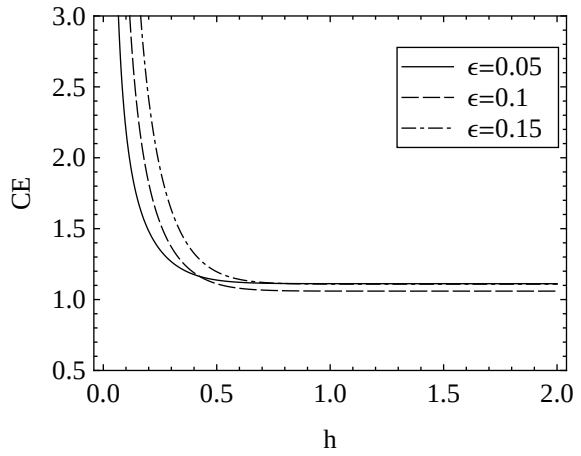

Figure 5.21: Dependence of the compliance of an infinite row of pin-loaded holes in an isotropic half-plane (5.43) on relative edge distance.

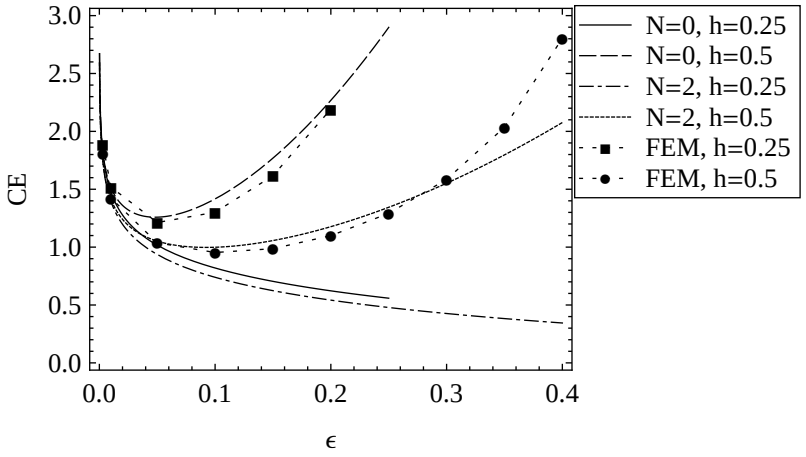

Figure 5.22: Dependence of the compliance of an infinite row of pin-loaded holes in an isotropic half-plane (5.44) on the relative hole radius.

Evaluating the compliance according to the definition (3.22) yields a rather lengthy expression

$$C = \frac{1}{24\pi^2(1+\kappa)G}\Big[24 + 12\pi + 12h\pi^2 + 32\kappa - 24h\pi^2\kappa + 8\kappa^2 + 12h\pi^2\kappa^2 + 6h\pi^2\kappa\coth(h\pi)$$
$$+ 18h\pi^2\kappa\coth(2h\pi) - 6h\pi^2\kappa\operatorname{csch}(2h\pi) + 24h^2\pi^3\operatorname{csch}(2h\pi)^2 - 3\pi\ln(4) - 6\pi\kappa\ln(4)$$
$$- 3\pi\kappa^2\ln(4) - 12\pi\kappa\ln(\pi) - 12\pi\kappa\ln(\epsilon) - 6\pi\ln(\sinh(2h\pi)) - 6\pi\kappa^2\ln(\sinh(2h\pi))\Big]$$

$$+\frac{1}{48G\pi}\Big[-6\pi-6\pi\kappa-8\,\mathrm{csch}(2h\pi)^2-3\pi\,\mathrm{csch}(2h\pi)^2+64h\pi\,\mathrm{csch}(2h\pi)^2$$
$$+8\kappa\,\mathrm{csch}(2h\pi)^2-3\pi\kappa\,\mathrm{csch}(2h\pi)^2+32h\pi\kappa\,\mathrm{csch}(2h\pi)^2+24h\pi^2\kappa\,\mathrm{csch}(2h\pi)^2$$
$$+8\cosh(4h\pi)\,\mathrm{csch}(2h\pi)^2+3\pi\cosh(4h\pi)\,\mathrm{csch}(2h\pi)^2-8\kappa\cosh(4h\pi)\,\mathrm{csch}(2h\pi)^2$$
$$+3\pi\kappa\cosh(4h\pi)\,\mathrm{csch}(2h\pi)^2-4\coth(2h\pi)\,\mathrm{csch}(2h\pi)^2-3\pi\coth(2h\pi)\,\mathrm{csch}(2h\pi)^2$$
$$+128h^2\pi^2\coth(2h\pi)\,\mathrm{csch}(2h\pi)^2+96h^2\pi^3\coth(2h\pi)\,\mathrm{csch}(2h\pi)^2-8\kappa\coth(2h\pi)\,\mathrm{csch}(2h\pi)^2$$
$$+4\cosh(6h\pi)\,\mathrm{csch}(2h\pi)^3+3\pi\cosh(6h\pi)\,\mathrm{csch}(2h\pi)^3+8\kappa\cosh(6h\pi)\,\mathrm{csch}(2h\pi)^3\Big]\epsilon+O(\epsilon^2). \tag{5.43}$$

As expected, this function tends to the result for the full plane (5.36) as $h \to \infty$. This formula can be further simplified for small values of h by means of Taylor expansion in h which gives

$$C=\frac{1}{24\pi^2(1+\kappa)G}\left[24+18\pi+32\kappa+12\pi\kappa-6\pi(1+\kappa^2)\ln(4\pi h)-12\pi\kappa\ln(2\pi\epsilon)\right]$$
$$+\frac{(-1+\kappa)^2h}{2(1+\kappa)G}-\frac{\pi\,(3-4\kappa+\kappa^2)\,h^2}{6(1+\kappa)G}$$
$$+\left[\frac{20+9\pi+12\kappa+3\pi\kappa}{24\pi^2hG}-\frac{-1+\kappa}{3\pi G}-\frac{(-4+3\pi)(-1+\kappa)h}{18G}\right]\epsilon+O(\epsilon^2)+O(h^3). \tag{5.44}$$

The dependence of the leading-order approximation of the compliance (5.43) on the parameter h is shown in Figure 5.21. It can be seen that the compliance converges rapidly to the result for the infinite plate and for $h > 0.5$, the parameter h has virtually no influence on the result.

The dependence of the compliance on the parameter ϵ is shown in Figure 5.22 for two relatively small values of h. The curves labelled 'FEM' have been obtained using the contact variant of the FEM model described in Section 4.4. The discrepancy between the asymptotic and numerical solution, which is larger here than in the case of full plane, is in the first place due to the inaccuracy of the assumed distribution of contact stresses and to some extent also due to the omission of higher-order terms in h.

5.3 Load distribution on pin-loaded holes

The compatibility conditions required for the determination of the load distribution on bolts were presented in Section 3.4. In this section, these compatibility conditions are combined with the asymptotic solution of the underlying plane problem in order to obtain the load distribution on bolts in form of an asymptotic series.

In this work, it is assumed for simplicity that the distribution of the contact pressure is equal on all bolts and is independent of the load magnitude. Therefore, the asymptotic series for the load distribution coefficients can be obtained in the following manner. First,

the coefficients λ_p are written in form of an asymptotic series

$$\lambda_p = \sum_{n=0}^{\infty} \lambda_p^n \epsilon^n. \tag{5.45}$$

The complex potentials and the resulting displacements are then computed by one of the Algorithms 4.2 or 4.3. Finally, the asymptotic series for the displacements is substituted into the compatibility conditions and a set of linear algebraic equations for the unknown coefficients λ_p^n, $p = 1, \ldots, N_A$, $n = 0, \ldots, N$ is obtained by comparing the left- and right-hand-side of the compatibility conditions term-by-term.

5.3.1 A finite row of holes perpendicular to the load direction

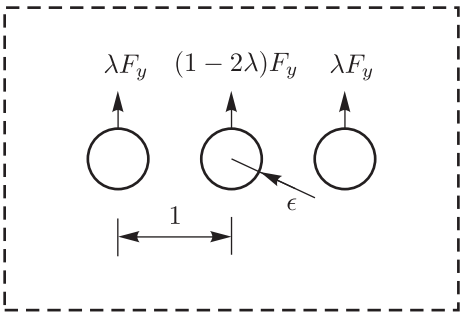

Figure 5.23: An infinite plane containing three pin-loaded holes.

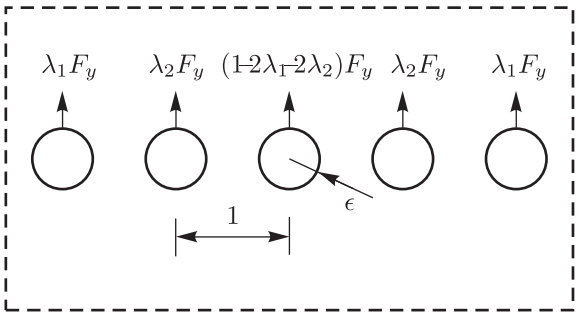

Figure 5.24: An infinite plane containing five pin-loaded holes.

As the first example, consider an infinite isotropic plate containing three pin-loaded holes of radius ϵ and respective distance 1 as shown in Figure 5.23. This elastic plate is connected to a rigid one, the corresponding compatibility condition (3.26) becomes

$$V_1 = V_2 = V_3, \tag{5.46}$$

where the displacements are given as

$$V_p = v(c_p + i\epsilon), \quad p = 1, 2, 3. \tag{5.47}$$

The force transmitted over all holes is F_y. From the symmetry of the problem it follows that the forces transmitted over the left and the right bolt are equal. The corresponding load transfer coefficient λ introduced in Figure 5.23 is assumed to have the form of an asymptotic series

$$\lambda = \sum_{n=0}^{\infty} \lambda^n \epsilon^n. \tag{5.48}$$

Algorithm 4.2 with

$$N_H = 3, \quad c_p = p - 1, \quad \rho_p = 1, \hat{\varphi}_0^n(z) = 0, \quad \hat{\psi}_0^n(z) = 0, \tag{5.49a}$$

$$\hat{\varphi}_1^n(\zeta) = \hat{\varphi}_3^n(\zeta) = \lambda^n F_y \hat{\varphi}_{\mathrm{BL}}(\zeta), \quad \hat{\psi}_1^n(\zeta) = \hat{\psi}_3^n(\zeta) = \lambda^n F_y \hat{\psi}_{\mathrm{BL}}(\zeta), \tag{5.49b}$$

$$\hat{\varphi}_2^n(\zeta) = (\delta_{n0} - 2\lambda^n) F_y \hat{\varphi}_{\mathrm{BL}}(\zeta), \quad \hat{\psi}_2^n(\zeta) = (\delta_{n0} - 2\lambda^n) F_y \hat{\psi}_{\mathrm{BL}}(\zeta), \tag{5.49c}$$

$$F_1^n = F_3^n = \lambda^n i F_y, \quad F_2^n = \lambda^n i F_y, \tag{5.49d}$$

where the functions $\hat{\varphi}_{\mathrm{BL}}(\zeta)$ and $\hat{\psi}_{\mathrm{BL}}(\zeta)$ are defined in Section 3.2, gives the complex potentials

$$\varphi(z) = F_y \left[-\frac{i\big(\lambda \ln(-1+z) + (1-2\lambda)\ln(z) + \lambda \ln(1+z)\big)}{2\pi(1+\kappa)} - \frac{2\,(-1+z^2+2\lambda)\,\epsilon}{3\pi^2 z(-1+z^2)} \right.$$
$$\left. + \frac{i(2-2\kappa-3\lambda+3\kappa\lambda)\epsilon^2}{2\pi(1+\kappa)(-1+z^2)} + \frac{(-4z^2+4\lambda+3z^2\lambda)\,\epsilon^3}{3\pi^2 z(-1+z^2)} \right] + O(\epsilon^4), \tag{5.50}$$

$$\psi(z) = F_y \left[-\frac{i\kappa\big(\lambda \ln(-1+z) + (1-2\lambda)\ln(z) + \lambda \ln(1+z)\big)}{2\pi(1+\kappa)} + \frac{i\lambda}{\pi(1+\kappa)(-1+z^2)} \right.$$
$$- \frac{2\big(3+3z^4-6\lambda+2z^2(-3+5\lambda)\big)\epsilon}{3\pi^2 z(-1+z^2)^2} + \frac{i(-1+\kappa)(-2+3\lambda)\,(1+z^2)\,\epsilon^2}{2\pi(1+\kappa)\,(-1+z^2)^2}$$
$$\left. + \frac{\big(-8\lambda+16z^2\lambda+z^4(-8+6\lambda)\big)\epsilon^3}{3\pi^2 z(-1+z^2)^2} \right] + O(\epsilon^4). \tag{5.51}$$

In these expressions, a truncation of the series (5.48) to an appropriate order has to be substituted for λ. Evaluating the displacements V_1 and V_2 by means of (5.47), substituting them into the equation (5.46), comparing likewise powers of ϵ, solving for λ^n, $n = 1, \ldots, N$ and substituting the solution into (5.48) yields the final result

$$\lambda = \frac{1}{3} + \frac{\frac{1}{3}\pi\kappa \ln(2)}{8 + 3\pi + \kappa(10 - \pi \ln(2)) + 2\kappa^2 - 3\pi\kappa \ln(\epsilon)} + O(\epsilon^2). \tag{5.52}$$

The dependence of the parameter λ on the relative hole radius ϵ is plotted in Figure 5.25. In this example, the parameter ϵ lies in the interval $0 < \epsilon < 1/2$. The curve $N = 0$ corresponds to the equation (5.52), the curve $N = 2$ shows the influence of the quadratic correction. The points labelled 'FEM' represent results obtained by the contact variant of the FEM model described in Section 4.4. As can be seen, the curve $N = 0$ agrees well with the numerical curve in the technically relevant domain $\epsilon < 0.2$, the quadratic correction being significant for large values of ϵ. The slight difference between both curves near $\epsilon = 0$ is caused by the inaccuracy of the assumed form of contact stresses.

When the number of the holes is increased to five as shown in Figure 5.24, the load distribution due to the symmetry is described by two coefficients λ_1 and λ_2 introduced in Figure 5.24. Proceeding in the same manner as in the first example, one obtains long formulae for the load distribution coefficients that can be written as

$$\lambda_1 = \frac{\lambda_1^{N0} + \lambda_1^{N1} \ln(\epsilon) + \lambda_1^{N2} \ln(\epsilon)^2}{\lambda_1^{D0} + \lambda_1^{D1} \ln(\epsilon) + \lambda_1^{D2} \ln(\epsilon)^2} + O(\epsilon^2), \quad \lambda_2 = \frac{\lambda_2^{N0} + \lambda_2^{N1} \ln(\epsilon) + \lambda_2^{N2} \ln(\epsilon)^2}{\lambda_2^{D0} + \lambda_2^{D1} \ln(\epsilon) + \lambda_2^{D2} \ln(\epsilon)^2} + O(\epsilon^2), \tag{5.53}$$

where

$$\lambda_1^{N0} = 4(8+3\pi)^2 + 4(8+3\pi)\big(20+3\pi\ln(3)\big)\kappa + 12\big(44-3\pi^2\ln(2)^2+4\pi+10\pi\ln(3)\big)\kappa^2 + 8\big(20+3\pi\ln(3)\big)\kappa^3 + 16\kappa^4, \quad (5.54a)$$

$$\lambda_2^{N0} = 4(8+3\pi)^2 - 4(8+3\pi)\big(-20+6\pi\ln(2)-3\pi\ln(3)\big)\kappa + 12\big(44+4\pi-20\pi\ln(2)+10\pi\ln(3)-6\pi^2\ln(2)^2+3\pi^2\ln(2)\ln(3)\big)\kappa^2 + 8\big(20-6\pi\ln(2)+3\pi\ln(3)\big)\kappa^3 + 16\kappa^4, \quad (5.54b)$$

$$\lambda_1^{N1} = -24\pi(8+3\pi)\kappa - 12\pi\big(20+3\pi\ln(3)\big)\kappa^2 - 48\pi\kappa^3, \quad (5.54c)$$

$$\lambda_2^{N1} = -24(\pi(8+3\pi))\kappa + 12\pi\big(-20+6\pi\ln(2)-3\pi\ln(3)\big)\kappa^2 - 48\pi\kappa^3, \quad (5.54d)$$

$$\lambda_1^{N2} = \lambda_2^{N2} = 36\pi^2\kappa^2, \quad (5.54e)$$

$$\lambda_1^{D0} = \lambda_2^{D0} = 20(8+3\pi)^2 + 4(8+3\pi)\big(100-15\pi\ln(2)+12\pi\ln(3)\big)\kappa - 12\big(-220-20\pi+50\pi\ln(2)+40\pi\ln(3)+18\pi^2\ln(2)^2-12\pi^2\ln(2)\ln(3)+3\pi^2\ln(3)^2\big)\kappa^2 + \big(800-120\pi\ln(2)+96\pi\ln(3)\big)\kappa^3 + 80\kappa^4, \quad (5.54f)$$

$$\lambda_1^{D1} = -120\pi(8+3\pi)\kappa - 12\pi\big(100-15\pi\ln(2)+12\pi\ln(3)\big)\kappa^2 - 240\pi\kappa^3, \quad (5.54g)$$

$$\lambda_1^{D2} = \lambda_2^{D2} = 180\pi^2\kappa^2. \quad (5.54h)$$

The dependence of the leading-order approximation of the load transfer coefficients on the relative hole radius is plotted along with a finite-element solution in Figure 5.26. Similarly as in the previous example, this approximation gives satisfactory results in the technically relevant domain $\epsilon < 0.2$.

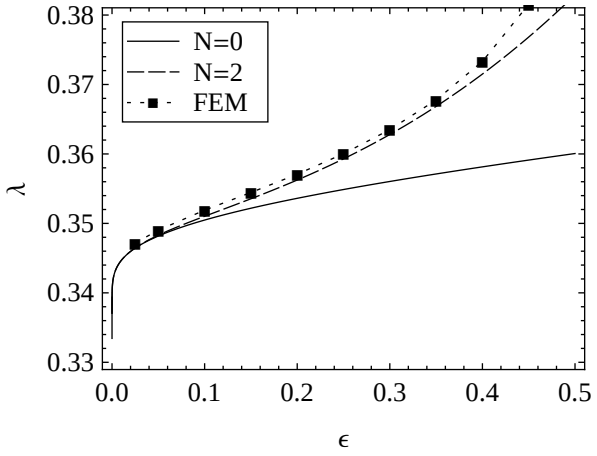

Figure 5.25: Dependence of the load distribution coefficient (5.52) on the relative hole radius.

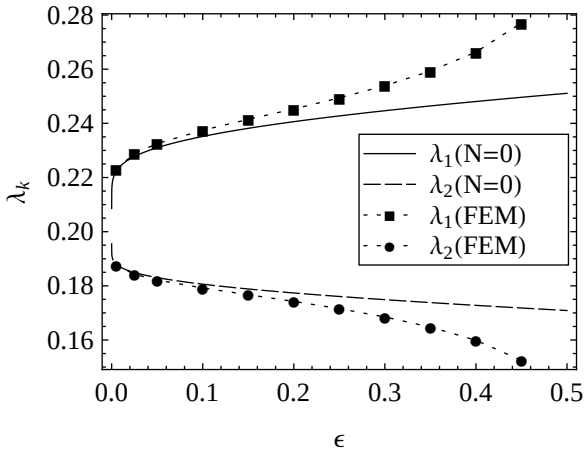

Figure 5.26: Dependence of the load distribution coefficients (5.53) on the relative hole radius.

Now, the influence of a finite edge at the distance h from the row is investigated (cf. Figure 5.27). The same procedure as above gives a lengthy formula for the load distribution coefficient in terms of the edge distance h that converges to the result for the full plane as $h \to \infty$. For small values of h, a compact approximation can be obtained by performing a

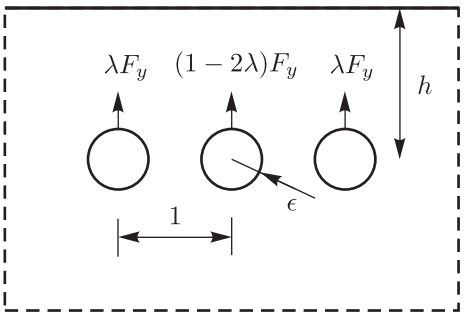

Figure 5.27: An half-plane containing three pin-loaded holes.

Taylor series expansion

$$\lambda = \frac{1}{3} + \frac{\frac{1}{3}\pi\ln(2)(1+\kappa)^2}{\big(16{+}9\pi{+}2\ln(2)\big){+}\big(20{+}6\pi{+}\ln(2)\big)\kappa{+}2\big(2{+}\ln(2)\big)\kappa^2{-}3\pi(1{+}\kappa^2)\ln(h){-}6\pi\kappa\ln(\epsilon)} + O(\epsilon^2) + O(h^2). \quad (5.55)$$

The exact dependence of the load distribution coefficient on the edge distance for two values of the relative radius along with the approximation (5.55) is plotted in Figure 5.28.

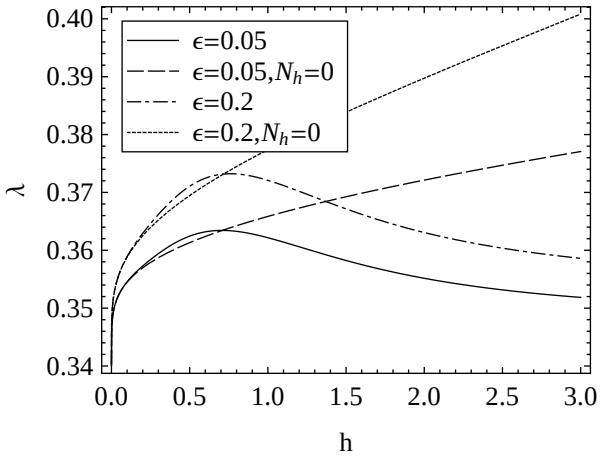

Figure 5.28: Dependence of the load distribution coefficient for three holes in a half-plane on the relative hole radius. The curves denoted $N_h = 0$ correspond to the Taylor expansion (5.55), the other curves to the exact dependency on h.

The solution in the anisotropic case proceeds in the same manner using the Algorithm 4.3 with the following settings:

$$N_H = 3, \quad c_p = p - 1, \quad \rho_p = 1, \quad m_p = 1, \quad \hat{\varphi}^n_{0j}(z_j) = 0, \quad (5.56a)$$

$$\hat{\varphi}^n_{1j}(\zeta_j) = \hat{\varphi}^n_{3j}(\zeta_j) = \lambda^n F_y \hat{\varphi}_{j\mathrm{BL}}(\zeta_j), \quad F^n_1 = F^n_3 = \lambda^n i F_y, \quad (5.56b)$$

$$\hat{\varphi}^n_{2j}(\zeta_j) = (\delta_{n0} - 2\lambda^n) F_y \hat{\varphi}_{j\mathrm{BL}}(\zeta_j), \quad F^n_2 = (\delta_{n0} - 2\lambda^n) i F_y, \quad (5.56c)$$

where the functions $\hat{\varphi}_{j\mathrm{BL}}(\zeta_j)$ have been defined in Section 3.2. Although the algorithm can be evaluated for arbitrary material behaviour, the results in the case of general material parameters are lengthy. Compact closed-form results can be obtained assuming strong orthotropy. Below, the leading-order terms for each of the cases listed in Section 2.3.3 are given. In the case of large E_1, the leading-order approximation reads

$$\lambda = \frac{1}{3} + \frac{\frac{2}{3}\pi\ln(2)\left(1+\sqrt{\frac{G_{12}}{E_2}}\right)}{32-3\pi-2\pi\ln(2)+(32+9\pi-2\pi\ln(2))\sqrt{\frac{G_{12}}{E_2}}-6\pi\left(1+\sqrt{\frac{G_{12}}{E_2}}\right)\ln\left(\epsilon\sqrt{\frac{G_{12}}{E_2}}\right)} + O(\epsilon^2) + O\left(\frac{E_2}{E_1}\right), \quad (5.57)$$

in the case of large E_2, it becomes

$$\lambda = \frac{1}{3} + \frac{\frac{2}{3}\pi\ln(2)}{32-3\pi-2\pi\ln(2)-(16+3\pi)\sqrt{\frac{G_{12}}{E_1}}-6\pi\ln\left(\epsilon\sqrt{\frac{G_{12}}{E_2}}\right)} + O(\epsilon^2) + O\left(\frac{E_1}{E_2}\right) \quad (5.58)$$

and finally in the case of large E_1 and E_2, it takes the form

$$\lambda = \frac{1}{3} + \frac{\frac{2}{3}\pi\ln(2)}{32-3\pi-2\pi\ln(2)-6\pi\ln\left(\epsilon\sqrt{\frac{G_{12}}{E_2}}\right)} + O(\epsilon^2) + O\left(\frac{G_{12}}{E_1}\right). \quad (5.59)$$

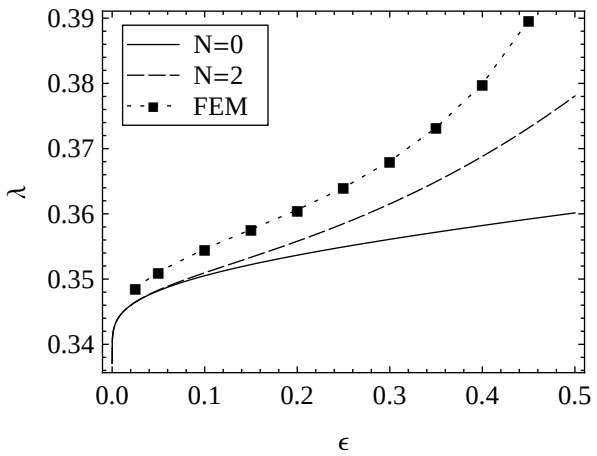

Figure 5.29: Dependence of the load distribution coefficient (5.57) on the relative hole radius.

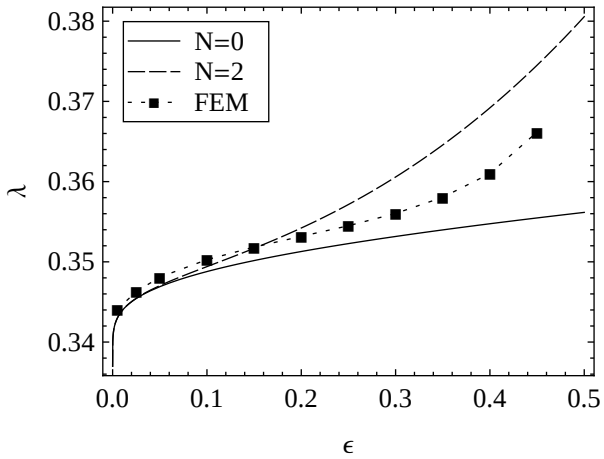

Figure 5.30: Dependence of the load distribution coefficient (5.59) on the relative hole radius.

The dependencies (5.57) and (5.59) are plotted along with the second order correction in Figures 5.29 and 5.30, respectively. In Figure 5.29, an unidirectional layer of T300/Epoxy is used while in Figure 5.30, a laminate with the layup $[\pm 0/90°]_s$ is assumed. Comparison with a numerical solution especially in the first case shows a discrepancy from the analytical solution even for small values of ϵ. It is caused by the departure of the contact pressure

distribution from the assumed form. The material parameters in this example have been chosen in such a way that the omission of the terms involving higher powers of the parameter accounting for strong orthotropy has only an insignificant impact of the numerical values of the results.

Finally, note that the load distribution coefficients (5.52), (5.53), (5.55) and (5.57) – (5.59) fulfil the intuitively expected relation

$$\lim_{\epsilon \to 0} \lambda = \frac{1}{N_H}, \tag{5.60}$$

which means that in the limit $\epsilon \to 0$, all holes carry the same load.

5.3.2 A finite row of holes parallel to the load direction

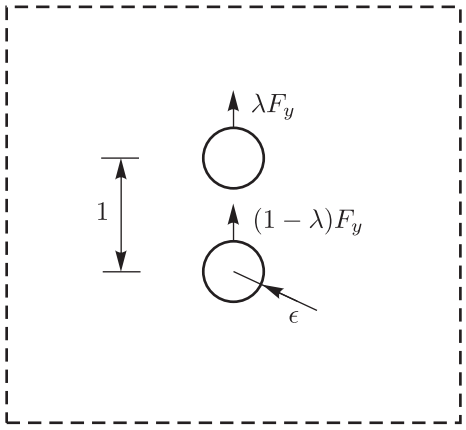

Figure 5.31: An infinite plane containing two pin-loaded holes.

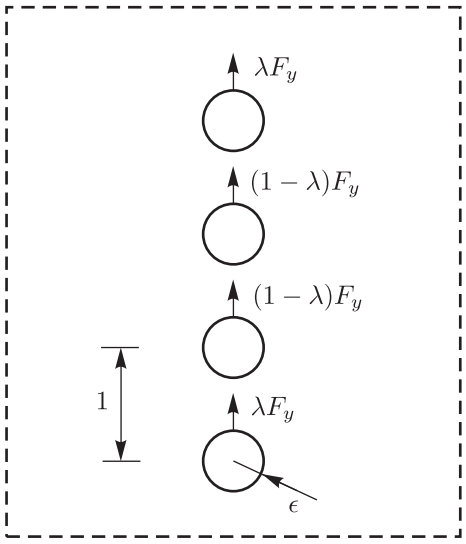

Figure 5.32: An infinite plane containing four pin-loaded holes.

Consider an infinite isotropic plate connected to a rigid plate by two bolts of radius ϵ and respective distance 1 as shown in Figure 5.31. The corresponding compatibility condition (3.26) becomes

$$V_1 = V_2. \tag{5.61}$$

Proceeding similarly as in the previous example, the Algorithm 4.2 with the settings

$$N_H = 2, \quad c_p = i(3/2 - p), \quad \rho_p = 1, \hat{\varphi}_0^n(z) = 0, \quad \hat{\psi}_0^n(z) = 0, \tag{5.62a}$$

$$\hat{\varphi}_1^n(\zeta_1) = \lambda^n F_y \hat{\varphi}_{\mathrm{BL}}(\zeta_1), \quad \hat{\psi}_1^n(\zeta_1) = \lambda^n F_y \hat{\psi}_{\mathrm{BL}}(\zeta_1), \tag{5.62b}$$

$$\hat{\varphi}_2^n(\zeta_2) = (\delta_{n0} - \lambda^n) F_y \hat{\varphi}_{\mathrm{BL}}(\zeta_2), \quad \hat{\psi}_2^n(\zeta_2) = (\delta_{n0} - \lambda^n) F_y \hat{\psi}_{\mathrm{BL}}(\zeta_2), \tag{5.62c}$$

$$F_1^n = \lambda^n i F_y, \quad F_2^n = (\delta_{n0} - \lambda^n) i F_y \tag{5.62d}$$

gives the load transfer coefficient

$$\lambda = \frac{1}{2} + \frac{-16 + 6\pi + (-20 + 9\pi)\kappa + (-4 + 3\pi)\kappa^2}{32 - 3\pi + (40 + 3\pi)\kappa + 8\kappa^2 - 12\pi\kappa \ln(\epsilon)}\epsilon + O(\epsilon^3). \tag{5.63}$$

This function along with the second order correction is plotted in Figure 5.33. In can be seen that the function does not match well with the finite element results even in the domain of very small values of ϵ. The comparison with the finite element calculation shows that this discrepancy is caused by the inaccuracy of the assumed contact pressure distribution. Although the contact angle on both holes stays close to the assumed value 90°, the form of stress distribution changes in a way that is not captured in the simple model (3.4). This problem can be somewhat artificially solved by assuming a more general approximation of the contact pressure such as that described by the equation (3.5). The constants m_1 and m_2 corresponding to holes 1 and 2 are assumed to have the form of an asymptotic series

$$m_p = \sum_{n=1}^{\infty} m_p^n \epsilon^n. \tag{5.64}$$

This more general assumption on the stress distribution leads to the following generalisation of the formula (5.63):

$$\lambda = \frac{1}{2} + \frac{-16 + 6\pi + (-20 + 9\pi)\kappa + (-4 + 3\pi)\kappa^2}{32 - 3\pi + (40 + 3\pi)\kappa + 8\kappa^2 - 12\pi\kappa \ln(\epsilon)}\epsilon + \\ + \frac{\frac{1}{20}(m_1^1 - m_2^1)\big(32 + 30\pi + (72 + 15\pi)\kappa\big)}{32 - 3\pi + (40 + 3\pi)\kappa + 8\kappa^2 - 12\pi\kappa \ln(\epsilon)}\epsilon + O(\epsilon^3). \tag{5.65}$$

The up to now unknown constants m_1^1 and m_2^1 have to be determined from the contact condition. One possibility to obtain two additional equations for the determination of these constants is by forcing the contact condition to hold in the integral mean over the contact area. This gives numerical values $m_1^1 = 0.45$, $m_2^1 = -0.45$. The corrected solution is plotted along with the original one in Figure 5.33. As can be seen, this correction gives satisfactory results for small values of ϵ. This example shows the limits of the considered modelling.

Similarly to the previous example, the results in the case of general anisotropic material behaviour tend to be very lengthy and a compact closed-form formula can only be written in the case of strong orthotropy. For E_1 large, the load distribution coefficient reads

$$\lambda = \frac{1}{2} + \frac{(-8 + 3\pi)\left(2 + \sqrt{\frac{E_2}{G_{12}}} + \sqrt{\frac{G_{12}}{E_2}}\right)}{32 - 3\pi - (32 + 9\pi)\sqrt{\frac{G_{12}}{E_1}} - 6\pi\left(1 + \frac{G_{12}}{E_1}\right)\ln(\epsilon)}\epsilon + O(\epsilon^3) + O\left(\left(\frac{E_2}{E_1}\right)^0\right) \tag{5.66}$$

and for large E_2, it takes the form

$$\lambda = \frac{1}{2} + \frac{(-8 + 3\pi)\left(1 + \sqrt{\frac{G_{12}}{E_2}}\right) + (-4 + 3\pi)\frac{G_{12}}{\sqrt{E_1 E_2}} + 4\sqrt{\frac{G_{12}}{E_1}} + 4\frac{G_{12}}{E_1}\sqrt{\frac{G_{12}}{E_2}}}{(32 - 3\pi)\sqrt{\frac{G_{12}}{E_2}} - (16 + 3\pi)\frac{G_{12}}{E_1}\sqrt{\frac{E_1}{E_2}} - 6\pi\sqrt{\frac{G_{12}}{E_2}}\ln(\epsilon)}\epsilon + O(\epsilon^3) \\ + O\left(\frac{E_1}{E_2}\right), \tag{5.67}$$

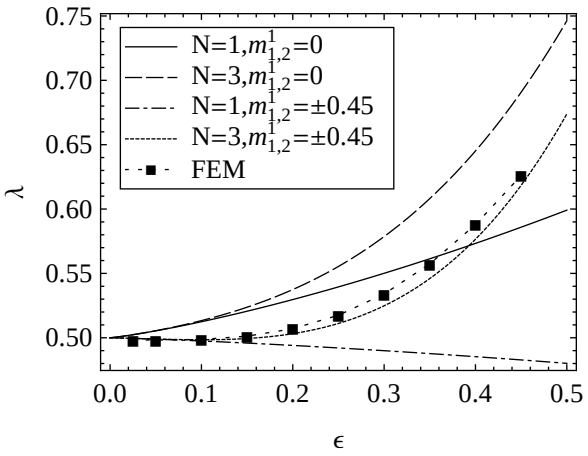

Figure 5.33: Dependence of the load distribution coefficient for two holes in an infinite plane on the relative hole radius. Curves $m^1_{1,2} = 0$ represent the equation (5.63), curves $m^1_{1,2} = \pm 0.45$ the equation (5.65).

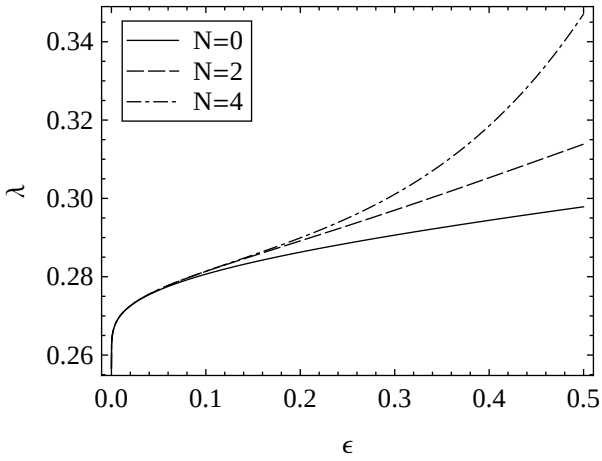

Figure 5.34: Dependence of the load distribution coefficient (5.69) on the relative hole radius.

whereas the leading order term in the case of large E_1 and E_2 is very complex even in this simple case. These equations suffer from the same drawback as the equation (5.63), i.e. they do not take into account the influence of the departure of the contact pressure from the assumed one, which plays an important role in this configuration.

Finally, consider a joint of two identical isotropic plates joined by a row of four bolts in a row parallel to the direction of the transmitted load. From the symmetry conditions follows that the load distribution can be described by a single parameter λ as shown in Figure 5.32 and that the corresponding compatibility condition reads

$$V_1 = V_2. \tag{5.68}$$

Algorithm 4.2 with $N_H = 4$, $c_p = i(5/2 - p)$, other settings being equal to (5.49) along with the procedure described in the previous paragraph gives the following expression for the load distribution coefficient:

$$\lambda = \frac{1}{4} + \frac{3\pi\kappa\ln(3)}{16(1+\kappa)(4+\kappa) + 6\pi\big(-1+\kappa+4\kappa\ln(2)-2\kappa\ln(3)\big) - 24\pi\kappa\ln(\epsilon)} + O(\epsilon^2). \tag{5.69}$$

The dependence of this function along with higher-order approximations is shown in Figure 5.34.

5.3.3 Infinite plane containing two infinite rows of holes

An infinite plane contains two rows of holes. The radius of all holes is ϵ, the horizontal spacing between the holes is 1 and the distance of the rows is also 1 (see Figure 5.35). The holes are loaded by the distribution of forces (3.13). The plane is connected to a rigid

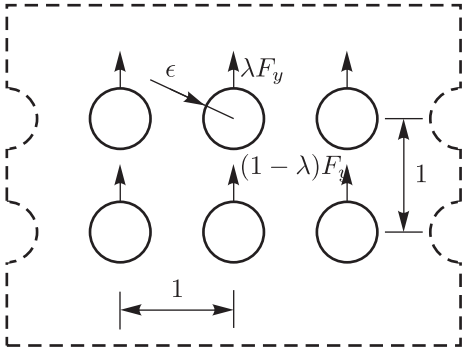

Figure 5.35: An infinite plane containing two infinite rows of pin-loaded holes.

plane, the compatibility condition (3.26) becomes

$$V_1 = V_2. \tag{5.70}$$

The distribution of the load among the rows is described by the parameter λ introduced in Figure 5.35. The Algorithm 4.2 with

$$N_H = \infty, \quad N_C = 2, \quad c_{pr} = r + (3/2 - p)i, \quad \rho_p = 1, \quad \hat{\varphi}_0^n(z) = \hat{\psi}_0^n(z) = 0, \tag{5.71a}$$

$$\hat{\varphi}_1^n(\zeta_1) = \lambda^n F_y \hat{\varphi}_{\mathrm{BL}}(\zeta_1), \quad \hat{\psi}_1^n(\zeta_1) = \lambda^n F_y \hat{\psi}_{\mathrm{BL}}(\zeta_1), \tag{5.71b}$$

$$\hat{\varphi}_2^n(\zeta_2) = (\delta_{n0} - \lambda^n) F_y \hat{\varphi}_{\mathrm{BL}}(\zeta_2), \quad \hat{\psi}_2^n(\zeta_2) = (\delta_{n0} - \lambda^n) F_y \hat{\psi}_{\mathrm{BL}}(\zeta_2), \tag{5.71c}$$

$$F_1^n = \lambda^n i F_y, \quad F_2^n = (\delta_{n0} - \lambda^n) i F_y \tag{5.71d}$$

along with the procedure described in the beginning of this section leads to

$$\lambda = \frac{1}{2} - \frac{18\pi^2(\kappa - 1)}{-36\pi^2 \coth(\pi) + 80 + 27\pi + (104 + 9\pi)\kappa + 24\kappa^2 - 36\pi\kappa \ln\bigl(\pi\, \mathrm{csch}(\pi)\epsilon\bigr)} + O(\epsilon). \tag{5.72}$$

The dependence of the parameter λ on the parameter ϵ is plotted in Figure 5.36. In this example, the parameter ϵ lies in the interval $0 < \epsilon < 1/2$, the limiting value $\epsilon = 1/2$ corresponding to the situation when all neighbouring holes touch each other. The curve $N = 0$ corresponds to the equation (5.72), the curve $N = 2$ shows the influence of the quadratic correction. The points labelled 'FEM' represent results obtained by the contact variant of the FEM model described in Section 4.4. Similarly as in the examples of Section 5.3.1, the curve $N = 0$ agrees well with the numerical curve in the technically relevant domain $\epsilon < 0.2$, the quadratic correction being significant for large values of ϵ. The slight difference between both curves near $\epsilon = 0$ is caused by the inaccuracy of the assumed form of contact stresses.

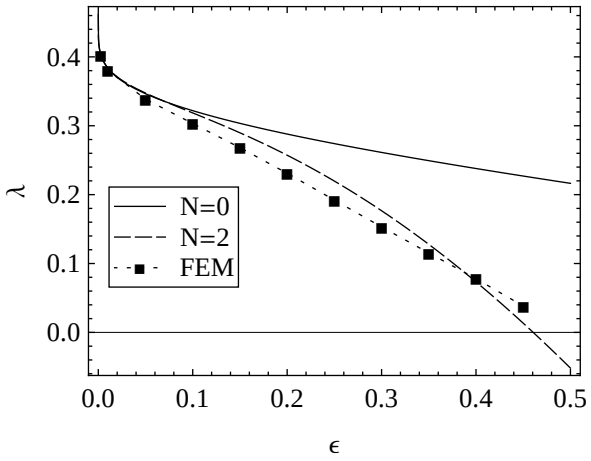

Figure 5.36: Dependence of the load distribution coefficient (5.72) on the relative hole radius.

5.4 Discussion

In this chapter, a collection of problems solved by the Algorithms 4.2 and 4.3 is presented. The first section of this chapter deals with stress concentration on unloaded holes. The main purpose of these problems is to evaluate the capabilities of the present method by means of simple examples in which a relatively high number of terms of the perturbation series can be calculated. A certain problem related to the nature of the asymptotic solution is the convergence of the asymptotic series. This problem is often indicated by alternating signs in the series. Numerical tests show that in the simplest example of a single hole in an isotropic half-plane, the series converge for all admissible values of the small parameter. However, with increasing complexity of the geometric configuration the convergence worsens and the series are convergent only to a certain limiting value of the small parameter. The same behaviour is observed for anisotropic materials. This problem can be solved by some of the methods for the improvement of convergence of asymptotic series, the most successful of them being the method of Padé approximants. Besides that, even if a series is divergent, its first few terms give a satisfactory approximation of the result for a large domain of values of the small parameter. In the case of anisotropic material behaviour, the dependence of the series coefficients on the material parameters is always very complex. Their simplification can be achieved by assuming strong anisotropy and performing the Taylor series expansion with respect to a small parameter accounting for the strong anisotropy. In this manner, compact formula for an anisotropic material can be obtained.

The second section of this chapter deals with the compliance of pin-loaded holes defined earlier in Section 3.3. Since a finite number of holes in an infinite or semi-infinite domain always gives infinite compliance, only infinite rows of pin-loaded holes are considered. Analytical results for an isotropic plane and a half-plane are presented. The convergence of the result with respect to the relative hole radius as well as with respect to the approximation of the contact pressure proved to be sufficient in the technically relevant domain. This allows to construct a compact formula suitable for practical computations. The result for a half-plane tends quickly to that for a full plane as the edge distance tends

to infinity. For small values of the edge distance, a compact closed-form expression can be obtained by using Taylor series expansion. Unfortunately, similar results cannot be obtained for anisotropic material behaviour. The reason is that although the solution for anisotropic plates follows the same lines as for isotropic plates, it leads to infinite sums that cannot be evaluated analytically.

The last section of this chapter is devoted to the calculation of load distribution on bolted joints on the basis of the procedure sketched in Section 3.4. Several relatively simple configurations involving a finite number of holes in both isotropic and anisotropic plates and two infinite rows in an isotropic plane are considered. Compact formulae can be obtained for isotropic material behaviour. For anisotropic materials, this is possible only by assuming strong anisotropy. A certain limitation of the presented results is the assumed distribution of the contact pressure in the bolt-to-plate contact. Comparative finite element analysis shows that when the bolts lie on a line perpendicular to the load direction, the assumed stress distribution corresponds well to that obtained in a finite element calculation and so do the load distribution coefficients. However, when the bolts lie on a line parallel to the direction of the transmitted force, the contact distribution differs on each bolt which has a significant impact on the resulting load distribution. This has been observed even in the simplest configuration consisting of two holes in an infinite isotropic plane.

Chapter 6

Summary and outlook

In this thesis, the complex potential method along with the method of compound asymptotic expansions is applied to the analysis of selected problems of plane elasticity related to double-lap bolted joints. The contribution of the thesis lies in the construction of several closed-form approximations of solutions to the considered problems.

After a brief introduction of the basic theoretical concepts in Chapter 2, a mathematical model of a double-lap bolted joint is presented in Chapter 3. A very simple model is chosen in order to make the analytical treatment possible. This model assumes the (generalised) state of plane stress in each of the plates and a simple sinusoidal distribution of contact pressure in the bolt-to-hole contact and leads to the first fundamental problem of the plane theory of elasticity.

In Chapter 4, a formal asymptotic solution of the first fundamental problem for an infinite plane or half-plane weakened by a finite number or an infinite symmetric array of small holes is derived. Several types of deformations with three different underlying partial differential equations are considered, namely antiplane strain described by the Laplace equation, plane stress and plane strain in isotropic plates described by the bipotential equation and plane stress and generalised plane stress in anisotropic plates described by a more general linear elliptic fourth-order partial differential equation with constant coefficients. In all cases, an asymptotic expansion of the complex potentials is derived which is uniformly valid in the whole domain, i.e. in the vicinity of each of the holes as well as in the far-field. From these potentials, expansions of all other quantities of interest such as stresses, displacements or forces can be obtained by simple algebraic operations. The solution is summarised in form of algorithms for a computer algebra system and implemented in MATHEMATICA. Furthermore, a fully parametrised finite element model of the considered problem has been created using the commercial FE Software ABAQUS and its PYTHON programming interface in order to verify the results in an independent way.

In Chapter 5, the general asymptotic solution introduced in Chapter 4 is applied to three types of problems. The first one is the problem of stress concentration on unloaded holes. Although it describes the stress concentration of a by-pass load on a bolted joint, its main purpose is to evaluate the capability of the method by means of simple examples where a sufficiently high number of terms of the asymptotic series can be generated. The

second type of problems involves the compliance of an infinite row of pin-loaded holes. A closed-form approximate formula for the compliance of an infinite row of pin-loaded holes in an infinite isotropic plane and a half-plane is derived. This formula, as opposed to semi-empirical formulae commonly used in the industrial environment, correctly takes into account the contributions of the plane deformation of the plates to the overall compliance of the joint. Finally, the third type deals with the determination of the load distribution on both finite number of bolts as well as infinite rows of bolts. Closed-form approximations of the load distribution factor for these configurations are presented.

The choice of the examples and their applicability is limited to some extent by the very simple contact model used. The assumed sinusoidal distribution of the contact stress in the pin-to-hole contact gives satisfactory results for the compliance of an infinite row of pin-loaded holes in the case of zero clearance. It also gives satisfactory results for the load distribution on bolts in some situations, although sometimes, a significant departure of the contact stress from the assumed one is observed which has a non-negligible impact on the result. On the other hand, the presented model is by no means capable of capturing the effects of bolt-hole clearance. It is also not sufficiently precise for a strength analysis. Therefore, no examples involving stress concentration on pin-loaded holes are given in this thesis.

A certain problem related to the nature of the proposed solution is the convergence of the asymptotic series. As expected from the nature of the asymptotic solution, the discrepancy between the asymptotic solution and a reference numerical one is the smallest for small radii and with increasing radii, it generally increases. However, results with the presented order of approximation are sufficiently accurate in the technically relevant domain.

The performance of the method for anisotropic material behaviour is rather disappointing. Although the derivation of the method and its implementation basically follows the same lines as in the isotropic case, the analytic evaluation of the algorithm turns out to be more complicated. When numerical values are assigned to the material parameters before the algorithm is executed, solutions for a finite number of holes can be obtained in form of a series with numerical coefficients. However, the formulae describing the dependence on the material parameters are too complex for practical use even in the simplest situations such as stress concentration on a single hole in a half-plane. A certain simplification can be achieved by assuming strong orthotropy and performing a Taylor expansion in terms of the corresponding small parameter. It appears that such an expansion exhibits good convergence and can therefore be used also for moderately orthotropic materials. It was not possible to obtain analytical results for infinite rows of holes in anisotropic plates because the proposed algorithm leads to infinite sums that cannot be be evaluated analytically.

The presented work offers the possibility of further extension in several directions. The first one is related to the anisotropic material behaviour. As shown in Chapter 5, one possible way of simplifying the results for anisotropic materials is by using the approximation of strong orthotropy. Within this thesis, first, the solution for a general anisotropic material is constructed from which the approximation for a strongly anisotropic material is derived a posteriori. Another approach, originally proposed in the works of Spencer [89] or Manevitch and Pavlenko [59] is to first simplify the underlying boundary value problem using this assumption and then to treat this generally simpler problem. The application

of this approach in combination with the treatment of the small holes in the same manner as in this thesis could be a way towards the solution of problems involving infinite rows of holes in anisotropic plates. This approach might also be extended to problems involving extension-bending coupling.

Another line of possible future research could be focused on the improvement of the contact model. The challenge is to find a more accurate model than the one used in this thesis which would still be simple enough to allow a closed-form analytical approximation of the solution of the plane problem.

Finally, it should be kept in mind that all solutions proposed in this thesis rely on a wide range of assumptions. Therefore, before the results of this thesis can be applied to practical problems, it has to be validated experimentally whether these assumptions are at least approximately fulfilled and to what extent the proposed solutions are capable of describing the reality.

Bibliography

[1] Abramowitz, M. and Stegun, I. A. *Handbook of mathematical functions*. United States Government Printing, 1972.

[2] Altenbach, H., Altenbach, J. and Kissing, W. *Mechanics of composite structural elements*. Foundations of engineering mechanics. Springer-Verlag, 2004.

[3] Aluko, O. and Whitworth, H. Analysis of stress distribution around pin loaded holes in orthotropic plates. *Composite Structures*, 86(4):308 – 313, 2008.

[4] Andrianov, I. V. and Manevitch, L. I. *Asymptotology: Ideas, Methods, and Applications*. Springer, 2002.

[5] Anton, M. *Bolt stiffness in carbon fibre reinforced plastics*. Master's thesis, Technische Universität Darmstadt, 2011.

[6] Baker, G. and Graves-Morris, P. *Padé approximants*. Encyclopedia of mathematics and its applications. Cambridge University Press, 1996.

[7] Becker, W. A complex potential method for plate problems with bending extension coupling. *Archive of Applied Mechanics*, 61:318–326, 1991.

[8] Becker, W. and Gross, D. *Mechanik elastischer Körper und Strukturen*. Springer-Verlag Berlin Heidelberg, 2002.

[9] Berbinau, P. and Soutis, C. A new approach for solving mixed boundary value problems along holes in orthotropic plates. *International Journal of Solids and Structures*, 38(1):143 – 159, 2001.

[10] Camanho, P. and Matthews, F. Stress analysis and strength prediction of mechanically fastened joints in frp: a review. *Composites Part A: Applied Science and Manufacturing*, 28(6):529 – 547, 1997.

[11] Chao, C. K., Shen, M. H. and Fung, C. K. On multiple circular inclusions in plane thermoelasticity. *International Journal of Solids and Structures*, 34(15):1873 – 1892, 1997.

[12] Christensen, R. *Mechanics of composite materials*. Dover books on engineering. Dover Publications, 2005.

[13] Dassault Systèmes Simulia Corp. Abaqus, version 6.10. Providence, RI, USA, 2010.

[14] de Jong, T. *On the calculation of stresses in pin-loaded anisotropic plates.* Ph.D. thesis, Technische Universiteit Delft, 1987.

[15] Duan, Z., Kienzler, R. and Herrmann, G. An integral equation method and its application to defect mechanics. *Journal of the Mechanics and Physics of Solids*, 34(6):539 – 561, 1986.

[16] Dyke, M. D. V. *Perturbation methods in fluid dynamics.* Parabolic Press, 1975.

[17] Ekh, J. and Schön, J. Effect of secondary bending on strength prediction of composite, single shear lap joints. *Composites Science and Technology*, 65(6):953 – 965, 2005.

[18] Ekh, J. and Schön, J. Load transfer in multirow, single shear, composite-to-aluminium lap joints. *Composites Science and Technology*, 66:875 – 885, 2006.

[19] Ekh, J. and Schön, J. Finite element modeling and optimization of load transfer in multi-fastener joints using structural elements. *Composite Structures*, 82(2):245 – 256, 2008.

[20] Ekh, J., Schön, J. and Melin, L. G. Secondary bending in multi fastener, composite-to-aluminium single shear lap joints. *Composites Part B: Engineering*, 36(3):195 – 208, 2005.

[21] Engels, H. *Analyse und Optimierung lokaler Laminat-Lochverstärkungen und Laminat-Lochreparaturen.* Ph.D. thesis, Universität Siegen, 2003.

[22] Engels, H. and Becker, W. Closed-form analysis of external patch repairs of laminates. *Composite Structures*, 56(3):259 – 268, 2002.

[23] Engels, H., Zakharov, D. and Becker, W. The plane problem of an elliptically reinforced circular hole in an anisotropic plate or laminate. *Archive of Applied Mechanics*, 71:601–612, 2001.

[24] Frizzell, R., McCarthy, C. and McCarthy, M. Simulating damage and delamination in fibre metal laminate joints using a three-dimensional damage model with cohesive elements and damage regularisation. *Composites Science and Technology*, 71(9):1225 – 1235, 2011.

[25] Gong, S. and Meguid, S. Interacting circular inhomogeneities in plane elastostatics. *Acta Mechanica*, 99:49–60, 1993.

[26] Gray, P. and McCarthy, C. A global bolted joint model for finite element analysis of load distributions in multi-bolt composite joints. *Composites Part B: Engineering*, 41(4):317 – 325, 2010.

[27] Grüber, B. *Beitrag zur Strukturanalyse von anisotropen Schichtverbunden mit elastischen Einschlüssen und Bolzen.* Ph.D. thesis, Technische Universität Dresden, 2004.

[28] Grüber, B., Hufenbach, W., Kroll, L., Lepper, M. and Zhou, B. Stress concentration analysis of fibre-reinforced multilayered composites with pin-loaded holes. *Composites Science and Technology*, 67(7-8):1439 – 1450, 2007.

[29] Haddon, R. A. W. Stress in an infinite plate with two unequal circular holes. *The Quarterly Journal of Mechanics and Applied Mathematics*, 20(3):277–291, 1967.

[30] Henrici, P. *Applied and computational complex analysis.* v. 1-2. Wiley, 1974.

[31] Hinch, E. J. *Perturbation Methods.* Cambridge University Press, 1991.

[32] Howell, P., Kozyreff, G. and Ockendon, J. *Applied solid mechanics.* Cambridge texts in applied mathematics. Cambridge University Press, 2009.

[33] Howland, R. C. J. and Knight, R. C. Stress functions for a plate containing groups of circular holes. *Phil. Trans. R. Soc. Lond.*, 238:357–392, 1939.

[34] Hühne, C., Zerbst, A.-K., Kuhlmann, G., Steenbock, C. and Rolfes, R. Progressive damage analysis of composite bolted joints with liquid shim layers using constant and continuous degradation models. *Composite Structures*, 92(2):189 – 200, 2010.

[35] Huth, H. Zum Einfluss der Nietnachgiebigkeit mehrreihiger Nietverbindungen auf die Lastübertragungs- und Lebensdauervorhersage. Technical report, Fraunhofer-Institut für Betriebsfestigkeit Darmstadt, 1984.

[36] Huth, H. *Fatigue in mechanically fastened composite and metallic joints: a symposium*, chapter Influence of fastener flexibility on the prediction of load transfer and fatigue life for multiple-row joints, pages 221–250. ASTM, 1986.

[37] Il'in, A. A boundary value problem for the elliptic equation of second order in a domain with a narrow slit. *Mathematics of the USSR - Sbornik*, 28:459–480, 1976.

[38] Il'in, A. M. *Matching of asymptotic expansions of solutions of boundary value problems.* American Mathematical Society, 1992.

[39] Isida, M. *Methods of analysis and solutions of crack problems*, chapter Method of Laurent series expansion for internal crack problems, pages 56–130. Noordhoff International Publishing Leyden, 1973.

[40] Johnson, K. and Johnson, K. *Contact mechanics.* Cambridge University Press, 1987.

[41] Johnson, R. S. *Singular Perturbation Theory.* Springer, 2004.

[42] Jones, R. *Mechanics of composite materials.* Scripta Book Co., 1975.

[43] Kevorkian, J. and Cole, J. *Perturbation Methods in Applied Mathematics.* Applied Mathematical Sciences. Springer, 2010.

[44] Kozlov, V., Maz'ya, V. and Movchan, A. *Asymptotic Analysis of Fields in Multi-Structures.* Clarendon Press, 1999.

[45] Kozlov, V., Movchan, A. and Maz'ya, V. Asymptotic analysis of a mixed boundary value problem in a multistructure. *Asymptotic analysis*, 8:105–143, 1994.

[46] Kozlov, V., Movchan, A. and Maz'ya, V. Asymptotic representation of elastic fields in a multistructure. *Asymptotic analysis*, 11:343–415, 1995.

[47] Kradinov, V., Barut, A., Madenci, E. and Ambur, D. Bolted double-lap composite joints under mechanical and thermal loading. *International Journal of Solids and Structures*, 38(44-45):7801 – 7837, 2001.

[48] Kradinov, V., Madenci, E. and Ambur, D. Application of genetic algorithm for optimum design of bolted composite lap joints. *Composite Structures*, 77(2):148 – 159, 2007.

[49] Kradinov, V., Madenci, E. and Ambur, D. R. Bolted lap joints of laminates with varying thickness and metallic inserts. *Composite Structures*, 68(1):75 – 85, 2005.

[50] Kratochvil, J. and Becker, W. Asymptotic analysis of stresses in an isotropic linear elastic plane or half-plane weakened by a finite number of holes. *Archive of Applied Mechanics*, pages 1–12. 10.1007/s00419-011-0587-z.

[51] Kratochvil, J. and Becker, W. Structural analysis of composite bolted joints using the complex potential method. *Composite Structures*, 92(10):2512 – 2516, 2010.

[52] Kratochvil, J. and Becker, W. Asymptotic analysis of the interaction of a finite number of holes in an elastic plane or half-plane. *PAMM*, 11(1):237–238, 2011.

[53] Kushch, V., Shmegera, S. and Buryachenko, V. Elastic equilibrium of a half plane containing a finite array of elliptic inclusions. *International Journal of Solids and Structures*, 43(11-12):3459 – 3483, 2006.

[54] Lang, S. *Complex Analysis*. Springer, 1998.

[55] Leguillon, D. and Sanchez-Palencia, E. *Computation of singular solutions in elliptic problems and elasticity*. Recherches en mathématiques appliquées. Wiley, 1987.

[56] Lekhnitskii, S. *Anisotropic Plates*. Gordon and Breach Science Publishers, 1968.

[57] Ling, C.-B. On the stresses in a plate containing two circular holes. *Journal of Applied Physics*, 19:77–82, 1948.

[58] Madenci, E., Ileri, L. and Starnes, J. Analysis of pin-loaded holes in composite laminates under combined bearing-bypass and shear loading. *International Journal of Solids and Structures*, 32(14):2053 – 2062, 1995.

[59] Manevitch, L. and Pavlenko, A. *Asymptotic methods in the micromechanics of composite materials*. Kiev Visha Shkola, 1991. (in Russian).

[60] Mangalgiri, P., Dattaguru, B. and Rao, A. Fasteners in composite plates: effects of interfacial friction. *Computers and Mathematics with Applications*, 11(10):1057 – 1068, 1985.

[61] Mangalgiri, P., Ramamurthy, T., Dattaguru, B. and Rao, A. Elastic analysis of pin joints in plates under some combined pin and plate loads. *International Journal of Mechanical Sciences*, 29(8):577 – 585, 1987.

[62] Mazja, V. G., Nazarow, S. A. and Plamenewskii, B. A. *Asymptotische Theorie elliptischer Randwertaufgaben in singulär gestörten Gebieten.* Akademie-Verlag Berlin, B.1 1991; B.2 1992.

[63] Maz'ya, V. G., Nazarov, S. A. and Plamenevskij, B. A. Asymptotic solutions of elliptic boundary value problems when the domain is varied close to conical points. *Soviet physics / Doklady*, 24:904–905, 1979.

[64] Maz'ya, V. G., Nazarov, S. A. and Plamenevskij, B. A. *Asymptotic Theory of Elliptic Boundary Value Problems in Singularly Perturbed Domains.* Birkhäuser, 2000.

[65] McCarthy, C. and McCarthy, M. Three-dimensional finite element analysis of single-bolt, single-lap composite bolted joints: part II - effects of bolt-hole clearance. *Composite Structures*, 71(2):159 – 175, 2005.

[66] McCarthy, C., McCarthy, M. and Lawlor, V. Progressive damage analysis of multi-bolt composite joints with variable bolt-hole clearances. *Composites Part B: Engineering*, 36(4):290 – 305, 2005.

[67] McCarthy, M., McCarthy, C., Lawlor, V. and Stanley, W. Three-dimensional finite element analysis of single-bolt, single-lap composite bolted joints: part I - model development and validation. *Composite Structures*, 71(2):140 – 158, 2005.

[68] McCarthy, M. A., McCarthy, C. T. and Padhi, G. S. A simple method for determining the effects of bolt-hole clearance on load distribution in single-column multi-bolt composite joints. *Composite Structures*, 73(1):78 – 87, 2006.

[69] Milne-Thomson, L. *Plane elastic systems.* Ergebnisse der angewandten Mathematik. Springer-Verlag, 1968.

[70] Mindlin, R. D. Stress distribution around a hole near the edge of a plate under tension. *Proceedings of the Society for Experimental Stress Analysis*, V(2):56–68, 1948.

[71] Muskhelishvili, N. I. *Some Basic Problems of the Mathematical Theory of Elasticity.* P. Nordhoof Ltd, 1963.

[72] Nelson, W. D., Bunin, B. L. and Hart-Smith, L. J. *Critical joints in large composite aircraft structure.* NASA CR-3710, 1983.

[73] Neuber, H. *Kerbspannungslehre.* Springer, 2001.

[74] Persson, A. *On the stress distribution of cylindrical elastic bodies in contact.* Ph.D. thesis, Chalmers Techniska Högskola, 1964.

[75] Pilkey, W. D. and Pilkey, D. F. *Peterson's Stress Concentration Factors*. John Wiley & Sons, 2008.

[76] Postupka, S., Kühweg, A. and Anderts, F. Determination of the bolt flexibility. In *ECCM-8*. 2008.

[77] Prandtl, L. Über Flüssigkeitsbewegung bei sehr kleiner Reibung. In *3rd International Mathematics Congress, Heidelberg*. 1904.

[78] Radaj, D. and Schilberth, G. *Kerbspannungen an Ausschnitten und Einschlüssen*. Deutscher Verlag für Schweißtechnik, 1977.

[79] Rangavittal, H., Naidu, A., Dattaguru, B. and Ramamurthy, T. Analytical solutions for load transfer through smooth elastic pin in an infinite orthotropic plate. *Composite Structures*, 30(3):329 – 339, 1995.

[80] Rhee, J. and Rowlands, R. E. Stresses around extremely large or interacting multiple holes in orthotropic composites. *Computers & Structures*, 61(5):935 – 950, 1996.

[81] Rolbicki. Bolzenverbindungen in CFK-Laminaten (Konstruktive Hinweise). Technical report, LTH Faserverbund-Leichtbau, 1980.

[82] Sadd, M. H. *Elasticity: Theory, Applications and Numerics*. Academic Press, 2009.

[83] Savin, G. *Stress concentration around holes*. International series of monographs on aeronautics and astronautics: Solid and structural mechanics. Pergamon Press, 1961.

[84] Schmidt, P. Numerische Validierung asymptotischer Lösungen für Strukturen mit kleinen Löchern. Abschlussarbeit (B.Sc.), Technische Universität Darmstadt, 2012.

[85] Schürmann, H. *Konstruieren mit Faser-Kunststoff-Verbunden*. Springer Berlin Heidelberg, 2007.

[86] Sergeev, B., Madenci, E. and Ambur, D. R. Influence of bolt spacing and degree of anisotropy in single-lap joints. *Computers & Structures*, 76(1-3):89 – 103, 2000.

[87] Silva, M., Matalon, M. and Tortorelli, D. A. Higher order topological derivatives in elasticity. *International Journal of Solids and Structures*, 47(22-23):3053 – 3066, 2010.

[88] Sokolowski, J. and Zochowski, A. On the topological derivative in shape optimization. *SIAM Journal on Control and Optimization*, 37(4):1251–1272, 1999.

[89] Spencer, A. Boundary layers in highly anisotropic plane elasticity. *International Journal of Solids and Structures*, 10(10):1103 – 1123, 1974.

[90] Tate, M. B. and Rosenfeld, S. J. *Preliminary investigation of the loads carried by individual bolts in bolted joints*. Washington D.C.: National Advisory Committee for Aeronautics, 1946.

[91] Thoppul, S. D., Finegan, J. and Gibson, R. F. Mechanics of mechanically fastened joints in polymer-matrix composite structures - a review. *Composites Science and Technology*, 69:301 – 329, 2009.

[92] Tomas and Ireman. Three-dimensional stress analysis of bolted single-lap composite joints. *Composite Structures*, 43(3):195 – 216, 1998.

[93] Wei-Xun, F. and Chun-Tu, Q. Load distribution of multi-fastener laminated composite joints. *International Journal of Solids and Structures*, 30(21):3013 – 3023, 1993.

[94] Wolfram Research, Inc. Mathematica, version 8.0. Champaign, Illinois, 2010.

[95] Xiong, Y. An analytical method for failure prediction of multi-fastener composite joints. *International Journal of Solids and Structures*, 33(29):4395 – 4409, 1996.

[96] Xu, X. W., Yue, T. M. and Man, H. C. Stress analysis of finite composite laminate with multiple loaded holes. *International Journal of Solids and Structures*, 36(6):919 – 931, 1999.

[97] Zerres, P. *Ermittlung der Kraftflussverteilung und der Lastübertragung an zweischnittigen Niet- und Bolzenverbindungen zwischen CFK-Laminaten.* Master's thesis, Technische Universität Darmstadt, 2005.

Bisher sind in dieser Reihe erschienen

Band 1
Zur mikrorissinduzierten Schädigung spröder Materialien
B. Lauterbach, Dissertation 2001, ISBN 3-935868-01-4

Band 2
3D-Simulation der Mikrostrukturentwicklung in Zwei-Phasen-Materialien
R. Müller, Dissertation 2001, ISBN 3-935868-02-2

Band 3
Zur numerischen Simulation von Morphologieänderungen in mikroheterogenen Materialien
S. Kolling, Dissertation 2001, ISBN 3-935868-03-0

Band 4
Theoretische und numerische Untersuchung von Versagensmechanismen in Metall-Keramik-Verbundwerkstoffen
T. Emmel, Dissertation 2002, ISBN 3-935868-04-9

Band 5
On microcrack dominated problems in dynamics and statics of brittle fracture: a numerical study by boundary element techniques
S. Rafiee, Dissertation 2002, ISBN 3-935868-05-7

Band 6
Kontinuumsmechanik anisotroper Festkörper und Fluide
H. Ehrentraut, Habilitationsschrift 2002, ISBN 3-935868-06-5

Band 7
Plane unsteady inviscid incompressible hydrodynamics of a thin elastic profile
N. Blinkova, Dissertation 2002, ISBN 3-935868-07-3

Band 8
Anmerkungen zur Simulation von entfestigendem Materialverhalten
H. Baaser, Habilitationsschrift 2004, ISBN 3-935868-08-1

Band 9
Orts- und zeitadaptive DAE-Methoden zur Beschreibung elastisch-plastischen Materialverhaltens innerhalb der FEM
S. Eckert, Dissertation 2005, ISBN 3-935868-09-X

Band 10
Simulations of the Flow of the Ross Ice Shelf, Antarctica: Parameter Sensitivity Tests and Temperature-Dependent Rate Factor
A. Humbert, Dissertation 2005, ISBN 3-935868-10-3

Band 11
A Thermo-mechanical Continuum Theory with Internal Length of Cohesionless Granular Materials
Chung Fang, Dissertation 2006, ISBN 3-935868-11-1

Band 12
Modeling Dry Granular Avalanches past Different Obstructions: Numerical Simulation and Laboratory Analyses
Chiou Min-Ching, Dissertation 2006, ISBN 3-935868-12-X

Band 13
Configurational forces in defect mechanics and in computational methods
R. Müller, Habilitationsschrift 2005, ISBN 3-935868-13-8

Band 14
Hyperelastic dynamics in physical and material space
S. Kolling, Habilitationsschrift 2007, ISBN 978-3-935868-14-3

Band 15
Phenomenological modeling of ferroelectric material behavior
V. Mehling, Dissertation 2007, ISBN 978-3-935868-15-0

Band 16
Ein mischungsbasiertes Materialmodell zum Knochenumbau
R.-R. Kühn, Dissertation 2006, ISBN 978-3-935868-16-7

Band 17
Einige Erweiterungen der Rand-Finite-Elemente-Methode und deren Anwendung auf Randeffekte in ebenen Laminaten
J. Artel, Dissertation 2007, ISBN 978-3-935868-17-4

Band 18
Spannungskonzentrations-Effekte an Verstärkungspflaster-Ecken
H. Wigger, Dissertation 2008, ISBN 978-3-935868-18-1

Band 19
Rotationseffekte in der Kristallplastizität
C. Bröse, Dissertation 2007, ISBN 978-3-935868-19-8

Band 20
Finite-Element-Modelle zur Simulation von Delaminationen dünner Filme auf Substraten
V. D. Pham, Dissertation 2010, ISBN 978-3-935868-20-4

Band 21
Asymptotische Nahfeldanalysen ebener Multi-Materialverbindungsstellen mit der Methode komplexer Potentiale
C. Sator, Dissertation 2010, ISBN 978-3-935868-21-1

Band 22
Modellierung spröder Rissbildung an Spannungskonzentrationen mit der Bruchmechanik finiter Risse
J. Hebel, Dissertation 2010, ISBN 978-3-935868-22-8

Band 23
Some Contributions to the Homogenization of Macroscopically Isotropic Composites
V. Salit, Dissertation 2011, ISBN 978-3-935868-23-5

This work is devoted to the problem of the load transfer on double-lap bolted joints. For this purpose, the in-plane deformations of the plates involved in the joint are investigated within the framework of the complex potential method and the method of compound asymptotic expansions. First, the relative radius of the holes is introduced as a small parameter. Then, an asymptotic expansion of the complex potentials in terms of this small parameter is constructed. This expansion is uniformly valid in the whole domain, i.e. in the vicinity of the holes as well as in the far-field. Finally, this result is used to evaluate several practically relevant parameters such as the compliance of an infinite row of bolts or the load distribution on several bolts. The major advantage of the proposed method is that it leads to closed-form approximations that can easily be used by engineers in the industrial environment.

ISBN 978-3-935868-24-2